Shuting Lei
Department of Industrial and Manufacturing Systems Engineering,
Kansas State University,
Manhattan, KS 66506
e-mail: lei@ksu.edu

Xin Zhao
Department of Mechanical Engineering,
Clemson University,
Clemson, SC 29634
e-mail: xzhao5@clemson.edu

Xiaoming Yu
The College of Optics & Photonics,
University of Central Florida,
Orlando, FL 32816-8035
e-mail: yux@creol.ucf.edu

Anming Hu
Department of Mechanical, Aerospace and Biomedical Engineering,
University of Tennessee-Knoxville,
Knoxville, TN 37996
e-mail: ahu3@utk.edu

Sinisa Vukelic
Department of Mechanical Engineering,
Columbia University,
New York, NY 10027
e-mail: sv2147@columbia.edu

Martin B. G. Jun
School of Mechanical Engineering,
Purdue University,
West Lafayette, IN 47907
e-mail: mbgjun@purdue.edu

Hang-Eun Joe
School of Mechanical Engineering,
Purdue University,
West Lafayette, IN 47907
e-mail: hjoe@purdue.edu

Y. Lawrence Yao
Department of Mechanical Engineering,
Columbia University,
New York, NY 10027
e-mail: yly1@columbia.edu

Yung C. Shin
School of Mechanical Engineering,
Purdue University,
West Lafayette, IN 47907
e-mail: shin@purdue.edu

Ultrafast Laser Applications in Manufacturing Processes: A State-of-the-Art Review

With the invention of chirped pulse amplification for lasers in the mid-1980s, high power ultrafast lasers entered into the world as a disruptive tool, with potential impact on a broad range of application areas. Since then, ultrafast lasers have revolutionized laser–matter interaction and unleashed their potential applications in manufacturing processes. With unprecedented short pulse duration and high laser intensity, focused optical energy can be delivered to precisely define material locations on a time scale much faster than thermal diffusion to the surrounding area. This unique characteristic has fundamentally changed the way laser interacts with matter and enabled numerous manufacturing innovations over the past few decades. In this paper, an overview of ultrafast laser technology with an emphasis on femtosecond laser is provided first, including its development, type, working principle, and characteristics. Then, ultrafast laser applications in manufacturing processes are reviewed, with a focus on micro/nanomachining, surface structuring, thin film scribing, machining in bulk of materials, additive manufacturing, bio manufacturing, super high resolution machining, and numerical simulation. Both fundamental studies and process development are covered in this review. Insights gained on ultrafast laser interaction with matter through both theoretical and numerical researches are summarized. Manufacturing process innovations targeting various application areas are described. Industrial applications of ultrafast laser-based manufacturing processes are illustrated. Finally, future research directions in ultrafast laser-based manufacturing processes are discussed. [DOI: 10.1115/1.4045969]

1 Introduction

Ultrafast lasers, or more precisely known as ultrashort pulse lasers, utilize mode locking to produce pulses with femtosecond (fs) or picosecond (ps) durations [1]. Because this paper concerns ultrafast laser applications in manufacturing processes that involve strong laser–matter interaction with typical electron–phonon coupling on a timescale of picoseconds [2], femtosecond lasers will be emphasized in this review. An fs laser when used in manufacturing modifies or ablates materials with high-intensity ultrashort pulses of <1 ps duration to create high precision features at the micro and nanoscales in a highly localized and controlled manner. Although nanosecond (ns) and ps lasers have been widely used in the field of laser micromachining, fs lasers offer superior quality in micromachining and are often indispensable in nanomanufacturing. With rapid development in fs laser technology, especially the maturity of economical and reliable fs fiber lasers,

Manuscript received May 16, 2019; final manuscript received November 26, 2019; published online January 14, 2020. Editor: Y. Lawrence Yao.

more fs lasers will be used in the future. Hence, this paper aims to review the progress made in the past mainly in fs laser-based manufacturing processes and point out emerging application areas and directions for potential future research. Because of the vast literature devoted in this field in the past few decades, this review attempts to provide an insightful overview of representative work in each topic area without losing the broadness in scope. In addition, due to the huge variety of manufacturing processes involving fs lasers, this review will mainly focus on fs laser-based subtractive and additive processes.

2 A Brief History of Ultrafast Laser Development

The pursuit of ultrashort pulse durations traces back to the 1960s, soon after the first demonstration of a ruby laser by Theodore Maiman [3]. Pioneering mode locking research of solid-state and organic dye lasers was reported in the 1960s and 1970s, including both experimental investigations [4,5] and theoretical studies [6]. A turning point in ultrafast laser development came with the report of a sub 100 fs self-mode-locked Ti:sapphire laser by Spence et al. [7], while demonstrating the advantage of solid-state lasers over organic dye lasers in practicality and efficiency [8]. Subsequent rapid advances in the 1990s witnessed a continuous drop of pulse duration to as short as below 10 fs [9]. While ultrashort pulses directly from a laser oscillator with nanojoule energy at megahertz repetition rates may be more applicable for information processing and communications, highly energetic pulses are required for heavy duty micro/nanomaterials processing in manufacturing.

In 1985, a revolutionary development was made by Strickland and Mourou with the invention of chirped pulse amplification (CPA) to create ultrashort, ultrahigh intensity laser pulses [10], for which they were awarded a Nobel Prize in Physics in 2018. The CPA approach first stretches the mode-locked low power ultrashort pulses in time by a factor of $\sim 10^4$ from its original duration using gratings. Then, these long pulses with much lower peak power are safely amplified by several orders of magnitude while avoiding damage to the gain medium through nonlinear processes. Finally, these amplified pulses are recompressed in time to their original pulse duration, achieving orders of magnitude higher peak power than an ultrafast laser can generate. Without question, CPA removed a tremendous roadblock in the quest for high power ultrafast lasers by enabling the efficient amplification of ultrafast pulses to high energy within a compact package and thus opened a new era in ultrafast laser development. Now, CPA lasers are widely used in the world for both scientific research and industrial applications, with average power exceeding 100 W [11], peak power reaching terawatt levels [12], pulse duration dropping below 10 fs [13], repetition rate reaching megahertz [11], and wavelength covering extreme ultraviolet (XUV) to mid-infrared (MIR) [14,15].

As another class and an important addition to the portfolio of ultrafast laser source, ultrafast fiber lasers started to attract attention in the 1980s with the development of fiber lasers and fiber amplifiers [16]. Early interest in ultrafast fiber lasers was driven by the demand for shorter pulses in communications. For industrial applications such as materials processing, high average power fs fiber lasers were developed utilizing CPA and large-mode-area hollow-core photonic fiber technology [17]. Femtosecond fiber lasers generally use Yb-, Er-, or Tm-doped gain media and emit in the near-infrared (NIR) regime. A range of commercial femtosecond fiber lasers are now available which can operate at <100 fs pulse duration, megahertz repetition rate, gigawatts peak power, and kilowatt level average power. The potentially high throughput and low cost of ownership make femtosecond fiber lasers attractive in industrial applications.

3 Ultrafast Laser Machining Characteristics

3.1 Ultrafast Laser–Matter Interaction. Ultrafast lasers possess three key distinctive properties compared to lasers with longer pulse durations: ultrashort pulse duration, ultrahigh intensity, and large spectral bandwidth. The first two properties in particular give rise to some unique physical phenomena enabled via ultrafast laser–matter interaction in manufacturing applications. Because of their <1 ps pulse duration, ultrashort pulses in principle do not allow heat to diffuse into the surrounding area and thus prevent large thermal damage. Figure 1 illustrates the drastic differences between long pulse and ultrashort pulse laser micromachining [18]. For long pulses (e.g., >1 ns), the material has time to be heated up and melt at the focal volume and to diffuse into the surrounding material. A portion of the molten material is vaporized and ejected as high-velocity microdroplets while the rest of the melt re-solidifies, resulting in poor machining quality that is characterized by a heat-affected zone (HAZ), recast, dross, and microcracks. In contrast, for ultrashort pulses (e.g., <1 ps), the thermal diffusion length is generally much smaller than the laser penetration length. Hence, ultrashort pulses induce rapid ionization and directly turn the material at the irradiated volume into a mixture of plasma, vapor, and nanodroplets with subsequent ejection. Negligible melting and heat diffusion into the surrounding lead to a highly clean and precise machining quality that is free of the defects associated with longer pulse durations.

Some new phenomena in ultrashort pulse–matter interaction with dielectrics stem from the ultrahigh intensity that a focused pulse can reach (>10^{18} W/cm^2, the relativistic regime). As laser intensity is above a threshold value, a normally transparent material begins to absorb laser radiation through multiphoton absorption, which is responsible for generating some initial seed electrons from a dielectric or semiconductor material for the subsequent avalanche ionization, plasma formation, and material breakdown. Since multiphoton absorption is a nonlinear process that does not rely on seed electrons provided by defects or contaminants, the breakdown threshold for a material is definite and can be accurately determined. This deterministic nature of ultrafast laser–matter interaction lends itself to numerous new applications in manufacturing processes. For example, nanoscale features are made possible without a nanoscale focal spot size. This diffraction limit defying performance can be achieved by controlling the Gaussian intensity profile in such a way that only a small portion of the beam in the middle of the spot reaches the threshold intensity, effectively reducing the useful portion of the beam to below the wavelength value and thus submicron/nanoscale features can be created on the target sample. Another fascinating phenomenon owing to this nonlinear laser–matter interaction is the ability to access inside a material. This is usually done by tightly focusing a laser beam into a material

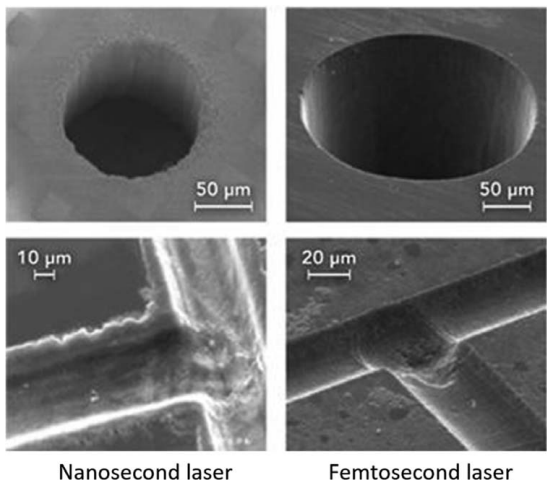

Fig. 1 Illustration of laser–matter interaction with long pulse (left) and ultrashort pulse (right) [18] (reprinted with permission from IntechOpen)

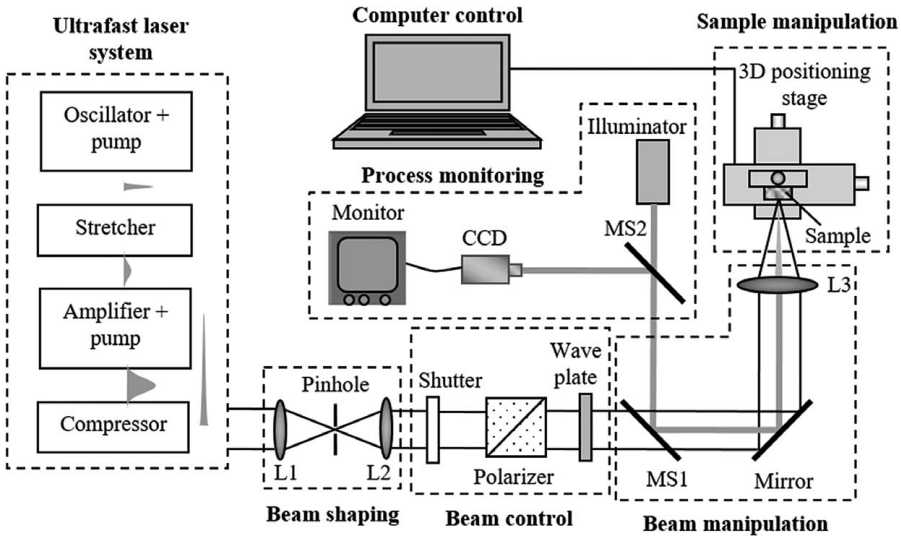

Fig. 2 A typical setup of the femtosecond laser machining system showing various functional modules

with a high numerical aperture (NA) objective lens so that only the focal volume inside the material reaches the damage threshold.

3.2 Typical Experimental Setup for Ultrafast Laser Machining. Figure 2 shows a typical ultrafast laser machining setup, which consists of the following main modules: ultrafast fs laser system, beam shaping, beam control, beam delivery and focusing, process monitoring, motorized 3D positioning stage, and computer control. Most of the current ultrafast fs lasers use Ti:sapphire as a gain medium because of its broad bandwidth. Low energy (~nJ) and high repetition rate (~100 MHz) ultrashort pulses are first generated in a mode-locked oscillator pumped by a solid-state laser. These pulses are then amplified through the technique known as chirped pulse amplification to microjoule and millijoule level for machining applications. Typical commercially available systems can produce pulses with tens of fs duration at about 800 nm wavelength and up to 10 kHz repetition rate. The average output powers can reach several watts. This power output does not allow a large amount of material removal and hence fs laser is most suitable for micro and nanomachining applications.

If the ultrashort pulses from the fs laser have fluctuations superimposed on a Gaussian intensity profile, a spatial filter as shown in Fig. 2 can be used to improve the beam quality by suppressing the noise and smoothing the beam profile. Also, wavefront correction techniques have been used to achieve high peak intensities at the focal spot [19]. In the beam control module, a high speed shutter is used to control the number of pulses. Pulse energy is adjusted with the combination of a polarizer and a half waveplate. Additional optics can be used to control the polarization state of the laser beam. In micromachining, fast laser scanning is often needed, which can be achieved in the beam manipulation module. Commercial laser beam scanning heads are available for this purpose. Figure 2 only illustrates simple beam delivery and focusing optics. The control of sample movement is done by the 3D positioning stage. Quality control is realized through the in-process monitoring module. One approach is through the use of a separate illumination source and CCD camera as shown in the figure. Another common practice is to use the reflected light from the ablation area to observe the processing site on the sample. Finally, the fs machining system is controlled by a computer with necessary application software for controlling various devices. There are several parameters to be controlled for fs laser machining: pulse energy, pulse duration, repetition rate, focal spot size, and polarization. In addition, sample movement and beam scanning need to be controlled based on the machining requirements.

4 Applications of Ultrafast Laser in Manufacturing Processes

4.1 Micro/Nanomachining. Ultrafast lasers are promising tools for ultrahigh precision machining due to the ultrafast laser absorption, heat transfer, material removal, and thus minimized HAZ formation. It is usually considered as a "cold" ablation process. It was demonstrated that femtosecond laser machining is much cleaner and smoother with sharp edges compared with machining by nanosecond laser pulses [20]. The ultrahigh laser intensity also enables it to process a rich diversity of materials, including brittle transparent materials by nonlinear absorption.

4.1.1 Micromachining. (a) Laser ablation: Laser micro/nanomachining is accomplished by laser ablation, which refers to the material removal process resulting from laser irradiation. Despite the property difference between different materials, it was shown that different materials behave similarly under the irradiation by femtosecond pulses at fluences below the threshold for plasma formation [21], implying that some very general mechanisms are responsible for the material removal process. It has been widely accepted that the possible ablation mechanisms include spallation [22,23], phase explosion [22–24], critical point phase separation [25], and fragmentation [22,26]. Spallation is caused by laser-induced tensile stress, which can cause the formation of voids and defects when its amplitude exceeds the matter bonding and trigger the consequent decomposition. Phase explosion, also known as explosive boiling, refers to the explosive decomposition of metastable material into a mixture of vapor and liquid when the material is superheated to temperatures close to the critical temperature. For critical point phase separation, the material is also rapidly heated to a temperature above critical point. During the fast expansion, the material is pushed into the metastable region by crossing the critical point, leading to a phase separation into an ablated vapor phase and an unablated solid/liquid phase. Fragmentation is the removal of small fragments due to laser-induced thermo-elastic stress and resultant nonuniform strain rates inside the material. The occurrence of these mechanisms depends on the incident laser parameters and target material properties. Generally, from low to high laser fluence, the dominating mechanism switches from spallation, to critical point phase separation, and to fragmentation. In addition, there is non-thermal ablation, such as Coulomb explosion induced by strong electric field near the surface [27–30]. It should be pointed out that although the ablation mechanisms discussed above occur and dominate in different fluence ranges, in many cases, two or more will take place simultaneously. In addition, processing environment also affects laser ablation mechanisms.

For example, Kudryashov et al. recently reported the damping of vapor/plume expansion in fs laser ablation of gold surface in isopropyl alcohol due to liquid confinement [31]. Cao et al. demonstrated that enhanced chemical reaction and electronic conductivity were responsible for the change of surface morphology when comparing fs laser ablation of silica in air and etching solutions [32].

(b) Effect of processing parameters: Ablation depth (per pulse) is defined as the depth of the crater ablated by one laser pulse, which is an important quantity to measure the efficiency of laser machining. It can be affected by various laser parameters, target material properties, and ambient environment.

Pulse duration: It was found that with the same laser fluence, the ablation depth decreases with pulse duration [33,34]. However, when the pulse duration is lower than 1 ps, the ablation depth does not change any more. This is because in this range, the pulse duration is lower than the electron–phonon relaxation time, and the thermal exchange is negligible during the laser irradiation [33,35–37].

Laser fluence: Laser fluence is another key factor to determine the ablation depth. It was observed in Ref. [35] that two ablation regimes exist during ultrafast laser ablation of copper, and the ablation depth (L) depends logarithmically on laser fluence in each regime:

$$L = \delta \ln\left(\frac{I}{I_{th}^{M}}\right) \quad \text{(low fluence)} \tag{1}$$

$$L = l \ln\left(\frac{I}{I_{th}^{H}}\right) \quad \text{(high fluence)} \tag{2}$$

where δ is the optical penetration depth, l is the electronic heat penetration depth, I is the laser fluence, I_{th}^{M} and I_{th}^{H} are the ablation thresholds for each regime. The existence of the two regimes is mainly due to the switch of the dominating energy transfer mechanism from optical penetration to heat diffusion. The phenomena were found to be universal for many other materials [38,39]. A third regime at even higher fluence was reported for some materials due to the collisionless absorption in vacuum and the early plasma absorption in air [36,40].

Laser-induced plasma: During laser ablation, the ablated materials can be partially or fully ionized, forming laser-induced plasma. Different from longer pulse ablations, this plasma (generated after hundreds of ps [41,42]) does not have any interaction with the incident pulse due to the ultrashort pulse duration. Therefore, the plasma shield effect is usually ignored for ultrafast laser machining. However, due to its extremely high laser intensity, an ultrafast laser pulse can create plasma in the ambient fluid by both direct photoionization and ionization by ejected electrons from the target surface. This plasma is called "early plasma" since it can be formed within tens of femtoseconds [43–45] and further absorb the incident laser energy. At high laser fluence, the early plasma can absorb up to 20% of the incident laser energy and thus reduce the ablation depth [43,44].

Multi-pulse ablation: Laser irradiation by multiple pulses is needed for many laser machining tasks. It has been shown that compared with the single-pulse ablation, the threshold fluence by multi-pulse ablation can be reduced, and the average ablation depth per unit incident fluence will be increased [46,47]. This phenomenon in general is called the incubation effect and could be caused by thermal accumulation [48], and enhanced absorption by pre-pulse surface modification [49], formation of micro- and nanostructures [47], and laser-induced defect formation [50].

When the time interval between pulses is reduced to extremely short (fs–ns), new mechanisms will come into play, and completely different ablation behavior will happen. It has been revealed that the ablation depth of metals will be suppressed by double-pulse ablation with ultrashort pulse intervals [51,52], possibly due to the formation of a second shock wave [53], the drop of electronic heat conductivity at high temperature [54,55], and the plasma shielding effect [52]. Different from metals, ablation of silicon will be enhanced by the same technique due to electron excitation by the first pulse to enhance the absorption of the second one [33,35–37,54,56–58].

(c) Processing techniques: Several processing techniques have been proposed to improve the micromachining efficiency and quality. Figure 3 shows the typical drilling strategies [59]. Single-pulse drilling is fast, but the achievable drilling depth is very limited. Percussion drilling uses laser pulses which move sequentially along the drilling direction, and deeper holes can be drilled. Trepanning combines percussion drilling with the circular movement of the laser beam relative to the target. Helical drilling is very similar to trepanning drilling, and the only difference is that the laser beam moves helically. The advantage of helical drilling over trepanning is that the machining position can always be maintained at the laser focal spot, and thus helical drilling suits better for deeper holes. These strategies can be easily modified to be suitable for other machining processes like scribing and cutting.

(d) Micromachining of various materials: Ultrafast lasers have been used for micromachining of various materials, such as metals [60–63], semiconductors [64–67], glass [68], organic materials [69], and composite materials [70], as shown in Figs. 4 and 5. It has the capability for deep-hole drilling, cutting, surface scribing, microstructuring, trimming, etc. Regardless of the material, machining quality and precision are very high with sharp edges and no cracks or debris. Ultrafast laser micromachining can be used in various applications, such as fuel injector nozzle drilling, stent

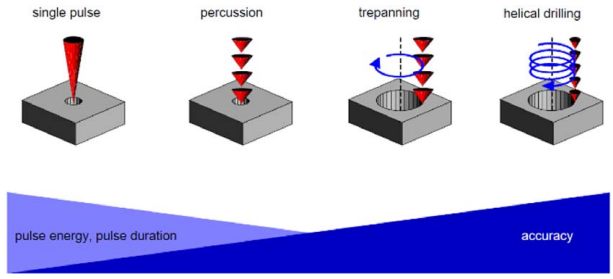

Fig. 3 Process strategies with increasing accuracy and decreasing pulse energy/duration, from left to right [59] (reprinted with permission from LIA)

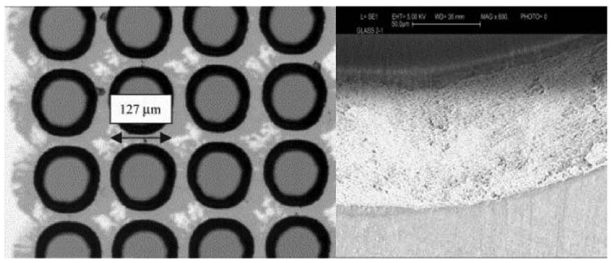

Fig. 4 Microholes drilled in doped glass (left) and the enlarged view (right) [68] (reprinted with permission from Elsevier)

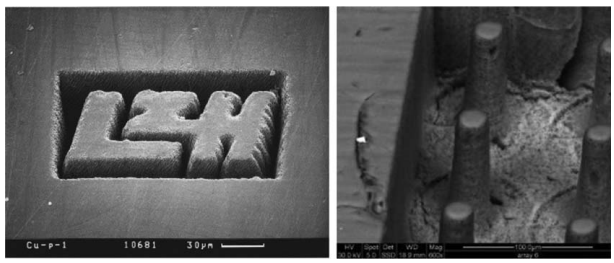

Fig. 5 Micromachining of copper (left) [35] and bovine cortical bone (right) [69] (reprinted with permission from SPIE)

fabrication, micro-device manufacturing, etc. In Ref. [71], it demonstrates that femtosecond laser possesses advantages for fuel injector nozzle drilling in edge sharpness, HAZ, and resolution compared with water-jet guided μs-laser and micro-EDM (electrical discharge machining).

The effects of processing conditions on machining quality and efficiency have been extensively studied for metals and semiconductors. It was found that by using shorter duration pulses, laser-induced thermal effects and HAZ will be suppressed. When the pulse duration is shorter than the electron–phonon relaxation time, clean ablation with minimized HAZ will be achieved [72]. However, with very short pulses, the laser fluence should be kept relatively low to avoid nonlinear beam profile distortion [73,74]. This issue can also be overcome by adopting vacuum environment leading to the absence of laser–air interaction [60–62]. With a too high laser fluence, although machining efficiency is high due to the high ablation depth, HAZ will also be increased which lowers the machining quality, losing the benefit of ultrafast laser machining. Therefore, a low laser fluence (slightly higher than the threshold) with a high repetition rate is a preferred combination for many cases [75,76]. Laser polarization was revealed to be important to control the drilling quality. Circular polarization is needed to drill a through-hole with a round exit [64,65].

Ultrafast lasers were also found capable of fabricating high aspect ratio and high quality microchannels in transparent materials which is difficult, if not impossible, using traditional machining techniques, due to the brittle structure and low thermal conductivity of the material. The first developed method was the laser-assisted chemical etching. The target was irradiated by femtosecond laser pulses, followed by heat treatment and dilute aqueous hydrofluoric solution etching [77,78]. The same technique without heat treatment was used to create microchannels with a high aspect ratio (50:1) [79–82]. The disadvantage of this technique is the requirement of a time consuming post-processing by toxic chemicals. An alternative microchannel fabrication method is direct laser drilling, which is fast with no post-processing [83–85]. It was found that drilling from the rear surface generates deeper holes than in the front surface, as the plasma formed by drilling from the rear surface is much weaker [85]. Distilled water and other liquids were reported to be helpful to raise the aspect ratio by reducing the redeposition of ablated materials [84,86]. Ultrasonic agitation [84] and post-annealing [87] were also found effective in improving the drilling process in terms of aspect ratio. A comparison of the air and vacuum drilling processes found that vacuum drilling increased the aspect ratio to over 100:1 in Ref. [88].

4.1.2 Nanomachining. Ultrafast laser ablation shows great advantages in minimizing the HAZ formation and has demonstrated superior capability in high precision micromachining. In principle, it possesses the potential for even higher resolution machining—nanomachining. In fact, the barrier for its application in nanomachining is not the HAZ but the diffraction limit of the laser spot size. In general, the focused laser spot size is limited by its wavelength, which cannot satisfy the requirement of nanomachining. To overcome this limitation, several methods have been successfully developed.

One method to achieve the ultrahigh fabrication resolution beyond the diffraction limit is to accurately control the peak laser intensity slightly higher than the processing threshold. Ultrafast laser ablation has deterministic thresholds for different materials, meaning that the material can be processed only when the laser intensity is higher than a certain threshold value. Therefore, using a Gaussian beam, higher fabrication resolution can be obtained by a low laser intensity where only the central part of the laser beam exceeds the threshold to induce ablation (Fig. 6). By using this method with femtosecond lasers from IR [89], visible [90], to ultraviolet (UV) [91] and extreme UV [92], sub-diffraction limit nanofeatures were successfully fabricated in different materials. With this method, nanomachining can be achieved with simple setup and simple objective lenses. This method was improved using a double-pulse setup (one IR pulse and one UV pulse with controlled interval), which can reduce the ablation threshold of fused silica by 90% [93,94] (Fig. 7). In Ref. [95], by adopting temporal airy pulses, high aspect ratio (30:1) nanochannels with diameters of hundreds of nanometers were fabricated. In principle, taking advantage of the threshold effect has no limit in the machining resolution, and features as small as 15 nm have been fabricated [90]. However, to achieve higher resolution, higher laser intensity control accuracy is required, which demands extremely stable laser energy output from the laser machines. In addition, the pulse-to-pulse energy fluctuation significantly limits the repeatability of this process with high resolution. Therefore, the reproducible fabrication resolution is usually limited to over 100 nm [92].

To achieve ultrahigh resolution far beyond the diffraction limit, another direction is to overcome the diffraction limit by novel beam focusing techniques. By applying femtosecond laser beams in optical near fields, such as scanning probe microscopy [96], near-field scanning optical microscopy [97], plasmonic nanolithography [98–100], microlens array nanolithography [101,102], and interference lithography [98,103], nano-features of tens of nanometers were successfully fabricated on various material surfaces including metals, semiconductors, and dielectrics.

As discussed in Sec. 4.1, ultrafast laser irradiation can create self-organized periodic nanostructures on surfaces. It is attributed to the periodic laser energy spatial modulation during laser irradiation. It was observed that by carefully controlling the laser intensity to be slightly higher than the ablation threshold, periodic nano-grooves can be created on a surface by single-pulse irradiation [104–107]. Furthermore, by adjusting the laser intensity, it is possible to control the number of nano-grooves, and only one nano-groove with a width of tens of nanometers can be fabricated with low laser intensity [106], as shown in Fig. 8.

4.2 Surface Structuring

4.2.1 Micro/Nanosurface Structures Produced by Femtosecond Lasers. Femtosecond laser has the ability to create either

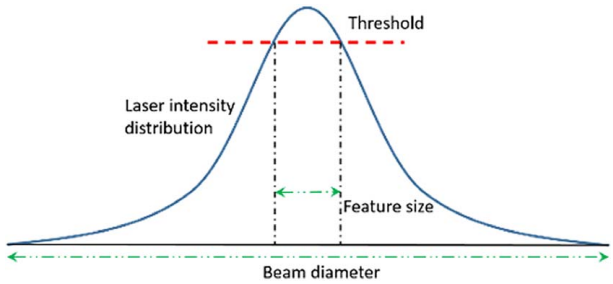

Fig. 6 Schematic of nanoablation by Gaussian beams

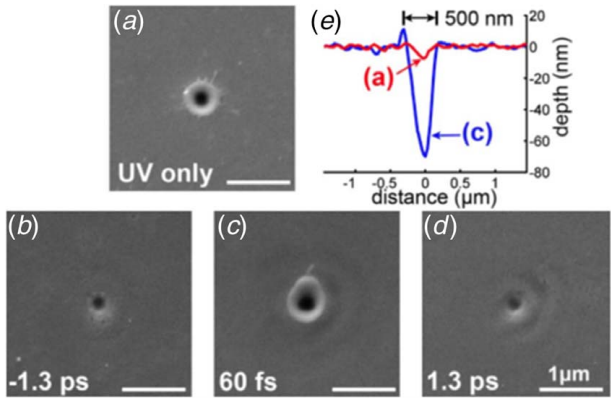

Fig. 7 Nanoholes ablated by (*a*) UV and (*b*)–(*d*) UV-IR pulse train with different delays [94] (reprinted with permission from OSA)

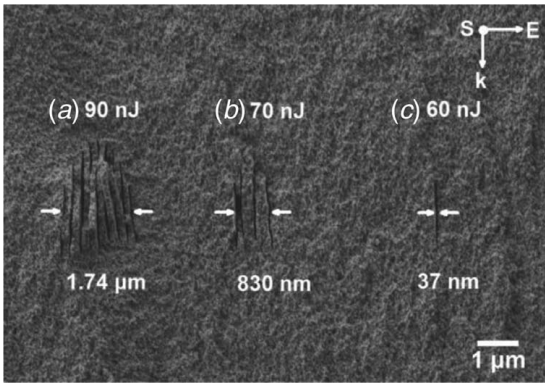

Fig. 8 Evolution from nanovoid array to single nanovoid with decreasing laser intensity [106] (reprinted with permission from OSA)

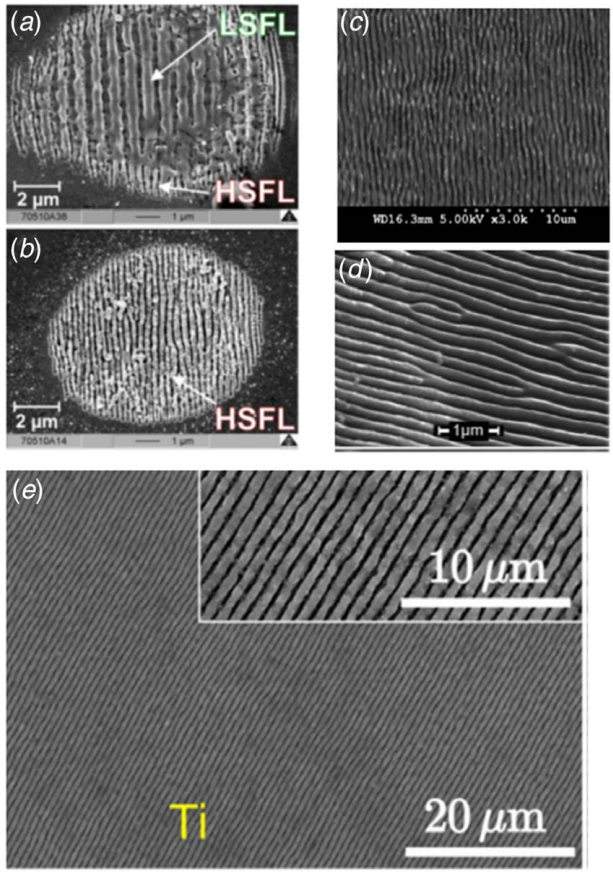

Fig. 9 LIPSS produced using fs laser: (*a*) and (*b*) LSFL and HSFL on ZnO [121] (reprinted with permission from AIP Publishing), (*c*) LSFL on silicon, (*d*) HSFL on diamond [122] (reprinted with permission from APS), and (e) highly regular LSFL on titanium [123] (reprinted with permission from Springer Nature)

ordered or random surface structures at both micro and nanoscales. The most commonly observed structure is the laser-induced periodic surface structure (LIPSS), also known as surface ripples. Although femtosecond lasers are routinely used to create LIPSS these days, this phenomenon was discovered more than 50 years ago by Birnbaum [108] with a ruby laser. Subsequent studies in the early days found similar periodic structures using various types of lasers [109–111]. With the emergence of high power fs lasers in the 1980s, surface structuring has shifted to the use of fs lasers and attracted worldwide attention. Today it remains an active research area with numerous new developments being reported over the past ten years, which will be the main focus of this part of the review. Among the many different structures produced using fs lasers, LIPSS are clearly the most widely studied one. LIPSS seems to be a universal phenomenon for a variety of materials including metals [112–115], semiconductors [116–118], polymers [119], and dielectrics [120]. There are two types of LIPSS being reported so far: low spatial frequency LIPSS (LSFL) and high spatial frequency LIPSS (HSFL). Figure 9 shows some examples of LIPSS structures found for different materials. The LIPSS structures are generally oriented perpendicular to the laser beam polarization direction for metals and semiconductors, and for dielectrics, the orientation can be both perpendicular and parallel [121,124]. By changing the laser beam to elliptical polarization, the ripples can be rotated; for circularly polarized beam, uniformly distributed bumps can be produced. The dependence of LIPSS orientation can also be changed with a double-beam irradiation scheme. With precisely controlled pulse delay of <1 fs resolution, i.e., by controlling the phase difference of the two incident pulses, the LIPSS formed on silicon was rotated by 90 deg [125]. In another study using double-beam irradiation, it was found that the polarization of the first pulse decides the LIPSS orientation for fused silica while for silicon the stronger pulse controls the orientation [120].

Under single-beam irradiation conditions, the spatial period of LSFL is close to the laser wavelength, but it can be smaller or larger depending on laser wavelength, incident angle, laser fluence, and material type [113,120,126]. Ambient air pressure was also found to affect the LSFL period in a study by Nivas et al., in which the ripple period on silicon decreases with increasing air pressure [127]. Using a double-pulse irradiation of nearly equal energy, Höhm et al. showed that time delay can reduce the LSFL period on silicon from 790 to 550 nm while the period remains nearly constant at about 760 nm for the same delay range [120]. Another study with two-color fs pulses (800/400 nm) showed that for titanium, the LSFL orientation and spatial period are determined by the second pulse [128]. Unlike LSFLs that occur for all major material types, HSFLs appear to be a phenomenon for dielectrics and semiconductors only. HSFLs have spatial periods much smaller than incidence laser wavelengths and are usually produced using ultrafast lasers below a material's ablation threshold [122]. They are often very sensitive to the number of laser shots and laser fluence [121,129]. A recent study by Beltaos et al. showed that with proper irradiation condition, sub-100 nm HSFL on multilayer graphene can be produced using a typical fs laser of 840 nm wavelength [130].

Various theoretical and numerical studies have been reported to explain the experimental observations of LIPSS formation, especially for LSFLs [108,109,123,126,131–134]. The most widely accepted one was developed by Sipe et al. [131], and it shows that inhomogeneous energy absorption as a result of the interference between the incident beam and the surface scattered electromagnetic wave field due to surface roughness is responsible for the formation of LIPSS structures. Later, Bonse et al. combined the Sipe model and the Drude model in their study and attributed the formation of LSFL to the interference of the defect-initiated surface plasma polaritons with the incident laser beam [126]. A further advancement was made by He et al. by extending the Sipe model to include excited states for materials like silicon [134]. Their simulation successfully revealed in real spatial coordinate ripple bending and bifurcation, two rarely investigated characteristics of LIPSS. A notable contribution was made recently by Gnilitskyi et al. [123] with the creation of long, highly uniform LIPSS (Fig. 9(*e*)) and the discovery of its origin. They found that the LIPSS regularity is governed by the decay length of the excited surface electromagnetic waves; and the shorter the decay length is, the more uniform the LIPSS is. Despite the successful theoretical development for LSFLs, the existing theories for LSFLs cannot explain the formation of HSFLs [124]. Based on some studies on HSFL using 800 nm fs lasers, it seems that the second harmonic at 400 nm

plays an essential role in forming HSFLs [121,129,135]. More work is definitely needed in this area.

Another widely known fs laser-induced ordered surface structure is micro cones/spikes. Figure 10 shows the spikes formed on silicon in the environment of SF_6 (Fig. 10(*a*)) and in water (Fig. 10(*b*)) and the conical structures on titanium (Fig. 10(*c*)) and steel (Fig. 10(*d*)). According to Carey et al., the spikes on silicon are formed after tens or hundreds of laser shots at about 100 fs pulse duration and medium fluence levels (e.g., 1–3 J/cm^2) [136]. The role of the first few laser pulses is to induce melting, vaporization, and/or chemical reaction at some selected sites based on the initial surface morphology, resulting in micro craters/ripples scattered over the surface. When the subsequent laser pulses strike this roughened surface, the incident laser light bounces off the sides of the protrusions and cause preferentially more absorption in the valleys than on the tips of the protrusions. Therefore, more ablation takes place in the valleys and sharp conical microstructures form after certain number of shots. Generally speaking, the necessary conditions for micro spike/cone formation involves relatively high laser fluence and a large number of laser shots (e.g., hundreds), and normally LIPSS is created first after a small number of shots before the transition to conical structures [139,140]. Interestingly, as micro cones grow with laser irradiation, LIPSS and random nanostructures can be found on the conical surface [138,139].

Besides the above-mentioned regular and periodic microstructures, many different types of surface patterns and structures have been demonstrated through beam shaping and multiple beam strategies, as shown in Fig. 11 for some interesting examples. Using a two-color (800/400 nm) fs pulses with controlled delay, dot-like matrix structure is created on Mo plate (Fig. 11(*a*)) [141]. The new pattern is not formed by a simple overlap of two sets of LIPSSs by the two individual beams, but rather through interaction of surface dynamics induced by the two beams. Figure 11(*b*) shows a feature created on Ni film with a donut-shaped, cylindrical vector fs laser beam that is azimuthally polarized [142]. A similar surface pattern is produced on silicon by Nivas et al. [145] using an optical vortex beam. Skoulas et al. demonstrated that a controlled scan of this type of beam enables creation of complex biomimetic structures exhibiting a combination of micro and nanoscale features [142]. Periodic arrays of nanotriangles are generated on tungsten using two cross-polarized collinear fs laser beams (Fig. 11(*c*)) [143]. The formation of nanotriangles is attributed to the interaction of three sets of periodic nano-grooves triggered by the excitation of surface plasmons from the two time-delayed fs pulses. With a single shot of four interfering fs laser beams at each spot, bump arrays on a gold film are formed as shown in Fig. 11(*d*) [144]. The interesting thing is that with increasing laser fluence, a bead appears first on the bump, then followed by a hole to finish. Recently, Oliveira et al. reported fs laser surface patterning of carbon fiber-reinforced polymer using laser interferometry [146]. Selective removal of the epoxy resin in the composite material was achieved with controllable pattern period and amplitude.

Other beam shaping techniques for surface structuring include the use of blazed gratings and spatial light modulator (SLM). High quality and more uniform LSFLs on a few metallic materials are produced using spatiotemporally modified fs pulses with a grating pair [147]. Almeida et al. [148] used a liquid-crystal SLM at the Fourier plane of a folded 4f zero-dispersion compressor to transform a 40 fs pulse to a train of several fs sub-pulses with an adjustable sub-pulse separation. It was found that LIPSSs produced by this pulse train are more pronounced with the largest enhancement in ripple amplitude obtained at a sub-pulse separation of 128 fs. Computationally efficient and accurate holograms are generated to produce diffractive multiple beams for parallel processing using SLM. Aided with a galvo scanning system, large area microhole patterns and 3D chessboard like structures are created on Ti6Al4V [149].

4.2.2 Surface Property and Potential Applications. Femtosecond laser surface structuring not only alters a material's surface morphology but often imparts some new functionality and properties to the surface, notably optical, mechanical, and chemical properties. Femtosecond laser textured silicon covered with micro spikes, often known as black silicon, is among the early findings to demonstrate nearly 100% absorptance in the visible range, and the spectrum can be extended to 2.5 μm when processed in an ambient SF6 gas environment [150]. A more recent work by Parmar and Shin [151] found that fs laser creates globular micro/nanostructures in air and elongated columnar structure in water, and both structures produce black silicon with wideband antireflection effect. Later, a similar effect was achieved with a parallel microgroove pattern produced by fs laser [152]. The groove period is 100 μm and the width and depth are about 50 μm in size. The antireflection effect extends to the mid-IR wavelength range. Enhanced surface optical property is also demonstrated for metals through fs laser micro/nanostructuring. A 95% absorptance

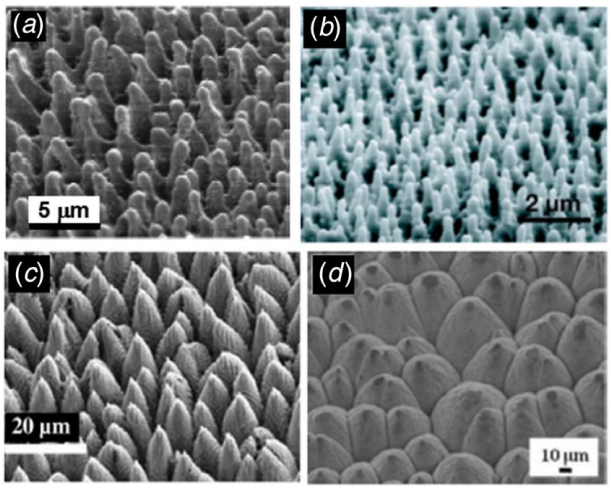

Fig. 10 Laser-induced micro cones/spikes on (*a*) silicon in SF_6 [136] (reprinted with permission from OSA), (*b*) silicon in water [137] (reprinted with permission from AIP Publishing), (c) titanium in air [138] (reprinted with permission from Springer Nature), and (*d*) stainless steel in air [139] (reprinted with permission from Elsevier)

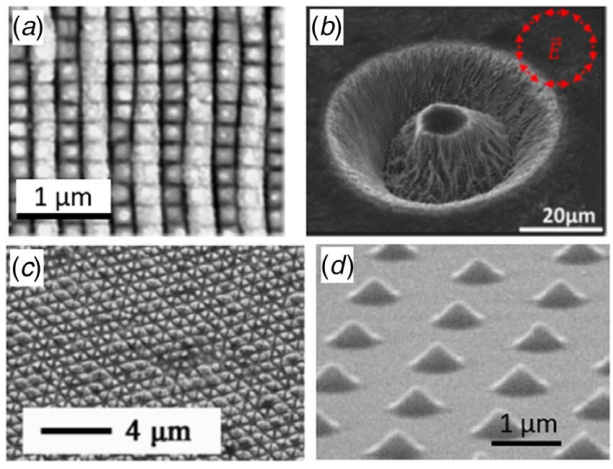

Fig. 11 Various surface structures induced by (*a*) two-color fs pulses [141] (reprinted with permission from OSA), (*b*) fs pulse of azimuthal polarization [142] (reprinted with permission from Springer Nature), (c) double fs pulses [143] (reprinted with permission from OSA), and (*d*) four interfering fs pulses [144] (reprinted with permission from The Japan Society of Applied Physics)

for black platinum (Fig. 12(*a*)) over the wavelength ranging from UV to near-IR is achieved with laser-induced micro/nanostructures on the surface [114]. Yang et al. [153] reported significant enhancement of thermal emission to about 100% for a NiTi alloy due to a microscale coral-like surface structure produced by an fs laser. Surface textured silicon and metals have a wide range of potential applications including solar cells, detectors, sensors, field emission devices, plasmonics, broadband thermal sources, radiative heat transfer devices, etc.

Another unique capability of fs laser is to modify and control material's wetting properties. Superwetting surfaces were created using fs laser for silicon and human enamel and dentin tissues by Vorobyev and Guo [154,155]. The structure consists of parallel microgrooves with a period of 100 μm with naturally formed micro/nanoscale morphology over the microgrooves. When water is dropped on the processed area, it spreads rapidly along the microgroove orientation and can even climb up the surface vertically. A similar microgroove micro/nano hierarchical structure created on platinum, titanium, and brass turned the surface superhydrophobic [156]. The wetting property of fs laser patterned surfaces is determined by the combined effect of surface morphology and surface chemistry. Skoulas et al. demonstrated the effect of surface morphology on wettability for a Ni film with different complex micro/nanostructures as shown in Fig. 12(*b*) which were created using a cylindrical vector fs laser beam [142]. Combining fs laser texturing and surface chemical treatment, the initial superhydrophilic metallic and dielectric surfaces after laser processing become superhydrophobic with contact angles exceeding 150 deg [157–159]. Materials with tailored wetting properties have potential applications in microfluidics, biomaterials, anti-icing, self-cleaning, etc. For example, Sarbada and Shin developed a fast and inexpensive method to create microfluidic devices with textured superhydrophobic inner channel walls for controllable fluid flow [160]. A textured superhydrophobic surface created on a copper mold was transferred to the inner surface of a polydimethylsiloxane (PDMS) microchannel that increased the fluid flow rate by 186%. While the above-mentioned studies concern surface wetting properties in air, a large body of work have been reported in the literature in recent years on fs laser-induced underwater superoleophobicity. In a comprehensive review article, Yong et al. presented various fs laser structured surfaces that display underwater superoloephobic behaviors based on the design principle of "in-air superhydrophilicity to underwater superoleophobicity" [161]. Potential industrial and military applications of superoloephobic surfaces were illustrated.

Femtosecond laser surface texturing for tribological applications has been an area of interest for almost 20 years. LIPSS has been generated and tested for friction and wear for various materials including metals, ceramics, and semiconductors. It has been shown that LIPSS can reduce friction under both regular sliding contact conditions [162] and harsh machining environment (i.e., chip-tool contact with high temperature, high pressure, and high speed) [163,164], which is especially true under lubricated conditions. Concerning wear, however, LIPSS created on titanium was found to be ineffective under reciprocal sliding tests and the authors concluded that the LIPSS amplitude should be larger than the contact deformation depth for a beneficial effect [165]. In contrast, fs laser textured cutting tools with microholes or microgrooves of tens or hundreds of microns in size have been shown to be effective in reducing friction and wear under both dry and lubricated conditions in machining applications [166,167]. This research area of textured tools has been active for about ten years, with a continuous flow of publications targeting new textured tool development and different machining operations [168,169].

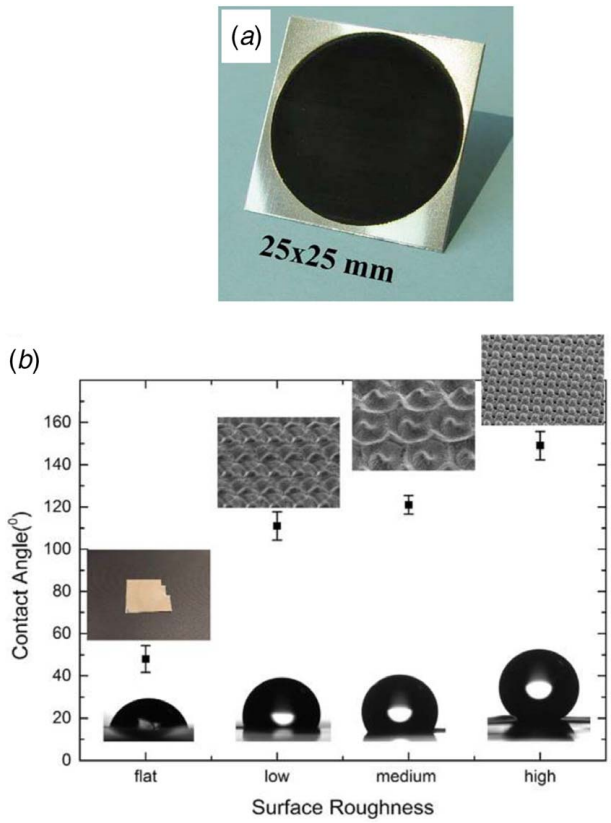

Fig. 12 Various fs laser functionalized surfaces: (*a*) black platinum [114] (reprinted with permission from AIP Publishing) and (*b*) wettability of Ni film with different structures [142] (reprinted with permission from Springer Nature)

4.3 Thin Film Machining. Femtosecond laser machining of thin film materials is driven by applications including thin film solar cells, MEMS, microelectronics, etc. In the production of a thin film solar device, a large solar panel is generally divided through laser scribing into narrow photovoltaic (PV) cells connected in series. Figure 13 shows a typical structure of a thin film solar cell. The typical thickness is up to a few hundred nanometers for the two contact films and a few hundred nanometers to a few microns for the middle PV film, depending on the solar cell type. Scribing is a key manufacturing process that consists of three steps (commonly known as the P1, P2, and P3 scribes as shown in Fig. 13), with different film deposition processes in between. The P1 scribe removes the first thin film (bottom contact) from the substrate and defines the individual cells. The P2 scribe removes the absorber film to form the series interconnects between cells. The P3 scribe removes the second contact film (top contact) only or together with the PV layer to isolate each cell. The three scribes plus the gaps in between form the dead area width, i.e., the area that does not contribute to power generation. From the standpoint of cell performance, the scribes should be narrow with straight walls so that the dead area is minimized. Scribing should have high depth resolution so that only the selected film is removed. The scribes should be clean and free from damage. Comparative studies for ns, ps, and fs laser scribing have shown that ns laser causes shunt between the top and bottom contact due to melting of the absorber film containing metallic elements

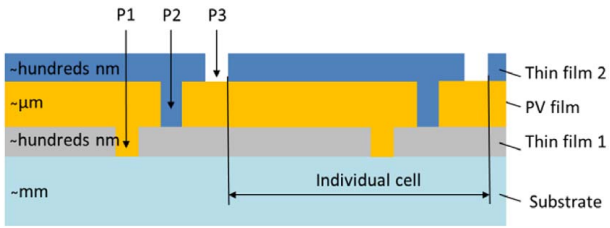

Fig. 13 Typical layered structure of thin film solar cell

[170]. In contrast, the benefits of fs and ps laser scribing are reduced thermal effects, less diffusion between layers, minimal cracking, and improved electrical performance [171]. However, sometimes a ps laser generates considerable melting in P3 scribing of a CIGS solar cell [172]. This problem can be mitigated through careful design of process parameters via experiments and 3D two-temperature modeling (TTM) of the scribing process, as shown in Fig. 14 by the high quality P2 and P3 scribing on a CIGS solar cell achieved by Zhao et al. [173,174].

An alternative process known as direct material lift-off was investigated for various solar cell structures [175–179]. In the lift-off process, absorption of laser irradiation occurs mainly at the interface, which causes rapid, localized heating and plasma formation so that the top layer is ejected. Although undesirable for direct film ablation, ns laser was able to achieve successful P2 scribing from glass side film lift-off for a CdTe-based solar cell [179]. Krause et al. demonstrated that all three scribing steps were successful for silicon-based thin film solar cells [178]. Markauskas et al. achieved lift-off for P2 and P3 scribing with both fs and ps lasers for CZTSe thin film cells [177]. In contrast, no lift-off was realized for a CIGS-based solar cell with both fs and ps laser at the wavelength of 1030 nm according to Gečys et al. [176], and the main reason is due to absorption throughout the thin film stack that lead to direct ablation. The dependence of the lift-off process on process conditions was demonstrated by Bayer et al. [175] in their study of perovskite film scribing. Three material removal mechanisms were identified as ablation only, lift-off, and ablation plus lift-off, as shown in Fig. 15. Depending on laser parameters and the irradiation method (e.g., film side or through glass), a specific mechanism may dominate the scribing process. An interesting technique named "rail-roading" patterning was presented by Jeoung et al. [180], in which two beams were focused on the surface with adjustable distance between the focal spots. When applied to scribing of a CIGS solar cell, it was found that the material removal displays features of both ablation and lift-off.

The desire for narrow scribes led to studies with tight focusing using microscope objective lenses. Clean, few micron P1 scribes were obtained for Mo on glass and indium tin oxide (ITO) on glass [181–183]. Extension to P2 is challenging because of the much thicker absorber layer. To overcome the short depth of focus intrinsic to tight focusing without sacrificing for small spot size, Bessel beams were used for P1 and P3 scribing of Mo on photo-initiator (PI) and ITO on glass [184,185]. The long central core of the zero-order Bessel beam is the useful part while the outside rings are undesirable because they may be strong enough to cause damage. To offset the detrimental ring effect of a Bessel beam, Yu et al. successfully constructed superposed Bessel beams using SLM to suppress ring damage observed with the zero-order Bessel beam [186]. One roadblock for industrial adoption of fs laser scribing is its low speed. Efforts have been made using fs lasers with a high repetition rate to reach scribing speeds on the order of m/s [187,188]. It was shown for a copper indium gallium diselenide (CIGS)-based solar cell that all P1, P2, and P3 can be done at the speed of 2 m/s using one laser source but different laser fluence [188].

Most other research conducted on fs laser thin film machining has targeted various applications including MEMS [189], microelectronics [190], photonics [191], biosensors [192], electrochromic films [193], etc. Hundred to two hundred nanometer sized grooves and craters were created through direct ablation on metallic thin films without the use of high NA microscope objective lenses [194,195]. The key is to have a highly stable laser beam and carefully controlled peak fluence to just a few percentage above the damage threshold, and a MHz level repetition rate seems to be beneficial for nanoscale machining. The effect of property mismatch at the interface for a Cr on glass substrate was brought out by Kim and Na [196], in which the glass serves as a thermal barrier for heat diffusion and induces a greater hydrodynamic (HD) flow and recoil pressure in the 500 nm thick film than the 200 nm film, resulting in different surface morphology. Besides the common method of single-beam direct ablation, laser-induced forward transfer was used to pattern a quartz substrate from a gold film donor plate [197]. Laser fluence had to be precisely controlled just above the threshold to enable efficient film transfer. Micromachining using a mask pattern was studied by Nakata et al. [198]. Microscale features in the form of lines and numbers were generated on a gold film with a single-shot exposure that has potential for fast and large area patterning.

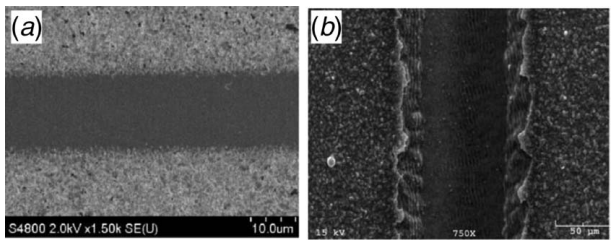

Fig. 14 SEM images of P2 and P3 scribing on CIGS [173,174] (reprinted with permission from Springer Nature): (*a*) P2: overlap ratio of 81% and laser fluence of 3 J/cm^2 for ablation depth of 1.75 μm, (*b*) P3: laser fluence of 4.5 J/cm^2 and overlap ratio of 87% for ablation depth of 1.95 μm

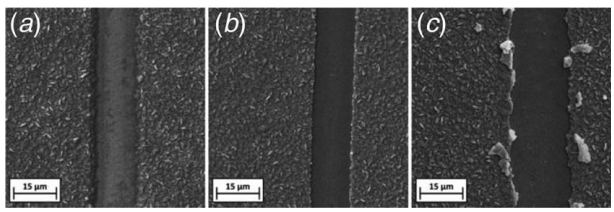

Fig. 15 SEM images of perovskite film scribing [175] (reprinted with permission from Springer Nature): (*a*) ablation, (*b*) ablation plus lift-off, and (*c*) lift-off. The scale bar is 15 μm.

4.4 Machining in Bulk of Materials

4.4.1 Machining Inside Transparent Materials. Ultrafast lasers possess unique capability of three-dimensional (3D) processing inside transparent materials. When a tightly focused ultrashort laser pulse irradiates onto a transparent target (photon energy lower than the band gap), the extremely high laser intensity will initiate the multiphoton absorption and excite electrons from valence band to conduction band. The material will be heated with a phase or structural modification, leading to a localized permanent property change. The occurrence of this process requires that the laser intensity is higher than the threshold of the multiphoton absorption, making it possible for localized 3D volume processing inside the sample by a tightly focused laser beam. Ultrafast laser processing inside transparent materials has been reviewed in a few recent publications [199–201]. Ultrafast laser irradiation induces phase and structural modification inside transparent materials. In this section, the mechanism of refractive index modification in different regimes is described and functional structures inside transparent materials fabricated by ultrafast lasers with a focus on femtosecond lasers are reviewed over the recent past.

(a) Types of refractive index modifications: The phase and structural changes according to the ultrafast laser parameters have been studied for various glasses such as porous glass [202], lithium niobium silicate glass [203], and silica fibers [204]. The ultrafast-laser-induced refractive index modification is categorized into three different regimes (or types): regime I (smooth refractive index changes), regime II (birefringent zones), and regime III (micro-voids or damages) [205,206]. Type I modification occurs due to a multiphoton absorption process with the pulse energy below the ionization threshold, which results in isotropic smooth changes in refractive index. Type II modification occurs due to avalanche ionization and the local production of moderate plasma,

which results in ascribed either to laser-induced stress or self-ordered nano-gratings leading to anisotropic reflection. Type III modification occurs due to an excessive plasma production and subsequent Coulomb explosion, results in voids or disorganized damage features in the glass matrix [207,208]. Each type of modification has the threshold depending on pulse duration and pulse energy. For example, as shown in Fig. 16, type III modification is achieved inside the pure silica at high pulse energy (>300 nJ) and high pulse duration (>200 fs).

(b) Waveguides: Refractive index changes in bulk materials by fs laser have been employed for buried optical waveguides fabrication with various geometries [209]. The fs laser processing can modify the refractive index with arbitrary 3D designs in a single process step inside any materials, even in photo-insensitive materials. Abou Khalil et al. fabricated a series of 7 mm long straight waveguides inside a silver-containing zinc phosphate bulk glass using a 1030 nm femtosecond laser with 390 fs pulses and 0.02–0.15 μJ pulse energy [210]. Morris et al. fabricated the channel waveguides in Tm:Lu_2O_3 ceramic using a 1040 nm ultrafast laser with 200 fs pulses and 0.4–5 μJ pulse energy [211]. Pätzold et al. fabricated the straight and s-curve waveguides in a poly(methyl methacrylate) (PMMA) foil using a 1048 nm Yb:KYW laser with 600 fs pulses and 0.45 μJ pulse energy [212]. Consequently, the waveguides are usually fabricated by fs lasers with relatively low pulse energy as the type I modification.

(c) Bragg gratings: Bragg gratings are also inscribed inside the bulk materials by fs lasers. Bragg gratings are a periodic refractive index changes that perform as an optical filter that reflects a specific wavelength of light [213]. Femtosecond laser processing enables inscribing the gratings that are thermally stable up to the glass transition temperature in certain laser parameters [214]. It allows the ultrafast-laser-inscribed gratings to have a potential to be an element of the sensors for extreme conditions like high temperature [215,216]. Femtosecond laser processing has been used to fabricate waveguides composed of volume Bragg gratings in bulk materials such as diamond [217] and PMMA [218].

In recent studies, fs lasers are used to fabricate fiber Bragg gratings (FBGs) in various optical fibers such as a pure silica optical fiber [219], fluoride glass fibers [220], a cyclic transparent optical polymer fiber [221], trans-4-stilbenemthanol (TS)-doped PMMA optical fibers [222], and perfluorinated graded-index polymer optical fibers [223]. Femtosecond laser processing for fabrication of FBGs with novel geometries have been studied [224,225]. For example, as shown in Fig. 17, Ertorer et al. proposed damage-free beam delivery method using fs laser irradiation under oil immersion [226]. Since the filament is generated due to Kerr-lens self-focusing effects, uniform gratings with high aspect ratio were inscribed inside the optical fiber.

(d) Microfluidic structures: Femtosecond lasers are also used as a 3D micromachining tool for fabrication of fluidic devices with two strategies: fs laser-assisted wet chemical etching and liquid-assisted

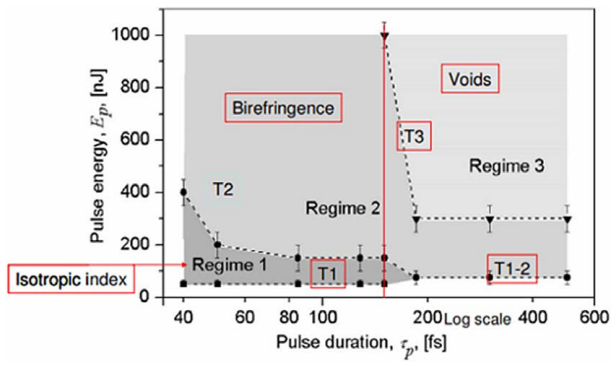

Fig. 16 Threshold pulse energies of an fs laser for different regimes of refractive index modification in fused silica [206] (reprinted with permission from OSA)

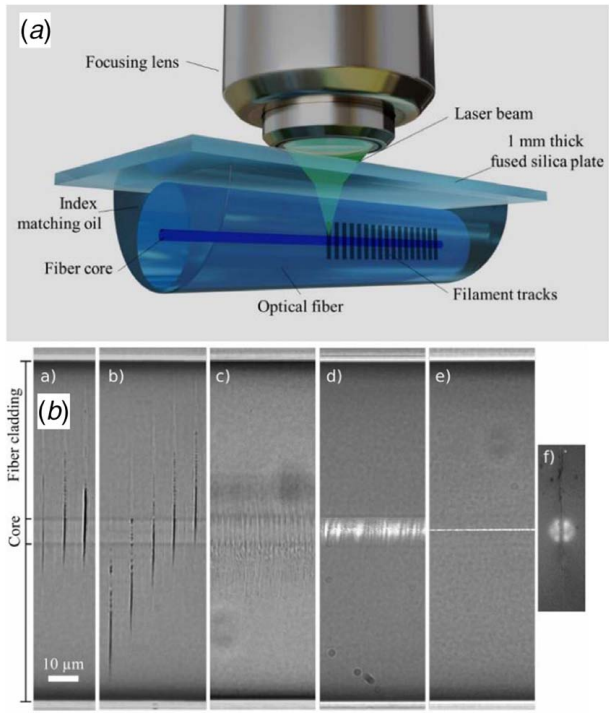

Fig. 17 (*a*) Schematic of the femtosecond laser writing of filament track Bragg gratings with oil immersion method and (*b*) microscope images of isolated filamentation tracks [226] (reprinted with permission from OSA)

fs laser drilling [227,228]. Femtosecond laser processing induces modification of chemical properties like etching rate [229] so that a wet etching process can be used to remove the irradiated region. Since the liquid like water assists to remove the debris during the laser processing, long and continuous channels can be fabricated inside the materials by the liquid-assisted fs laser drilling [86].

Recently, the fluidic devices with complex designs have been proposed to improve their integration and uniformity of microfluidic structures such as microfluidic channels, a microvalve, and a micropump in the microfluidics as shown in Fig. 18. Shan et al. proposed 3D multi-microchannel helical mixers fabricated by the fs laser-assisted wet etching method. They performed two-step wet etching in order to obtain the hollow spiral channels with high uniformity [230]. Wang et al. proposed a temporally shaped fs laser Bessel-beam-assisted chemical etching method to generate deep microchannels in fused silica. The etching depth was enhanced by a factor of 13 compared to the conventional method because of the advantage of the Bessel beam such as ultralong focal depth, an intense central core, and uniform intensity distribution [231]. Accordingly, fabrication of microfluidic structures with high integration and uniformity are achieved with optimized conditions for the fs laser processing and etching process.

Polymer-based fluidic structures fabricated by fs laser have also been studied. Roth et al. proposed fs laser processing for 3D-microfluidic channels fabrication inside PMMA bulk material. They fabricated the microchannels in two steps: fs laser irradiation and annealing. Non-periodic disruptions inside the focal volume generated by the fs laser irradiation become continuous channels with cross section larger than the focal volume after annealing. The height, width, and aspect ratio of the channels were adjusted by controlling laser conditions [232]. Martínez Vázquez et al. also used fs laser in the fabrication process for an optofluidic cytometry platform based on PMMA. The fs laser was used as a welding tool for the PMMA parts [233].

(e) Microscopic voids, nanocrystals, and dichroic structure: Femtosecond laser can also induce the formation of nanopores and voids inside the materials. A single void formation is caused

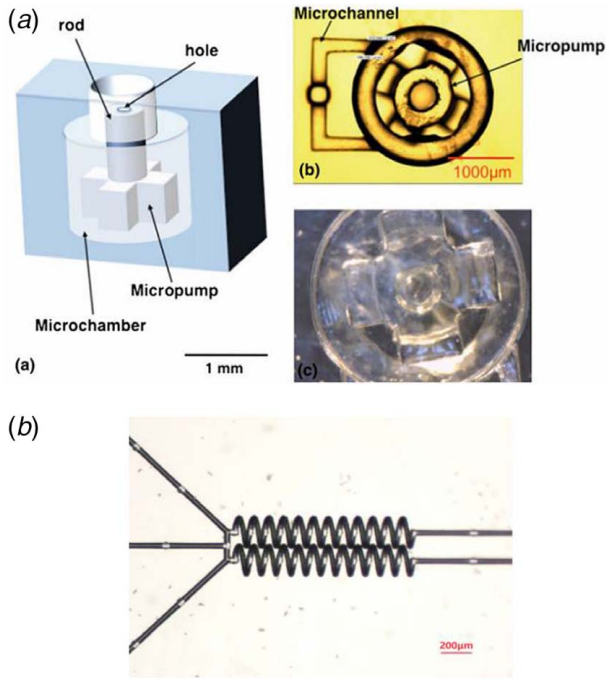

Fig. 18 (*a*) Micropump fabricated in a 3D-microfluidic structure in photosensitive glass and (*b*) multi-microchannel helical mixer fabricated by femtosecond laser inside fused silica (Refs. [227]—reprinted with permission from Springer Nature—and [230]—reprinted with permission from MDPI)

by strong explosion and shock wave formation in the decompaction regime. As shown in Fig. 19, the decompaction structure is observed for different laser scanning speeds. Ma et al. found that the periodic void structures can be controlled inside porous glasses by the mean pulse energy and the scanning speed [234]. Moreover, the ultrashort laser pulses induce microscopic voids in the direction of laser propagation due to self-focusing and filamentation, standing electron plasma wave, or spherical aberration.

The fs laser processing with high repetition rate can create thermal field in the laser focused area, which results in space-selective precipitation of various functional nanocrystals inside glasses [235]. The nanocrystals inside the glasses can be used for photonic applications such as laser frequency conversion devices, 3D optical-data storage, optical grating, 3D multicolored industrial art objects, and ultrafast all-optical switches.

Femtosecond laser irradiation inside an Ag nanoparticle containing glass was shown by Podlipensky et al. to change the spherical nanoparticles to oval shapes oriented in the laser polarization direction [236]. Permanent 3D anisotropic structures were created with the use of multi-wavelength fs pulses, which displays dichroic functionality. These structures are erasable using thermal annealing and thus could have applications as optical 3D storage devices.

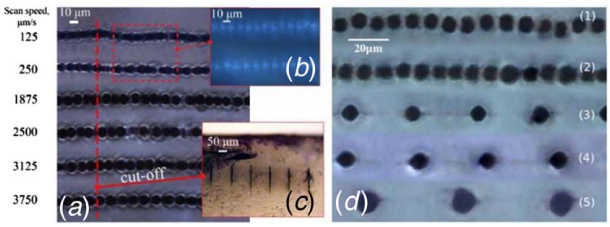

Fig. 19 (*a*)–(*c*) Optical images of decompaction regions obtained for different writing speeds and (*d*) image of periodic lines of voids formed inside of the porous glass [234] (reprinted with permission from OSA)

(f) Color centers: Femtosecond laser processing for single-crystal diamonds has increased in recent studies. Diamond has become a promising structure for spintronics and quantum information, thanks to the remarkable properties of a nitrogen-vacancy (NV) impurity [237]. The Yb:KGW laser with 20–26 nJ pulse energy and 230 fs pulse duration is focused inside the diamond using oil immersion lens. After laser processing, the diamond is annealed in a nitrogen atmosphere to produce the NV centers. It was found that the probability of creating single NVs is to be 80% for the laser pulse energy of 24 nJ [238]. Hadden et al. proposed the waveguide-coupled NVs, which enable optically linked single NVs for single-photon sources or solid-state qubit in quantum photonic applications [239]. The intrinsic structure of the fs laser modified region and the model of phase transition including graphitization and photolytic formation of vacancies have also been investigated in Refs. [240,241].

4.4.2 Machining Inside Non-Transparent Materials. Ultrafast lasers can also be used to create structures inside materials that are opaque to visible light. This is possible because as long as the photon energy is below the bandgap, laser beams can penetrate deep inside the material without significant linear absorption, and nonlinear light-matter interaction will initiate laser energy deposition at the beam focus. A commonly studied material that has scientific and technological significance is silicon, which has a bandgap of 1.1 eV at room temperature (corresponding to 1.1 μm laser wavelength in vacuum). A large body of work related to bulk processing in Si is stealth dicing of silicon wafers [242–246], which typically utilizes long-pulsed lasers to create internal defects followed by mechanical fracturing. When using femtosecond laser pulses for Si bulk processing, one needs to consider the high peak power and intensity that can create electronic and thermal non-equilibrium, which can in turn alter laser beam absorption and propagation. One can refer to the work by Verburg et al. who studied Si internal modification using 3.5 ns laser pulses at 1549 nm wavelength and also gave a short review on Si bulk processing using short (ns) and ultrashort (fs–ps) laser pulses [247]. A notable application of bulk processing is writing waveguides, as demonstrated using nanosecond [248,249] and femtosecond lasers [250,251]. Nanostructures inside Si induced by 1.24 μm femtosecond laser pulses were studied by Mori et al. [252]. The orientation of laser-induced structures can be controlled by the polarizations of two laser pulses, and the periodic nanostructures may have the same origin as "ripples" that have been observed in dielectrics [253,254]. In the studies by Grojo et al. [255], nonlinear absorption of Si at wavelengths longer than the linear absorption edge was found to pose a limit to the intensity that can be reached using femtosecond laser pulses. This is because nonlinear absorption taking place before the laser beam can reach its focus reduces laser energy and distorts beam profile. They also showed that this limit can be overcome by using solid-immersion focusing, which utilizes the high refractive index of silicon to increase the numerical aperture to ~3 [256]. Because of the transparency of silicon at wavelengths longer than 1.1 μm, ablation on the backside (beam exit surface) of silicon is possible, which has been demonstrated by several groups using fs–ns pulse durations [257–259]. Femtosecond laser beams with Gaussian and Bessel spatial profiles have been used to investigate beam propagation in the nonlinear regime and to drill high aspect ratio channels in silicon [255,260–262]. It has been shown recently that picosecond laser pulses can be used to create permanent internal modification in silicon, which offers an alternative to fabricating complex 3D structures [263].

4.5 Additive Manufacturing Using Ultrafast Lasers. Additive manufacturing that utilizes material melting, reflow and solidification, continuous-wave (CW), and long-pulsed lasers are often used to deposit thermal energy to initiate material phase change. 3D objects can also be additively manufactured using ultrafast lasers through linear or nonlinear laser–matter interaction. Recent

advances in using ultrafast lasers for additive manufacturing are reviewed in the following sections.

4.5.1 Multiphoton Polymerization. Lasers with UV wavelengths are commonly used in stereolithography, which utilizes linear absorption of organic molecules for UV light to induce cross linking of liquid photopolymers. Photopolymers typically consist of photoinitiators that will release reactive species upon UV laser radiation, and these species will initiate a chain reaction among monomers to form new bonds and cause solidification, thus "curing" the liquid photopolymer. This process requires short wavelengths (high photon energies) at which most photoinitiators are designed to have high absorption. It is possible to achieve photopolymerization through the simultaneous absorption of multiple, low-energy photons (multiphoton absorption), which is commonly referred to as multiphoton polymerization (MPP). One can refer to Refs. [264–270] for reviews of MPP and related applications. The most common form of MPP is two-photon polymerization (2PP) where two photons (typically visible to near-infrared wavelength) are absorbed simultaneously. However, three-photon polymerization is also possible [271]. Because the probability of simultaneously absorbing multiple photons is very small, in order for multiphoton absorption to take place, high peak laser intensities, typically on the order of 1 TW/cm^2 [272], are required. Such intensities can be provided by using ultrashort (<10 ps) laser pulses. 2PP has a few advantages compared to conventional single-photon stereolithography. Firstly, the laser beam can penetrate deep inside the photopolymer to initiate solidification only at the focal position, so the fabrication can in principle take place anywhere inside the photopolymer. This gives more freedom in the design of the fabrication process. Second, the fabrication resolution can be improved to the nanometer scale, because the material response scales with I^2, where I is laser intensity.

The principle of two-photon absorption was studied by Göppert-Mayer [273] and was experimentally demonstrated by Kaiser and Garrett [274]. The idea of two-photon polymerization was proposed and demonstrated in early 1990s [275,276]. In the concept proposed by Cabrera et al. [275], two laser beams cross each other in the photopolymer and 2PP occurs at the intersection. This concept has not been widely adopted because the structures that have been fabricated will obstruct the laser beams and cause distortion to the laser focus. Single-beam 2PP was realized by Strickler and Webb [276], who used a mode-locked dye laser at 630 nm wavelength and a 1.4 NA oil immersion objective lens to fabricate structures as small as 100 nm. This small size was possible because of the quadratic intensity dependence of two-photon absorption, together with the fact that the features were fabricated nearly at the threshold and that some material could have been removed during rinsing. 3D spiral structures were fabricated by Maruo et al. [277]. In their work, a femtosecond laser with 200 fs pulse duration and 790 nm center wavelength was focused inside the photopolymer that was optimized in UV wavelengths. The quality and resolution of 2PP had been improved significantly since then, and the same group reported the fabrication of a micro-sized bull using 2PP that has the size of a red blood cell in 2001 [278]. They also showed that micro-sized mechanical devices with movable parts can be fabricated.

Photopolymerization, especially in the nonlinear light-matter interaction regime, is a complex process involving many micro- and macro-scale phenomena which have not been fully understood. Avalanche ionization, which can contribute to free carrier generation in dielectrics [279,280], has found to have an influence in 2PP [281]. New insights into ultrafast dynamics in MPP can be obtained by studying optical nonlinearities [282] using, for example, the double-beam threshold measurement [283]. Spatial laser beam shaping is a powerful tool for MPP (and for laser material processing in general, see Sec. 5.2). Multiple foci can be generated using diffracting optical elements and spatial light modulator to fabricate structures in parallel [284]. Non-Gaussian beams, such as nondiffracting Bessel beams, have been used [285] to fabricate high aspect ratio structures, and new optical devices can be used to generate non-Gaussian beams [286]. Materials that can be used in MPP have been expanded to have more functionalities, high resolution, and the ability to respond to external stimuli [287,288]. MPP can be integrated with subtractive, laser machining processes for hybrid manufacturing [289].

4.5.2 Ultrafast Laser Additive Manufacturing of Metal, Glass, Ceramic, Semiconductor, and Biological Materials. The high peak power of ultrashort laser pulses can be utilized to achieve high temperature in materials to cause melting and solidification. Metal powders that have high melting temperature, such as tungsten, can be melted using femtosecond laser pulses at high repetition rate [290]. Copper has high thermal conductivity that prevents it from being additively manufactured using conventional lasers but can be fabricated using ultrafast lasers [291]. This is because high temperatures can be reached and localized in the material. Rapid heating and cooling associated with ultrafast laser treatment will cause residual stress that will degrade the performance of the fabricated part. It remains to be seen how to improve the quality of ultrafast laser additively manufactured parts. Femtosecond lasers can also be used to melt glass powders [292], where nonlinear absorption is likely to contribute to the energy absorption. Applying the above-mentioned MPP technique, polymer–ceramic hybrid materials can be used to fabricate micro-needles for medical applications [293]. It is worth pointing out that ultrafast lasers can also be used for post-processing of additively manufactured metal parts [294]. Figure 20 shows some examples of additively manufactured parts using ultrafast lasers.

In the above-mentioned additive manufacturing methods, heating and chemical reactions that are caused by laser energy deposition are used to directly introduce material change. Another approach to building 3D parts is to deposit or transfer materials that are more or less in their original state. This is best known as pulse laser deposition [295] and laser-induced forward transfer [296]. These methods have enabled additive manufacturing of semiconductor and biological materials.

4.6 Ultrafast Lasers in Biomedical Applications. In the past two decades, ultrafast lasers have become a mainstream in biomedical applications and found their place in clinical practice. The ability to alter biological media on a subcellular level without disrupting

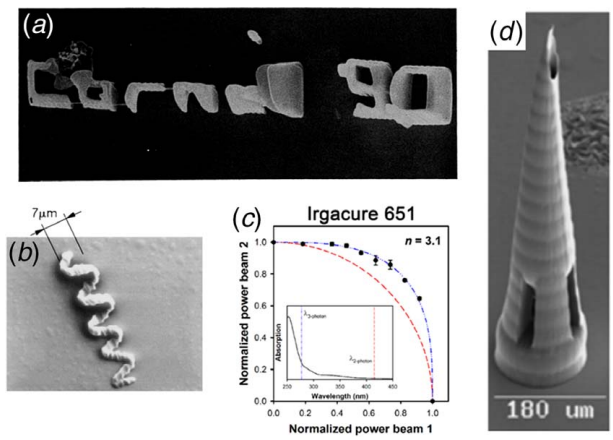

Fig. 20 Examples of additive manufacturing using ultrafast lasers. (*a*) Early work of microfabrication using 2PP [276] (reprinted with permission from SPIE) and (*b*) 3D spiral structures fabricated by 2PP [277] (reprinted with permission from OSA). (*c*) Determining the nonlinear absorption order (*n*) using the two-beam initiation threshold method [283] (reprinted with permission from Wiley-VCH). (*g*) A micro-needle printed using 2PP in polymer–ceramic hybrid materials [293] (reprinted with permission from Wiley-Blackwell).

cell viability highlights the use of ultrafast lasers in research, whereas high precision and modest heat-affected zone are primary factors in adopting these lasers in clinical applications, especially ophthalmology. Furthermore, the latest research demonstrates the ability to enhance material properties of collagen rich tissues without disruption, which opens a completely new avenue for applications and may in the future transfer to manufacturing as well, perhaps as means for inorganic polymer treatment.

Nonlinear absorption, a unique property of the ultrafast laser, enables treatment of the interior of target material without affecting its outside surface. Proper use of optical and laser parameters provides control over different processing regimes, photodisruption (PT) and ablation via thermal accumulation, both of which are known processes in nontraditional manufacturing. PT is an underlying mechanism in femtosecond laser-assisted corneal refractive surgeries, an application already mature in clinical practice. Amplified pulse trains at few kHz repetition rate with pulse energies above the damage threshold are used for bubble formation [297–301], which plays a key role in the surgery process. Cuts are created by the superposition of a series of cavitation bubbles.

Nanoscale femtosecond applications have been present for about a decade and can be broadly characterized by use of long series of pulses from femtosecond laser oscillators with repetition rates on the order of 80 MHz and pulse energies around the optical breakdown threshold [302–305]. Stuart and co-workers have been developing a theoretical framework for nanoscale applications of femtosecond lasers in biological media [306–308]. Most reported studies focus on a subcellular level for cell and tissue studies [309,310]. A number of researchers have focused on the nanosurgeries in which ablation is used to remove cellular components without affecting the viability of the cell itself. König and co-workers have been performing nanodissection of human chromosomes with femtosecond laser pulses [301,311,312]. Tirlapur and König [303] utilized ultrafast lasers for generation of reactive oxygen species (ROS) in mammalian cells to induce their apoptosis-like death. At the moment, there are few prospective clinical applications with one being removal of the small content of biomaterial for very precise subsequent proteomic or genomic analysis [313].

Advantages of using oscillator systems in biological applications are numerous, including increased resolution, reduced trauma to surrounding tissue due to smaller total energy deposition, and affordability of oscillator systems in comparison to the chirped amplified systems capable of producing pulses with significantly higher energy.

Femtosecond lasers are used in vision correction surgeries, anterior lamellar corneal transplantation, keratomileusis, channel creation for corneal implants [314], as well as cataract surgeries. Laser *in situ* keratomileusis (LASIK) is a vision correction surgery composed of flap formation via a mechanical microtome followed by the photoablation of the stromal tissue with an excimer laser. The femtosecond laser was introduced to replace the mechanical microkeratome to create a flap in the so-called femtosecond LASIK [315]. In the next generation surgery called small incision lenticule extraction (ReLEx smile) [316–318], a femtosecond laser alone is used to reshape the cornea by directly creating channels within its interior without removing the epithelium, the outermost layer of the cornea.

Juhasz et al. [319] conducted initial studies on the use of femtosecond lasers in laser-assisted corneal surgery in the mid-1990s. They used water to model shock wave generation and subsequent cavity formation and applied the same method to bovine corneas. Furthermore, it has been shown that femtosecond generated flaps have numerous advantages in comparison to mechanical keratomes including decreased risk of infection and reduced intraocular pressure during the procedure, greater precision, and more uniform thickness [315,320]. Lubatschowski has investigated the differences in laser–tissue interaction and beam delivery of different commercial systems tailored for refractive surgery [321]. Repetition rate effects on affected tissue have also been studied [322]. Significant differences in the nature of cell death as a function of laser repetition rate have been observed. At lower repetition rates, the laser pulse energy required to create a cut is higher resulting in predominant cell death by necrosis rather than apoptosis. As necrosis causes release of intracellular contents into the surrounding tissue, there is more inflammatory cell influx after flap formation. Revealing the cavitation bubble formation mechanisms at different processing and beam delivery regimes will help to optimize laser parameters, control the creation of bubbles, and reduce complications.

Recently, Vukelic and co-workers introduced a novel ultrafast laser–tissue interaction regime that relies on photochemical effect induced by ultrashort laser pulses rather than tissue disruption [323,324]. The approach restricts the laser regime such that the treatment is always below the optical breakdown level, and thus relies on the ionization potential for alteration of corneal geometry (Fig. 21). If a femtosecond laser operates below the energy level

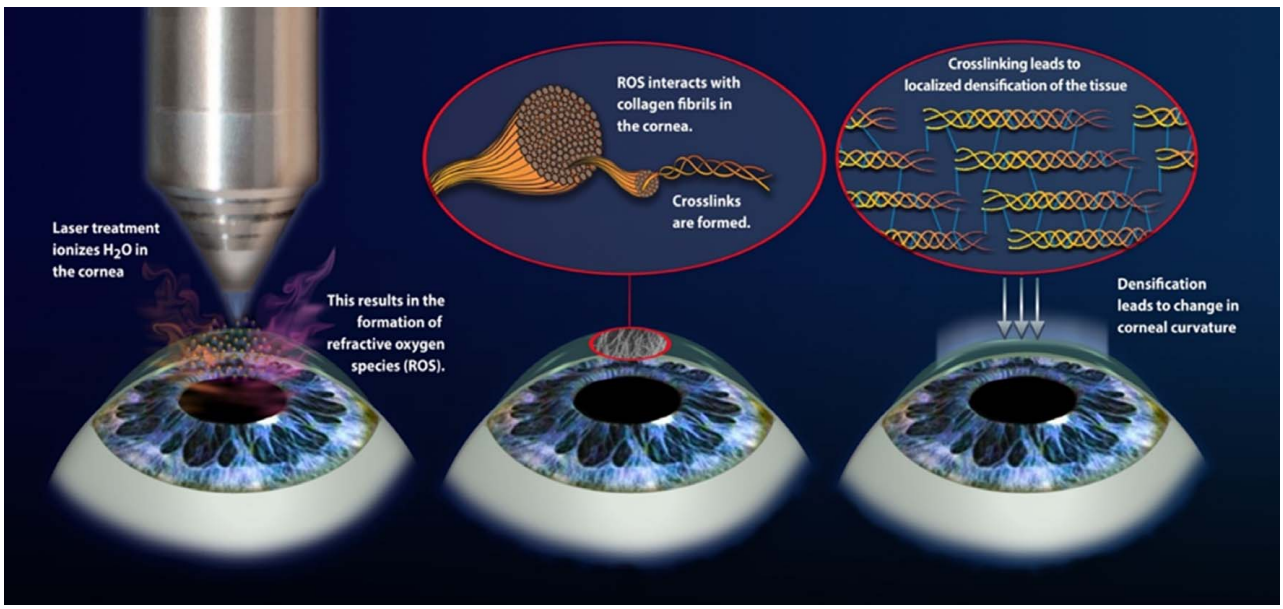

Fig. 21 Step-by-step illustration of the use of the proposed laser-assisted process for the non-invasive correction of refractive errors

required for optical breakdown, ionization of atoms within the focal volume is still possible, because the ionization probability has a number of resonance maxima due to intermediate transition of the atom to an excited state. In the vicinity of such maximum, the ionization cross section increases by several orders of magnitude enabling ionization even if the frequency of the incoming electromagnetic wave is lower than the ionization potential. Such a scenario enables formation of an ionization field, which locally ionizes and dissociates water content in the tissue, creating ROS. When applied to collagenous tissues, the reaction between ROS and surrounding proteins results in crosslink formation (Fig. 21), giving rise to spatially resolved alterations in mechanical properties. Carefully tailored alterations of mechanical properties of collagen stroma can be utilized to change the overall corneal curvature that may be leveraged for the correction of refractive errors. Another explored application is strengthening of articular cartilage toward addressing early osteoarthritis [325,326].

4.7 Femtosecond Laser-Based Super-Resolution Manufacturing. The holy grail of nanoscience is to manufacture functional structures from the atomic scale to the macroscopic in three dimensions. The minimum size attainable by conventional laser direct writing is limited by Abbe's diffraction limit

$$d \approx \frac{\lambda}{2n \sin \alpha} \tag{3}$$

where d is the minimum beam diameter, λ is the wavelength, n is the refractive index of the medium where the light is focused, and α is the beam divergence angle. Current semiconductor chips are produced by photo-lithography with continuous shrinking of wavelength from UV, deep UV, to even extreme UV. The required mask masters are fabricated using e-beam lithography subject to the shorter de Broglie wavelength of a focused electron beam. This approach leads to nanomanufacturing equipment capital cost to reach the $100M level, thereby forming an economic barrier for extensive applications of nanodevices [327,328]. Based on the interaction between ultrafast laser and materials, there are two basic methods to overcome the optical diffraction limit: near-field optical manufacturing and innovative far-field nanolithography. Near-field optical manufacturing is intrinsically limited to the surface, i.e., to 2D, planar lithography [329] which can be conducted with either metallic tip-assisted laser processing or near scanning optical microscopy [330,331]. The key to realizing 3D nanolithography is to focus the pulsed laser into a diffraction-limited spot or a depletion region limited by a donut-shaped, stimulated light in a photon-sensitive medium [332].

A nonlinear multiphoton absorption procedure, such as 2PP, can enable precise manufacturing at a resolution near the diffraction limit [278,333,334]. The probability of the multiphoton absorption effect, p_n, is a power function of laser intensity I as follows [335]:

$$p_n = \delta_n I^n \tag{4}$$

where δ_n is the absorption cross section of n photons, which is dependent on the nth nonlinear coefficient of the optical medium. Therefore, the multiphoton effect can only occur at an extremely strong intensity, e.g., the central regime of a focused laser beam. As shown in Fig. 22(*a*), 2PP can be controlled by the laser intensity. When I is higher than I_o, the threshold, 2PP will occur at the central area. Theoretically, the size of 2PP is about $\lambda/(2.7n \sin \alpha)$, significantly smaller than the diffraction limit of $\lambda/(2n \sin \alpha)$ by single-photon absorption [332].

Serbin reports 2PP direct writing with tightly focused femtosecond laser pulses (60 fs, 90 MHz, 780 nm) using Ormocers as the photosensitive resin and a high numerical aperture, oil-immersed objective lens [333]. Figure 22(*b*) shows a 3D printed Venus micro-statue [333] and Fig. 22(*c*) presents a woodpile-style photonic crystal [334]. The woodpile structure of the photonic crystal reported in Ref. [333] possesses a rod diameter of 300 nm and

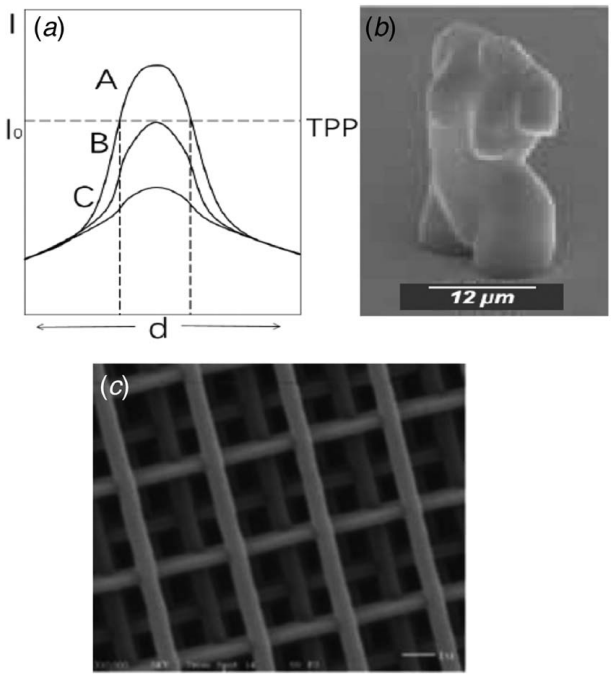

Fig. 22 (*a*) Gaussian beam intensity for 2PP, (*b*) printed Venus micro-statue [333] (reprinted with permission from OSA), and (*c*) a printed woodpile-style photonic crystal [334]

rod spacing of 900 nm. Although a photonic band gap is evident at the near-IR band in the photonic crystal, the crystal does not possess a complete photonic band structure due to fabrication imperfections.

Super-resolution manufacturing beyond the diffraction limit has been achieved by a stimulated emission depletion (STED) mechanism inside a photon-sensitive polymer. An insoluble, photo-induced, cross-linked polymerization can be used for super-resolution manufacturing. There are three primary methods to realize a super-resolution depletion-limited focal spot. With STED lithography [336,337], monomer molecules are first excited via two-photon absorption. The excited molecules are brought back to the ground state by the ring-shaped, stimulated light at a short wavelength via a stimulated emission. Therefore, only surviving radicals in the central regime can undergo polymerization. Alternatively, resolution augmentation through photo-induced deactivation lithography excites PI molecules via two-photon absorption, generating a long-lived intermediate state. Upon further ring-shaped light excitation, the intermediate state is activated and does not lead to cross-linking polymerization [338]. Finally, two-color photo-initiation/inhibition lithography [339] excites PI molecules via *one-photon* excitation and generated radicals. The photo-inhibitor molecules are excited by another ring-shaped light at a different wavelength via one-photon absorption, generating non-initiating radicals, which can terminate the polymerization of excited radicals. In summary, all these methods involve photosensitive polymers and realize a depletion-limited focusing through a spatially controlled ultrafast photochemistry.

In a typical STED configuration, the diameter of the exposure area can be calculated by the formula [340,341]

$$d \approx \frac{\lambda}{2n \sin \alpha \sqrt{1 + bI_{\text{STED}}/I_S}} \tag{5}$$

where $n \sin \alpha$ is the numerical aperture, the same as in Eq. (3), b is a systematic coefficient dependent on the beam shape, I_{STED} is the intensity of the depletion light, and I_s is the switching intensity at which half of radicals will be depleted through a stimulated emission. It is apparent that one can reduce the exposure area by

increasing I_{STED}/I_S ratios. Figure 23 shows a comparison among the e-beam, 2PP, and STED lithography approaches. Although e-beam lithography can reach a resolution around 10 nm, it is still a near-planar manufacturing (2.5 dimensional) technique. Additionally, it requires operations to be accomplished in an ultrahigh vacuum chamber. 2PP is a facile 3D manufacturing technique with resolution close to the diffraction limit. STED is an ultra-precise 3D manufacturing beyond the diffraction limit.

Gan et al. have demonstrated deep sub-diffraction optical beam lithography with a 9 nm feature size based on the STED mechanism [342]. They chose 2,5-bis(p-dimethylaminocinn amylidene)-cyclopentanone as the two-photon initiator and the monomer was SR399 or SR444. A 800 nm 140 fs 80 MHz laser was used as the writing beam and the depletion light was a 375 nm CW laser. The donut-shaped light was generated through a planar vortex phase plate. Two-line resolution of 52 nm has been achieved at a depletion intensity of 2.42 μW/cm^2. Shown in Fig. 24, microscale optical cloaking has also been demonstrated with a specially designed photonic crystal with lattice varying from 500 nm to 900 nm [343].

Although STED is a well-established method for overcoming the diffraction limit, there has been limited progress in direct writing of nanostructures using different materials other than polymers. Cao et al. reported gold nanoparticles generated by using ion-doped hybrid photoresin [344]. Frölich et al. reported a titania woodpile-style photonic crystal with a complete photonic bandgap via STED direct writing and a double-inversion procedure [345]. If a metallic nanostructure can be fabricated via STED direct writing, the super-resolution manufacturing can pave the way to various nanodevices for energy, environment, and biomedical applications.

4.8 Numerical Methods. The ultrafast laser has demonstrated its superiority for material processing and manufacturing. To further explore its application, it is critical to understand the ultrafast laser–matter interaction, which is a complex multi-physics process. In general, when materials are irradiated by an ultrashort laser pulse, the laser beam energy is first absorbed by free electrons (metals) or bonded electrons (semiconductors and dielectrics). By absorbing the incident laser beam energy, the electrons inside the target are heated to an extremely high temperature in a very short amount of time. The electrons will transfer the energy to the lattice, leading to phase change, structural modification, and ablation as described in Sec. 4.3.1. The ejected material will be partially or fully ionized to form plasma. On the other hand, when the electrons near the target surface gain enough energy, surface electron emission (photoelectric or thermionic) will occur [346–348]. The ejected hot electrons are energetic enough to ionize the ambient gas, forming an early stage plasma in several or tens of femtoseconds [349,350]. Due to the complexity of the process, numerical modeling is demanded to elucidate the underlying mechanisms. Extensive studies have been devoted to investigating the physics of ultrafast laser–matter interaction, and multiple useful models have been developed.

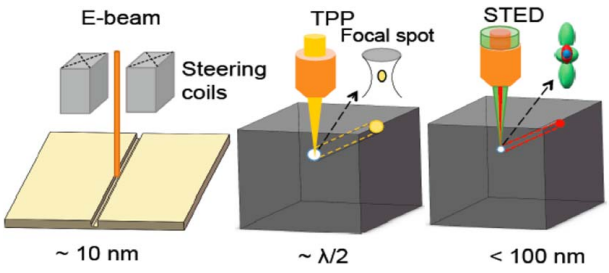

Fig. 23 Comparison of e-beam, 2PP, and STED lithography. These figures are modified from Ref. [342].

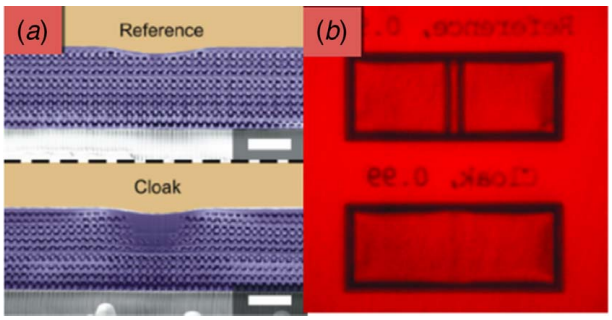

Fig. 24 STED direct writing of photonic crystal and 3D optical cloak. (*a*) Photonic crystals (reference) with a lattice of 500 nm and a cloak with a lattice ranging from 500 nm to 900 nm, the bar is 2 μm and (*b*) top-view of two golden lines under photonic crystal (above) and a cloak (below). Note that the lines disappeared beneath the optical cloak [343] (reprinted with permission from OSA).

The TTM has been widely used to describe the energy transfer inside the target during ultrafast laser ablation. The basic governing equations are

$$\frac{\partial}{\partial t}(C_e T_e) = \nabla \cdot (K_e \nabla T_e) - G(T_e - T_l) + S \tag{6}$$

$$\frac{\partial}{\partial t}(C_l T_l) = \nabla \cdot (K_l \nabla T_l) + G(T_e - T_l) \tag{7}$$

where t is the time, G is the electron–phonon coupling factor, S is the laser source term, C_e/C_l and K_e/K_l are the thermal capacities and thermal conductivities of electrons and lattice, respectively. The electrons and the lattice are treated as two separate systems with energy coupling between them. This approach is based on the fact that laser energy is first absorbed by electrons in the material, and then the electrons are relaxed by coupling with phonons. Anisimov et al. proposed the parabolic TTM [351], which can be generally used for pulses below 10 ps. However, it is not applicable for pulses shorter than 100 fs, because laser–plasma/plume interaction is not considered, and thermal equilibrium in the electron system is assumed for all time. Hyperbolic TTM [352,353] was then developed for pulse duration shorter than 100 fs, considering electron non-thermalization. To further improve TTM, a semi-classical TTM was established by Chen et al. [354] to include the effects of non-equilibrium electron transportation and electron drifting. TTM was further combined with rate equations to consider the electron number density evolution during laser ablation of dielectrics and semiconductors [355]. One requirement for accurate prediction of ablation depth with TTM for a wide range of materials is to consider the correct thermal properties such as C_e and k_e as well as the electron–phonon coupling factor at very high temperatures. Wu and Shin used the quotidian equations of state (EOS) and the model of Lee and More with TTM and demonstrated the efficacy in accurately predicting ablation depth of various metals [356] and semiconductors and dielectrics [357] over a wide range of fluence and laser pulse durations.

One issue with the commonly used TTM is that the predicted ablation depth is not deterministic at high fluence because the model does not consider heat loss by material ejection. In Refs. [358,359], TTM was improved to solve this issue by considering the energy loss through a dynamic description of the ablation process with material removal. TTM has its advantages in simplicity, computational efficiency, and decent prediction accuracy. However, it is a pure thermal model, which cannot describe the non-thermal processes (Coulomb explosion, laser-induced shock wave, etc.), plasma generation and evolution, and laser–plasma interaction.

HD models describe the evolution of the irradiated materials, with considerations of conservations of mass, momentum, and energy on the continuum level [360]. HD models have been developed to describe the material removal and plasma expansion behavior during laser ablation [34,361–366]. It has been widely applied to longer pulse ablation processes and is proved to be valid for

various processing conditions [364,367]. However, for ultrafast laser ablation, the surface hot electron emission and resultant early stage plasma generation are very important and need to be integrated into the HD model. In the model developed by Bulgakova et al. [368], the effect of the hot electron emission process was accounted for and the electron transport inside the target was calculated. Chen and Mao applied a one-dimensional HD model to simulate the early stage plasma behavior during femtosecond laser ablation [369]. Colombier et al. incorporated TTM into their hydrodynamic model to account for the electron-ion coupling effect and thus more accurate simulation results on laser ablation were obtained [363]. Zhao and Shin developed a multi-fluid HD model to capture the dynamics of electrons, ions, and atoms separately [40,349] and successfully simulated both early plasma and plume plasma. The application of the HD model is limited by its disadvantages in the following aspects. First, EOS have to be combined with the HD model to provide thermal and optical properties of materials in a wide range of temperature and density. Therefore, the accuracy of a HD model strongly relies on the accuracy of EOS, which is not satisfactory in many cases. Second, as a continuum model, a HD model is not capable of capturing the non-equilibrium transformation and other ultrafast dynamics during the initial stage of ablation.

The molecular dynamics (MD) methods have been developed owing to the advancement of knowledge in solid-state physics and quantum mechanics. Once the intermolecular potential is given, MD can be used to simulate many problems with their specific external forces following the Newton's second law. MD provides an explicit atomistic representation of target heating, material removal, and expansion and solves problems that cannot be accounted for by continuum models, such as highly non-equilibrium states and fast phase transformations induced by ultrashort laser pulse irradiation [370]. It has been widely used to investigate the ultrashort laser pulse ablation of different materials in different fluence ranges [22,24–26,371,372], providing insight into the material removal mechanisms and fast transitions in the very early stage. MD model itself does not consider the electron relaxation dynamics. To improve it, Schäfer et al. established TTM-MD models by combining MD and TTM models together [373]. The thermal evolution of the electron system and its coupling with the lattice are involved in these models. In Refs. [374,375], an alternative improvement to MD models was proposed by coupling it with a Monte Carlo (MC) method, which was adopted to describe the electron dynamics during ablation. The ionization process and fast phase change of the electrons during ablation were described by the MC method, and the simulation results were improved. Inogamov et al. used an integrated model by a HD model and a MD model, where the HD model was applied to solve the early stage heating and expansion of electrons/lattice, and the MD model was adopted to describe the lattice atom motion and removal process later [376]. Hu et al. improved the MC-MD model by adding the particle in cell (PIC) method to calculate the Coulomb interaction between charged particles and the beam propagation method (BPM) to handle the interaction of early plasma with the incident laser beam [45]. As a result, the early plasma dynamics could be simulated with good accuracy in comparison with experimental measurements. This MD/MC-PIC-BPM model was further combined with an HD model in Ref. [42], where the output of the MD/MC-PIC-BPM model served as the initial stage of the HD model, and thus the plume plasma evolution in a longer time scale up to tens of ns could be covered. MD models have their own disadvantages in its computational cost. As a consequence, it can only simulate the ablation process in a very small simulation domain and time scale, which are not sufficient to capture the ablation process of the bulk material.

5 Recent Development in Ultrafast Laser-Based Manufacturing

5.1 Mechanism of Ultrafast Laser-Induced Damage Studied by the Pump–Probe Technique. For any laser-based processing technologies, it is crucial to have a fundamental understanding of how ultrashort laser pulses interact with materials, and what the key parameters are that influence the laser processing outcome. This is particularly important for ultrafast laser material processing, which involves light-matter interaction under extreme conditions. This section will review recent studies on the mechanism of ultrafast laser-induced damage of materials, with a focus on obtaining time-resolved information of ultrafast laser-induced material dynamics. Reviews of ultrafast laser–matter interaction at and above the damage threshold can be found elsewhere [377–379].

A useful tool for the study of ultrafast laser–solid interaction is the pump–probe technique, which is an *in situ*, nondestructive measurement of laser-induced phenomena in materials. In a typical pump–probe setup, a strong laser pulse ("pump") induces disturbance to the material, and a weak pulse ("probe") interacts with the disturbance whose information will be "encoded" in the probe pulse. By analyzing the transmission, reflection, phase, or a combination of these optical constants of the probe pulse as a function of the delay between the pump and the probe pulse, time-resolved information about laser-induced changes can be extracted. With ultrashort laser pulses, the temporal resolution of this technique is suitable for studying fast dynamics such as electron ionization and relaxation, laser-induced plasma, and shock waves. This technique has been used by many researchers in recent studies of laser-induced damage and modification in solid materials. Mouskeftaras et al. used a pump–probe interferometry technique to measure the change of refractive index with 100 fs temporal resolution [380]. Their results suggest that avalanche ionization does not play a dominant role for ultrashort pulse irradiation. Mauclair et al. used pump–probe optical transmission microscopy and phase contract microscopy to study ultrashort pulse-induced positive and negative refractive index change in fused silica and borosilicate glass [381]. Fast and slow material responses were observed, indicating the effect of carrier dynamics and material phase change. Pump–probe shadowgraphs were recorded in a study by Zhao and Shin on the dynamics of early plasma generation in femtosecond laser ablation of silicon [30]. Coulomb explosion caused by electron emission was found to increase material ablation rate. Using a train of two femtosecond laser pulses, Zhang et al. showed that nanostructures originated from electron dynamics can be controlled by changing the delay between the two pulses [382]. These nanostructures can be used in surface-enhanced Raman scattering. Garcia-Lechuga et al. observed an interesting ring pattern in pump–probe time-resolved microscopy [383,384]. These patterns resemble Newton's rings and are caused by light interference between an expanding layer of ablated material and the interface of a non-ablated substrate [384]. Similar patterns were observed by Rapp et al. in femtosecond laser ablation of silicon nitride [385]. Wædegaard et al. studied the evolution from free carrier generation to material ablation in single-crystal sapphire using pump–probe spectral interferometry and reflectivity measurement [386]. Pump–probe spectroscopy was used by Acharya et al. to study ultrafast carrier dynamics in ZnO and $BaTiO_3$ thin films [387]. The presence of excitons was observed, and excitons can be excited to inject carriers in hetero-structures. These experimental studies can often be used in conjunction with modeling and simulation [388–390] to reveal how ultrashort laser pulses interact with materials in the above-threshold regime.

5.2 Spatial Beam Shaping and Temporal Pulse Shaping for Ultrafast Laser Material Processing. Material processing using ultrafast lasers is most commonly conducted using laser pulses at kHz–MHz repetition rate, with Gaussian spatial beam profile, and at near-infrared fundamental wavelength. These conditions are used because they are the laser parameters from most commercially available ultrafast laser systems. However, for material processing applications, the optimal processing parameter set often varies from material to material, and even with the same material, different processing modes (drilling, cutting, surface texturing, etc.) require the tuning of processing conditions. This section is focused on

recent advances in using temporal pulse shaping and spatial beam shaping techniques to tailor ultrafast laser material processing for improved manufacturing outcomes.

5.2.1 Temporal Pulse Shaping. Temporal pulse shaping can be achieved by a variety of techniques, and the most commonly used methods in laser material processing are Fourier synthesis of spectrally modulated waveforms and the interferometric method based on Michelson and Mach–Zehnder interferometers [391,392]. Li et al. adopted the interferometric method to create a pulse pair, which was used to determine the damage threshold as a function of the delay between the two pulses in dielectric materials [393]. Their work showed that the decay of free carriers must be taken into account when analyzing the laser damage threshold measurement. Choi et al. used three laser beams (two pump beams and one probe beam) to investigate the dynamics of plasma and shock wave in femtosecond laser ablation of crystalline silicon [394]. An increase of ablation volume was observed when the two pump pulses are at ~10 ps delay, and the increase was due to a better energy coupling to the sample, because at short delays (1–5 ps), liquid film or hot surface plasma formed by the first pulse will increase the reflection of the second pulse, while at longer delays (>10 ps), the ejected material will reduce the transmission of the second pulse. The work by Qi et al. on femtosecond laser ablation of silicon showed that the energy coupling is enhanced at long delay because the density of the plasma formed by the first pulse will decrease, allowing deep penetration of the second pulse [395]. In a study with fused silica, Chowdhury et al. noticed that the depth of the laser ablated hole is maximum when two pulses are overlapped at zero delay, and the depth decreased as the delay increases. This is explained as the screening by the plasma produced by the first pulse [396]. The effect of femtosecond laser pulse train processing was investigated theoretically by Zhang et al. [397]. It was found that photoionization of self-trapped excitons is important for understanding femtosecond laser ablation and controlling laser processing results. A pulse train consisting of four femtosecond laser pulses with varying delays was generated in a twofold Michelson interferometer, and this pulse train was used to process metal, semiconductor, and dielectric samples, which were found to require the optimization of delays according to the materials used [398]. Pulse trains with an asymmetric temporal profile were generated by the Fourier synthesis method by Englert et al., and it was found that electron ionization in fused silica and sapphire depends on the type of the pulse trains, which are useful in tailoring laser processing for high bandgap materials at the nanometer scale [399–401]. Ahn et al. observed that the aspect ratio of femtosecond laser drilled holes in glass can be increased by using secondary pulses at 100–1000 ps delays [402]. High aspect ratio channels can also be obtained using pulses at high repetition rates, which can induce the heat accumulation effect [403]. The mechanism of the increased aspect ratio was investigated by Götte et al. using temporal airy pulses [404]. It was shown that delayed energy deposition can achieve larger laser penetration depth compared to single-pulse processing.

Various groups also use two or multiple pulses each of which has a different wavelength. Because materials often have wavelength-dependent reflection and absorption, choosing wavelengths for individual pulses in the pulse train is another dimension to tailor laser material processing. Gyamfi et al. studied the laser damage threshold of dielectric high-reflection coatings for a sequence of two pulses with different wavelengths, the fundamental 780 nm wavelength and its second harmonic at 390 nm [405]. Their work revealed the role of conduction-band electrons and their effect on laser damage threshold. Yu et al. used a pair of femtosecond laser pulses at 266 and 800 nm to investigate multiphoton and avalanche ionization [406–408]. It was shown that these two ionization pathways can be controlled individually by utilizing the wavelength-dependent absorption, and nanostructures can be fabricated more efficiently using a combination of short and long wavelengths.

5.2.2 Spatial Beam Shaping. It has been recognized that laser beams with a conventional Gaussian spatial profile are not suitable for some laser processing applications. Researchers have been experimenting with non-Gaussian beams and choose the optimal beam shapes suitable for a particular application. There is a large body of work on spatial laser beam shaping, and an overview of this subject can be found in Refs. [409,410]. This section covers recent studies on applying spatial beam shaping for ultrafast laser processing of materials. The devices used for spatial beam shaping can be categorized into two types, passive devices (such as lenses and diffractive optical elements) and active devices (such as liquid-crystal spatial light modulators and deformable mirrors). Beam shaping is mostly achieved by modifying the amplitude or phase or both of the incident Gaussian optical field, either through iterative algorithms such as the Gerchberg–Saxton algorithm [411], or forward methods based on a priori knowledge of the relationship between the original and the resultant optical field. Depending on the arrangement of the optics, the final optical field can be an image (often scaled down) of a mask placed in the beam path or the Fourier transform of the mask. The most commonly used non-Gaussian profile is the so-called "top hat" or ("flat top") beam that has a uniform intensity distribution on the focal plane. Top hat beams are preferred in laser processing because the uniform intensity will not cause the center part of the Gaussian beam to create nonuniform processing results. Sanner et al. used a nonpixelated optically addressed liquid-crystal light valve to create top hat beams (among other beam shapes), and femtosecond laser drilling using the generated beams was demonstrated as shown in Figs. 25(*a*) and 25(*b*) [413,414]. Squared and circular top hat beams are generated by Li et al. using a spatial light modulator in an image-based configuration [415]. In that study, ultrafast laser machining was performed with titanium samples, and the machined features were found to be consistent with the designed beam shape.

Another type of beam shape that has drawn attention lately is the Bessel and annular beam. Bessel beam belongs to the propagation-invariant optical field whose transverse intensity distribution stays the same along the axial (beam propagation) direction [416], whereas annular (or doughnut) beams can be generated using the Bessel mode or other optical fields that have an intensity null at the center. If the location of the intensity null also has a phase

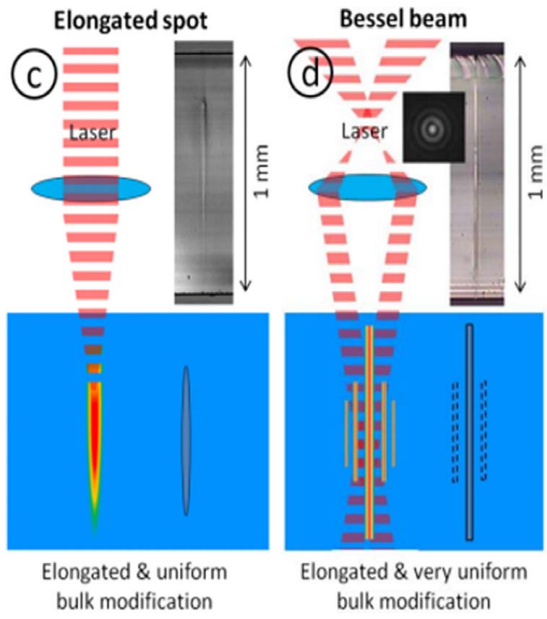

Fig. 25 Examples of material processing using spatial beam shaping in the axial direction to create Bessel-like beams [412] (reprinted with permission from LIA)

singularity, those annular beams are often called vortex beams or beams with orbital angular momentum. One can refer to Duocastella and Arnold for a review on using these beams for material processing [417]. Recently, Wetzel et al. reported femtosecond laser ablation of graphene using vortex Bessel beams [418]. Damage morphologies can be controlled by single and a sequence of pulses that have different topological charges (orders of the phase singularity). The same type of beams were used by Sahin et al. to study femtosecond laser processing of Au/Cr thin films deposited on quartz substrates with different laser wavelengths and Bessel beam cone angles [419]. In a study by Cheng and Polynkin, self-focusing and beam deformation were shown to be important in femtosecond back-surface ablation of borosilicate glass [420]. The propagation of high-intensity Bessel beams in dielectrics and the associated nonlinear effects were studied by Xie et al. with the aim to control internal structural modification [421]. Using the zero-order Bessel beam, cutting of soda-lime glass and sapphire was demonstrated by Lopez et al. as shown in Figs. 25(*c*) and 25(*d*) [412]. The side walls of the cut surface have good smoothness, and the side lobes of the Bessel beam have to be taken into consideration even though they have lower intensities than the central lobe. While Bessel beam cutting of glass has been successively demonstrated, applying femtosecond Bessel beam to cut semiconductor materials is still challenging. Grojo et al. used an optical parametric amplifier (OPA) to generate femtosecond laser pulses at a wavelength of 1300 nm, which is transparent for silicon [255]. Their results show that the intensity reached inside silicon is below the damage threshold due to strong nonlinear absorption, which also deformed the Bessel beam profile at high intensities. Superposition of Bessel beams with higher orders can create petal-like beam patterns that still possess the nondiffracting property [422]. These beam shapes have been used in femtosecond laser scribing of glass and metal thin films [423] and two-photon polymerization [424]. A recent review by Stoian et al. gives an account of recent advances in femtosecond Bessel beam processing of materials [425].

5.3 Laser Material Processing With New Light Sources. Lasers used in ultrafast laser material processing typically are solid-state or fiber lasers that output ultrashort pulses with pulse duration of 100 fs to 10 ps, and fundamental wavelength in near infrared (800–1000 nm). With the development of new laser sources, researchers have been exploring new laser–matter interaction regimes which may lead to unprecedented processing results.

5.3.1 Laser-Induced Damage by Few-Cycle Laser Pulses. Laser-induced damage by few-cycle laser pulses (one optical cycle at 800 nm wavelength is 2.67 fs) was experimentally studied in the 1990s [426,427]. The mechanism of damage formation, such as multiphoton, tunneling, and avalanche ionization, was investigated, and the application for precision laser machining was predicted. Morphological changes of silicon including amorphization, melting, re-crystallization, nucleated vaporization, and ablation were studied with pulse duration down to 5 fs [428]. With the increasing availability of few-cycle pulsed lasers, more and more research has been conducted in this pulse duration range toward a better understanding of laser-induced damage. Sanner et al. created 7 fs pulses by self-phase modulation in a hollow-core fiber followed by pulse compression using chirped mirrors and found a correlation between the Keldysh parameter [429] and the determinism of the damage threshold, suggesting that tunneling ionization is predominant for few-cycle pulse durations [430]. Du et al. used few-cycle, UV pulses to study free carrier dynamics in dielectric coatings and found that free carriers in the conduction band will relax into self-trapped excitons, which will cause the incubation effect under repetitive radiation [431]. Utéza et al. studied laser ablation of fused silica in terms of ablation depth and diameter over pulse durations from 7 to 450 fs and concluded that short pulses can achieve high precision in axial material removal [13]. In a recent study, few-cycle pulses have been used to study laser-induced periodic structures [432]. It is found that shortening the pulse duration to a few optic cycles produces surface morphology very different from many-cycle pulses. The mechanism of few-cycle laser pulse-induced damage was studied by Kafka et al. in vacuum and air with single and multiple pulses [433], and a difference between the ambient environments was observed for the morphology of multiple pulse-induced damage. It has been pointed out that care must be taken when handling few-cycle laser pulses due to their high peak power and broad spectrum [434,435]. In particular, the assumption of quasi-monochromatic light, which is often used in describing electromagnetic waves, needs to be revisited for few-cycle pulses.

5.3.2 Laser-Induced Damage at New Spectral Range. The spectral range that can be used for ultrafast laser material processing has been extended from the typical UV-visible-near infrared to XUV and MIR. XUV pulses can be generated by high harmonic generation, and MIR pulses are typically generated by OPA. PMMA was ablated using XUV radiation with pulse duration of 30–100 fs from a free-electron laser [436]. The ablated surfaces exhibited good surface quality, and the results were compared with nanosecond and picosecond XUV ablation. Using an XUV/visible-NIR dual-beam setup, Mocek et al. and Jakubczak et al. investigated the surface structuring of amorphous carbon and PMMA [15,437]. The longer wavelengths (visible-NIR) can interact with the XUV pulse-induced carriers, so the absorption is enhanced. Femtosecond laser-induced damage in germanium (Ge) was studied by Malik et al. using an MIR wavelength of 3.9 μm [14]. Because Ge has low linear absorption at this wavelength, this study reveals nonlinear effects that will be of interest to laser processing applications. Recently, Austin et al. conducted single-shot laser damage experiment on Ge using a wavelength range from 0.78 to 3.6 μm [438]. It was found that the oxide layer together with a thin layer of Ge is removed by the laser beam, and a new model was proposed to address the discrepancies between the currently used models.

5.4 Scalable Nanomanufacturing by Ultrafast Lasers. Ultrafast lasers have shown superior capabilities in nanoscale manufacturing with high resolution, high quality, simple setup, and low request to the environment. To speed up the industrial application and commercialization of these techniques, it is essential to improve their scalability and fabricate nanostructures at an industrially relevant scale. The advance of the techniques of high speed motion stage and high speed galvanometer/polygonal scan head have significantly increased the processing speed for cutting, scribing, etc. However, more technical barriers need to be overcome to make these techniques scalable.

One approach to improve the scalability and throughput is to process multiple features simultaneously. Multiple parallel pulses can be generated by different techniques, such as diffractive optical elements [439], microlens array [440], periodical binary phase mask [441], and spatial light modulator [149,442,443]. The multiple parallel beams have been used to generate complex 2D and 3D structures on different materials. This method can efficiently reduce the processing time for high volume processing of the same feature.

Another effective method is to use non-diffractive Bessel beams instead of the commonly used Gaussian beams, as described in Sec. 5.2.2. Ideal zero-order Bessel beams are formed by axicon lenses from the axially symmetric interference of two plane waves to yield a high-intensity central core surrounded by lower intensity concentric rings. With the same beam diameter, the Bessel beam can maintain high-intensity over a distance much longer than the Rayleigh length of a Gaussian beam. Therefore, the Bessel beam is very efficient to fabricate high aspect ratio nanochannels [444–446]. Figure 26 shows a channel with a diameter of 400 nm and a length of 43 μm created by a single Bessel pulse in glass.

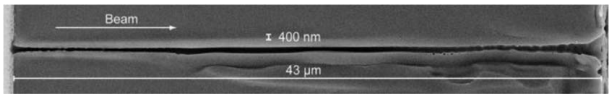

Fig. 26 A high aspect ratio nanochannel fabricated by a single femtosecond Bessel pulse [446] (reprinted with permission from AIP Publishing)

It should be pointed out that the Bessel beam is only effective to treat transparent materials to take advantage of its long intensity distribution length.

As described in Sec. 4.2, laser surface micro/nanostructuring could be a highly scalable technique. The nanoscale laser-induced periodic surface structures are formed and self-organized within the whole laser irradiation area. They are created within a few hundreds of ps and do not need super focusing of the laser beam. With the help of high speed laser scanning head, nanoscale surface structures can be potentially fabricated on a 1 m^2 surface within 30 min by a high repetition rate ultrafast laser (assuming 1.5 m/s scanning speed, 2 kHz repetition rate, 1 mm spot diameter, and 50% overlapping ratio).

5.5 Other Emerging Application Areas of Ultrafast Laser-Based Manufacturing. Ultrafast laser-based manufacturing is becoming a powerful and comprehensive platform for various applications. There are many innovative techniques invented for manufacturing emergent micro-to-nano devices and addressing the technical challenges of modern life. These fields include, but are not limited to, the following.

Ultrafast laser-based nanojoining is emergent as a crucial manufacturing method for nanodevices [447,448]. Nanojoining is an essential step to construct nanodevices through joining nanoscopic building blocks with strong bonds (metallic or covalent bonds, not a weak bonding force like Van der Waals, hydrogen bonds, or capillary force) and forming permanent bonding. It is important to point out that nanojoining is different from selected growth, which is a popular method to assemble nanomaterials, such as homogenous and heterogeneous nanowire junctions [449]. Nanojoining allows bottom-up manufacturing and assembles hybrid structures by joining dissimilar nanomaterials, maximizing the unique properties of nanomaterials. Femtosecond laser-induced sintering of silver nanoparticles has been demonstrated [450]. The experiment displayed that a very low laser fluence down to 900 $\mu J/cm^2$ is needed to melt silver nanoparticles. The self-localized joining mechanism is similar to plasmonic joining, in which silver nanowires are melted and joined at hot-spots due to localized plasmonic excitation [451,452]. It has been widely shown that nanoparticles can melt at a lower temperature than the bulk melting point due to size effects; molecular dynamics simulation predicts surface melting that also occurs at a lower temperature than the melting point of nanoparticles [453,454]. This result indicates that the sintering of nanomaterials can be induced by surface melting. Recently, silver nanowires were also joined with a focused 532 nm CW laser [455,456] and femtosecond laser [457]. Controllable multilevel memory is demonstrated in joined titania nanowires [458]. Moreover, a super-sensitive glucose sensor was fabricated by joining a single copper nanowire to silver film [459]. Shown in Fig. 27, a copper nanowire bridges a silver film gap cut by laser beam. After joining the two ends of the copper nanowire, electronic resistance decreased from 1 k Ω to 200 Ω. Such a joined single copper nanowire can sense glucose at a concentration as low as 10^{-6} M [459]. It is thus reasonable to predict that more applications of joined nanodevices can come to real world applications with further maturation of laser-based nanojoining.

New materials and new phases synthesized via femtosecond laser-induced micro-explosions have also appeared as a hot research topic [460]. Electron ejection due to ultrafast laser–matter interaction will lead to a Coulomb explosion of positively charged ions after laser-induced vaporization of electrons. This Coulomb explosion is confined in a microscale space in the vicinity of the focal spot. High-temperature and high-pressure conditions can be used for the synthesis of new materials, as well. Hu et al. reported that *sp*-bonded carbon chains can be formed on a graphite surface using femtosecond laser irradiation associated with the formation of amorphous tetrahedral carbon (diamond-like carbon) [461]. This *sp*-bonded carbon chain species can be precursors for various carbon allotropes, including carbon nanotubes, fullerenes, and carbynes [462]. Rapp et al. reported a new tetragonal polymorph of silicon induced by confined micro-explosions [463]. On the other hand, laser peening induced by fs laser pulses can be used as a powerful surface treatment tool for metals [464]. Femtosecond laser peening research was motivated by the process simplicity and high shock pressure attainable with fs pulses in comparison to ns laser peening. More recently, encouraging results in terms of compressive residual stress and hardness enhancement were reported in fs laser peening of aluminum [465] and steel [466] free from a protective coating and a transparent overlay. Hence, it can be said that ultrafast laser peening has shown promising results but more research is needed in this area.

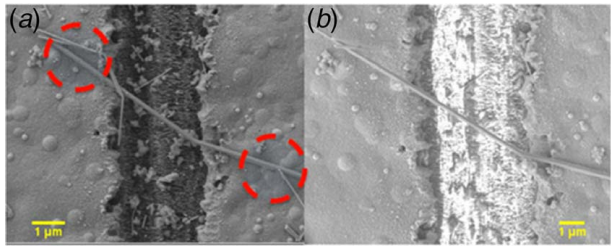

Fig. 27 Femtosecond laser joining of single Cu nanowire. The silver film width is 4 μm. (*a*) Before joining. Two dashed circles indicate the joining site. (*b*) After laser joining. The thin Cu nanowires were blown away by laser illumination.

6 Summary and Future Research Needs

This comprehensive review exposes a wide range of research activities utilizing ultrafast lasers, with a focus on fs laser applications in manufacturing processes. From surface structuring to machining in bulk to scalable manufacturing, fs lasers have been shown to be a crucial tool in the world of precision micro and nanomachining for a wide variety of materials, ranging from metals to dielectrics to biomaterials. Since the inception of high power ultrafast lasers over three decades ago, various advanced ultrafast light sources have emerged today and become more powerful (e.g., TW level), more colorful (from XUV to mid-IR), much shorter in pulse duration (e.g., attoseconds), and more economical (e.g., fs fiber laser), which opens up many new opportunities in manufacturing process innovation. Further down the road, here are some future research needs in ultrafast laser-based manufacturing.

(1) Laser–matter interaction under irradiation with ultrahigh intensities, few-cycle pulses, mid-IR wavelengths
(2) Micro/nanomachining using shaped beams
(3) Laser-induced material phase synthesis
(4) Additive manufacturing at micro/nanoscale (e.g., nanojoining)
(5) Micro/nanomachining at industrially relevant scale
(6) Micro/nanosurgery
(7) Nanowelding and nanojoining

References

[1] Paschotta, R., 2018, "Article on 'Ultrafast Lasers' in the Encyclopedia of Laser Physics and Technology," https://www.rp-photonics.com/ultrafast_lasers.html, Accessed February 6, 2018.
[2] Sadasivam, S., Chan, M. K. Y., and Darancet, P., 2017, "Theory of Thermal Relaxation of Electrons in Semiconductors," Phys. Rev. Lett., **119**(13), p. 136602.

[3] Rose, M., 2010, "A History of the Laser: A Trip Through the Light Fantastic," https://www.photonics.com/a42279/A_History_of_the_Laser_A_Trip Through_the_Light, Accessed February 3,2018.
[4] DeMaria, A. J., Stetser, D. A., and Heynau, H., 1966, "Self Mode Locking of Lasers With Saturable Absorbers," Appl. Phys. Lett., **8**(7), pp. 174–176.
[5] Shank, C. V., and Ippen, E. P., 1974, "Subpicosecond Kilowatt Pulses From a Mode Locked cw Dye Laser," Appl. Phys. Lett., **24**(8), pp. 373–376.
[6] Haus, H. A., 1975, "Theory of Mode Locking With a Fast Saturable Absorber," J. Appl. Phys., **46**(7), pp. 3049–3058.
[7] Spence, D. E., Kean, P. N., and Sibbett, W., 1991, "60-fsec Pulse Generation From a Self-Mode-Locked Ti:Sapphire Laser," Opt. Lett., **16**(1), pp. 42–44.
[8] Sibbett, W., Lagatsky, A. A., and Brown, C. T. A., 2012, "The Development and Application of Femtosecond Laser Systems," Opt. Express, **20**(7), pp. 6989–7001.
[9] Sutter, D. H., Jung, I. D., Kärtner, F. X., Matuschek, N., Morier-Genoud, F., Scheuer, V., Tilsch, M., Tschudi, T., and Keller, U., 1998, "Self-Starting 6.5-fs Pulses From a Ti: Sapphire Laser Using a Semiconductor Saturable Absorber and Double-Chirped Mirrors," IEEE J. Sel. Top. Quantum Electron., **4**(2), pp. 169–178.
[10] Strickland, D., and Mourou, G., 1985, "Compression of Amplified Chirped Optical Pulses," Opt. Commun., **56**(3), pp. 219–221.
[11] Mottay, E., Liu, X., Zhang, H., Mazur, E., Sanatinia, R., and Pfleging, W., 2016, "Industrial Applications of Ultrafast Laser Processing," MRS Bull., **41**(12), pp. 984–992.
[12] Lei, S., Yang, G., Wang, X., Chen, S., Prieb, A., and Ma, J., 2018, "High Energy Femtosecond Laser Peening of 2024 Aluminum Alloy," Procedia CIRP, **74**, pp. 357–361.
[13] Utéza, O., Sanner, N., Chimier, B., Brocas, A., Varkentina, N., Sentis, M., Lassonde, P., Légaré, F., and Kieffer, J. C., 2011, "Control of Material Removal of Fused Silica With Single Pulses of Few Optical Cycles to Sub-Picosecond Duration," Appl. Phys. A, **105**(1), pp. 131–141.
[14] Malik, R., Mills, B., Price, J. H. V., Petrovich, M., Moktadir, Z., Li, Z., and Rutt, H. N., 2013, "Determination of the Mid-IR Femtosecond Surface-Damage Threshold of Germanium," Appl. Phys. A, **113**(1), pp. 127–133.
[15] Mocek, T., Polan, J., Homer, P., Jakubczak, K., Rus, B., Kim, I. J., Kim, C. M., Lee, G. H., Nam, C. H., Hájková, V., Chalupský, J., and Juha, L., 2009, "Surface Modification of Organic Polymer by Dual Action of Extreme Ultraviolet/Visible-Near Infrared Ultrashort Pulses," J. Appl. Phys., **105**(2), p. 26105.
[16] Fermann, M. E., and Hartl, I., 2013, "Ultrafast Fiber Lasers," Nat. Photonics, **7**(11), pp. 868–874.
[17] Eidam, T., Hanf, S., Seise, E., Andersen, T. V., Gabler, T., Wirth, C., Schreiber, T., Limpert, J., and Tünnermann, A., 2010, "Femtosecond Fiber CPA System Emitting 830 W Average Output Power," Opt. Lett., **35**(2), pp. 94–96.
[18] Hamad, A. H., 2016, "Effects of Different Laser Pulse Regimes (Nanosecond, Picosecond and Femtosecond) on the Ablation of Materials for Production of Nanoparticles in Liquid Solution," *High Energy and Short Pulse Lasers*, R. Viskup, ed., IntechOpen, London.
[19] Sanner, N., Huot, N., Audouard, E., Larat, C., Laporte, P., and Huignard, J. P., 2005, "100-kHz Diffraction-Limited Femtosecond Laser Micromachining," Appl. Phys. B: Lasers Opt., **80**(1), pp. 27–30.
[20] Chichkov, B. N., Momma, C., Nolte, S., von Alvensleben, F., and Tünnermann, A., 1996, "Femtosecond, Picosecond and Nanosecond Laser Ablation of Solids," Appl. Phys. A, **63**(2), pp. 109–115.
[21] Sokolowski-Tinten, K., Bialkowski, J., Cavalleri, A., von der Linde, D., Oparin, A., Meyer-ter-Vehn, J., and Anisimov, S., 1998, "Transient States of Matter During Short Pulse Laser Ablation," Phys. Rev. Lett., **81**(1), pp. 224–227.
[22] Perez, D., and Lewis, L., 2003, "Molecular-Dynamics Study of Ablation of Solids Under Femtosecond Laser Pulses," Phys. Rev. B, **67**(18), p. 184102.
[23] Nedialkov, N. N., Imamova, S. E., Atanasov, P. A., Berger, P., and Dausinger, F., 2005, "Mechanism of Ultrashort Laser Ablation of Metals: Molecular Dynamics Simulation," Appl. Surf. Sci., **247**(1–4), pp. 243–248.
[24] Lorazo, P., Lewis, L. J., and Meunier, M., 2003, "Short-Pulse Laser Ablation of Solids: From Phase Explosion to Fragmentation," Phys. Rev. Lett., **91**(22), p. 225502.
[25] Vidal, F., Johnston, T. W., Laville, S., Barthélemy, O., Chaker, M., Le Drogoff, B., Margot, J., and Sabsabi, M., 2001, "Critical-Point Phase Separation in Laser Ablation of Conductors," Phys. Rev. Lett., **86**(12), pp. 2573–2576.
[26] Perez, D., and Lewis, L. J., 2002, "Ablation of Solids Under Femtosecond Laser Pulses," Phys. Rev. Lett., **89**(25), p. 255504.
[27] Stoian, R., Ashkenasi, D., Rosenfeld, A., and Campbell, E. E. B., 2000, "Coulomb Explosion in Ultrashort Pulsed Laser Ablation of Al_2O_3," Phys. Rev. B, **62**(19), pp. 13167–13173.
[28] Reif, J., Costache, F., Eckert, S., and Henyk, M., 2004, "Mechanisms of Ultra-Short Laser Pulse Ablation From Ionic Crystals," Appl. Phys. A, **79**(4–6), pp. 1229–1231.
[29] Bulgakova, N., Stoian, R., Rosenfeld, A., Hertel, I., and Campbell, E. E. B., 2004, "Electronic Transport and Consequences for Material Removal in Ultrafast Pulsed Laser Ablation of Materials," Phys. Rev. B, **69**(5), p. 054102.
[30] Zhao, X., and Shin, Y. C., 2013, "Coulomb Explosion and Early Plasma Generation During Femtosecond Laser Ablation of Silicon at High Laser Fluence," J. Phys. D: Appl. Phys., **46**(33), p. 335501.
[31] Kudryashov, S. I., Saraeva, I. N., Lednev, V. N., Pershin, S. M., Rudenko, A. A., and Ionin, A. A., 2018, "Single-Shot Femtosecond Laser Ablation of Gold Surface in Air and Isopropyl Alcohol," Appl. Phys. Lett., **112**(20), p. 203101.
[32] Cao, X. W., Chen, Q. D., Fan, H., Zhang, L., Juodkazis, S., and Sun, H. B., 2018, "Liquid-Assisted Femtosecond Laser Precision Machining of Silica," Nanomaterials, **8**(5), p. 287.
[33] Banks, P. S., Stuart, B. C., Komashko, A. M., Feit, M. D., Rubenchik, A. M., and Perry, M. D., 2000, "Femtosecond Laser Materials Processing," Proceedings of Commercial and Biomedical Applications of Ultrafast Lasers II, San Jose, CA, Jan. 24–25, Vol. 3934, pp. 14–21.
[34] Laville, S., Vidal, F., Johnston, T. W., Barthélemy, O., Chaker, M., Drogoff, B. L., Margot, J., and Sabsabi, M., 2002, "Fluid Modeling of the Laser Ablation Depth as a Function of the Pulse Duration for Conductors," Phys. Rev. E, **66**(6), p. 066415.
[35] Nolte, S., Momma, C., Jacobs, H., Tünnermann, A., Chichkov, B. N., Wellegehausen, B., and Welling, H., 1997, "Ablation of Metals by Ultrashort Laser Pulses," J. Opt. Soc. Am. B, **14**(10), pp. 2716–2722.
[36] Nedialkov, N. N., Imamova, S. E., and Atanasov, P. A., 2004, "Ablation of Metals by Ultrashort Laser Pulses," J. Phys. D: Appl. Phys., **37**(4), pp. 638–643.
[37] Hashida, M., Semerok, A. F., Gobert, O., Petite, G., Izawa, Y., and Wagner, J. F., 2002, "Ablation Threshold Dependence on Pulse Duration for Copper," Appl. Surf. Sci., **197–198**, pp. 862–867.
[38] Le Harzic, R., Breitling, D., Weikert, M., Sommer, S., Föhl, C., Dausinger, F., Valette, S., Donnet, C., and Audouard, E., 2005, "Ablation Comparison With Low and High Energy Densities for Cu and Al With Ultra-Short Laser Pulses," Appl. Phys. A, **80**(7), pp. 1589–1593.
[39] Furusawa, K., Takahashi, K., Kumagai, H., Midorikawa, K., and Obara, M., 1999, "Ablation Characteristics of Au, Ag, and Cu Metals Using a Femtosecond Ti:Sapphire Laser," Appl. Phys. A, **69**(7), pp. S359–S366.
[40] Zhao, X., and Shin, Y. C., 2013, "Femtosecond Laser Ablation of Aluminum in Vacuum and Air at High Laser Intensity," Appl. Surf. Sci., **283**, pp. 94–99.
[41] Zeng, X., Mao, X. L., Greif, R., and Russo, R. E., 2005, "Experimental Investigation of Ablation Efficiency and Plasma Expansion During Femtosecond and Nanosecond Laser Ablation of Silicon," Appl. Phys. A, **80**(2), pp. 237–241.
[42] Hu, W., Shin, Y. C., and King, G., 2012, "Characteristics of Plume Plasma and Its Effects on Ablation Depth During Ultrashort Laser Ablation of Copper in Air," J. Phys. D: Appl. Phys., **45**(35), p. 355204.
[43] Zhao, X., and Shin, Y. C., 2013, "Ablation Dynamics of Silicon by Femtosecond Laser and the Role of Early Plasma," ASME J. Manuf. Sci. Eng., **135**(6), p. 061015.
[44] Hu, W., Shin, Y. C., and King, G. B., 2011, "Effect of Air Breakdown With a Focusing Lens on Ultrashort Laser Ablation," Appl. Phys. Lett., **99**(23), pp. 1–4.
[45] Hu, W., Shin, Y. C., and King, G. B., 2011, "Early-Stage Plasma Dynamics With Air Ionization During Ultrashort Laser Ablation of Metal," Phys. Plasmas, **18**(9), p. 093302.
[46] Byskov-Nielsen, J., Savolainen, J. M., Christensen, M. S., and Balling, P., 2010, "Ultra-Short Pulse Laser Ablation of Metals: Threshold Fluence, Incubation Coefficient and Ablation Rates," Appl. Phys. A, **101**(1), pp. 97–101.
[47] Mannion, P. T., Magee, J., Coyne, E., O'Connor, G. M., and Glynn, T. J., 2004, "The Effect of Damage Accumulation Behaviour on Ablation Thresholds and Damage Morphology in Ultrafast Laser Micro-Machining of Common Metals in Air," Appl. Surf. Sci., **233**(1–4), pp. 275–287.
[48] Di Niso, F., Gaudiuso, C., Sibillano, T., Mezzapesa, F. P., Ancona, A., and Lugarà, P. M., 2014, "Role of Heat Accumulation on the Incubation Effect in Multi-Shot Laser Ablation of Stainless Steel at High Repetition Rates," Opt. Express, **22**(10), p. 12200.
[49] Neuenschwander, B., Jaeggi, B., Schmid, M., Dommann, A., Neels, A., Bandi, T., and Hennig, G., 2013, "Factors Controlling the Incubation in the Application of Ps Laser Pulses on Copper and Iron Surfaces," Proceedings of SPIE, 8607, Laser Applications in Microelectronic and Optoelectronic Manufacturing (LAMOM) XVIII, San Francisco, CA, Feb. 4–7, p. 86070D.
[50] Nedialkov, N. N., and Atanasov, P. A., 2006, "Molecular Dynamics Simulation Study of Deep Hole Drilling in Iron by Ultrashort Laser Pulses," Appl. Surf. Sci., **252**(13), pp. 4411–4415.
[51] Amoruso, S., Bruzzese, R., Wang, X., O'Connell, G., and Lunney, J. G., 2010, "Multidiagnostic Analysis of Ultrafast Laser Ablation of Metals With Pulse Pair Irradiation," J. Appl. Phys., **108**(11), pp. 1–10.
[52] Semerok, A., and Dutouquet, C., 2004, "Ultrashort Double Pulse Laser Ablation of Metals," Thin Solid Films, **453–454**, pp. 501–505.
[53] Povarnitsyn, M. E., Itina, T. E., Khishchenko, K. V., and Levashov, P. R., 2009, "Suppression of Ablation in Femtosecond Double-Pulse Experiments," Phys. Rev. Lett., **103**(19), p. 195002.
[54] Singha, S., Hu, Z., and Gordon, R. J., 2008, "Ablation and Plasma Emission Produced by Dual Femtosecond Laser Pulses," J. Appl. Phys., **104**(11), p. 113520.
[55] Penczak, J., Kupfer, R., Bar, I., and Gordon, R. J., 2014, "The Role of Plasma Shielding in Collinear Double-Pulse Femtosecond Laser-Induced Breakdown Spectroscopy," Spectrochim. Acta, Part B, **97**, pp. 34–41.
[56] Hu, Z., Singha, S., Liu, Y., and Gordon, R. J., 2007, "Mechanism for the Ablation of Si ⟨111⟩ With Pairs of Ultrashort Laser Pulses," Appl. Phys. Lett., **90**(13), pp. 2005–2008.
[57] Choi, T. Y., Hwang, D. J., and Grigoropoulos, C. P., 2002, "Femtosecond Laser Induced Ablation of Crystalline Silicon Upon Double Beam Irradiation," Appl. Surf. Sci., **197–198**, pp. 720–725.
[58] Zhao, X., and Shin, Y. C., 2014, "Ablation Enhancement of Silicon by Ultrashort Double-Pulse Laser Ablation," Appl. Phys. Lett., **105**(11), p. 111907.
[59] Abeln, T., Radtke, J., and Dausinger, F., 1999, "High Precision Drilling With Short-Pulsed Solid-State Lasers," Proceedings of ICALEO, San Diego, CA, Nov. 15-18.
[60] Foehl, C., Breitling, D., and Dausinger, F. H., 2003, "Precise Drilling of Steel With Ultrashort Pulsed Solid State Lasers," Proc. SPIE, **5121**, pp. 271–279.

[61] Foehihl, C., and Dausinger, F., 2003, "High Precision Deep Drilling With Ultrashort Pulses," Proc. SPIE, **5063**, pp. 346–351.
[62] Kamlage, G., Bauer, T., Ostendorf, A., and Chichkov, B. N., 2003, "Deep Drilling of Metals by Femtosecond Laser Pulses," Appl. Phys. A, **77**(2), pp. 307–310.
[63] Yang, J., Zhao, Y., Zhang, N., Liang, Y., and Wang, M., 2007, "Ablation of Metallic Targets by High-Intensity Ultrashort Laser Pulses," Phys. Rev. B, **76**(16), p. 165430.
[64] Crawford, T. H. R., Borowiec, A., and Haugen, H. K., 2005, "Femtosecond Laser Micromachining of Grooves in Silicon With 800 Nm Pulses," Appl. Phys. A, **80**(8), pp. 1717–1724.
[65] Borowiec, A., and Haugen, H. K., 2004, "Femtosecond Laser Micromachining of Grooves in Indium Phosphide," Appl. Phys. A, **79**(3), pp. 521–529.
[66] Matsumura, T., Nakatani, T., and Yagi, T., 2007, "Deep Drilling on a Silicon Plate With a Femtosecond Laser: Experiment and Model Analysis," Appl. Phys. A, **86**(1), pp. 107–114.
[67] Bärsch, N., Körber, K., Ostendorf, A., and Tönshoff, K. H., 2003, "Ablation and Cutting of Planar Silicon Devices Using Femtosecond Laser Pulses," Appl. Phys. A, **77**(2), pp. 237–242.
[68] Nikumb, S., Chen, Q., Li, C., Reshef, H., Zheng, H. Y., Qiu, H., and Low, D., 2005, "Precision Glass Machining, Drilling and Profile Cutting by Short Pulse Lasers," Thin Solid Films, **477**(1–2), pp. 216–221.
[69] Lim, Y. C., Altman, K. J., Farson, D. F., and Flores, K. M., 2009, "Micropillar Fabrication on Bovine Cortical Bone by Direct-Write Femtosecond Laser Ablation," J. Biomed. Opt., **14**(6), p. 064021.
[70] Liu, Y., Zhang, R., Li, W., Wang, J., Yang, X., Cheng, L., and Zhang, L., 2018, "Effect of Machining Parameter on Femtosecond Laser Drilling Processing on SiC/SiC Composites," Int. J. Adv. Manuf. Technol., **96**(5–8), pp. 1795–1811.
[71] Romoli, L., Lovicu, G., Rashed, C. A. A., Dini, G., De Sanctis, M., and Fiaschi, M., 2015, "Microstructural Changes Induced by Ultrashort Pulsed Lasers in Microdrilling of Fuel Nozzles," Procedia CIRP, **33**, pp. 508–513.
[72] Breitling, D., Ruf, A., and Dausinger, F., 2004, "Fundamental Aspects in Machining of Metals With Short and Ultrashort Laser Pulses," Proc. SPIE, **5339**, pp. 49–63.
[73] Breitling, D., Ruf, A., Berger, P. W., Dausinger, F., Klimentov, S. M., Pivovarov, P. A., Kononenko, T. V., and Konov, V. I., 2003, "Plasma Effects During Ablation and Drilling Using Pulsed Solid-State Lasers," Proceedings of SPIE, 5121, Laser Processing of Advanced Materials and Laser Microtechnologies, Moscow, Russia, June 22–27, 2002, pp. 24–33.
[74] Nibbering, E. T., Curley, P. F., Grillon, G., Prade, B. S., Franco, M., Salin, F., and Mysyrowicz, A., 1996, "Conical Emission From Self-Guided Femtosecond Pulses in Air," Opt. Lett., **21**(1), pp. 62–65.
[75] Ancona, A., Röser, F., Rademaker, K., Limpert, J., Nolte, S., and Tünnermann, A., 2008, "High Speed Laser Drilling of Metals Using a High Repetition Rate, High Average Power Ultrafast Fiber CPA System," Opt. Express, **16**(12), pp. 8958–8968.
[76] Lapczyna, M., Chen, K. P., Herman, P. R., Tan, H. W., and Marjoribanks, R. S., 1999, "Ultra High Repetition Rate (133 MHz) Laser Ablation of Aluminum With 1.2-Ps Pulses," Appl. Phys. A Mater. Sci. Process., **69**(7), pp. S883–S886.
[77] Kondo, Y., Qiu, J., Mitsuyu, T., Hirao, K., and Yoko, T., 1999, "Three-Dimensional Microdrilling of Glass by Multiphoton Process and Chemical Etching," Jpn. J. Appl. Phys., **38**(10A), pp. L1146–L1148.
[78] Cheng, Y., Sugioka, K., and Midorikawa, K., 2004, "Microfluidic Laser Embedded in Glass by Three-Dimensional Femtosecond Laser Microprocessing," Opt. Lett., **29**(17), pp. 2007–2009.
[79] Kiyama, S., Matsuo, S., Hashimoto, S., and Morihira, Y., 2009, "Examination of Etching Agent and Etching Mechanism on Femtosecond Laser Microfabrication of Channels Inside Vitreous Silica Substrates," J. Phys. Chem. C, **113**(27), pp. 11560–11566.
[80] Wortmann, D., Gottmann, J., Brandt, N., and Horn-Solle, H., 2008, "Micro- and Nanostructures Inside Sapphire by Fs-Laser Irradiation and Selective Etching," 2008 Conference on Quantum Electron and Conference on Lasers and Electro-Optics, CLEO/QELS, San Jose, CA, May 4–9, pp. 197–200.
[81] Bellouard, Y., Said, A., Dugan, M., and Bado, P., 2004, "Fabrication of High-Aspect Ratio, Micro-Fluidic Channels and Tunnels Using Femtosecond Laser Pulses and Chemical Etching," Opt. Express, **12**(10), pp. 2120–2129.
[82] Marcinkevičius, A., Juodkazis, S., Watanabe, M., Miwa, M., Matsuo, S., Misawa, H., and Nishii, J., 2001, "Femtosecond Laser-Assisted Three-Dimensional Microfabrication in Silica," Opt. Lett., **26**(5), pp. 277–279.
[83] Ran, A., Yan, L., Yan-Ping, D., Ying, F., Hong, Y., and Qi-Huang, G., 2004, "Laser Micro-Hole Drilling of Soda-Lime Glass With Femtosecond Pulses," Chin. Phys. Lett., **21**(12), pp. 2465–2468.
[84] Hwang, D. J., Choi, T. Y., and Grigoropoulos, C. P., 2004, "Liquid-Assisted Femtosecond Laser Drilling of Straight and Three-Dimensional Microchannels in Glass," Appl. Phys. A, **79**(3), pp. 605–612.
[85] Li, Y., Itoh, K., Watanabe, W., Yamada, K., Kuroda, D., Nishii, J., and Jiang, Y., 2001, "Three-Dimensional Hole Drilling of Silica Glass From the Rear Surface With Femtosecond Laser Pulses," Opt. Lett., **26**(23), pp. 1912–1914.
[86] Zhao, X., and Shin, Y. C., 2011, "Femtosecond Laser Drilling of High-Aspect Ratio Microchannels in Glass," Appl. Phys. A, **104**(2), pp. 713–719.
[87] Liao, Y., Ju, Y., Zhang, L., He, F., Zhang, Q., Shen, Y., Chen, D., Cheng, Y., Xu, Z., Sugioka, K., and Midorikawa, K., 2010, "Three-Dimensional Microfluidic Channel With Arbitrary Length and Configuration Fabricated Inside Glass by Femtosecond Laser Direct Writing," Opt. Lett., **35**(19), pp. 3225–3227.
[88] Xia, B., Jiang, L., Li, X., Yan, X., Zhao, W., and Lu, Y., 2015, "High Aspect Ratio, High-Quality Microholes in PMMA: A Comparison Between Femtosecond Laser Drilling in Air and in Vacuum," Appl. Phys. A, **119**(1), pp. 61–68.
[89] Pronko, P. P., Dutta, S. K., Squier, J., Rudd, J. V., Du, D., and Mourou, G., 1995, "Machining of Sub-Micron Holes Using a Femtosecond Laser at 800 nm," Opt. Commun., **114**(1–2), pp. 106–110.
[90] Joglekar, A. P., Liu, H., Spooner, G. J., Meyhöfer, E., Mourou, G., and Hunt, A. J., 2003, "A Study of the Deterministic Character of Optical Damage by Femtosecond Laser Pulses and Applications to Nanomachining," Appl. Phys. B, **77**(1), pp. 25–30.
[91] Simon, P., and Ihlemann, J., 1997, "Ablation of Submicron Structures on Metals and Semiconductors by Femtosecond UV-Laser Pulses," Appl. Surf. Sci., **109–110**, pp. 25–29.
[92] Bravo, H., Szapiro, B. T., Wachulak, P. W., Marconi, M. C., Chao, W., Anderson, E. H., Menoni, C. S., and Rocca, J. J., 2012, "Demonstration of Nanomachining With Focused Extreme Ultraviolet Laser Beams," IEEE J. Sel. Top. Quantum Electron., **18**(1), pp. 443–448.
[93] Yu, X., Bian, Q., Chang, Z., Corkum, P. B., and Lei, S., 2013, "Femtosecond Laser Nanomachining Initiated by Ultraviolet Multiphoton Ionization," Opt. Express, **21**(20), pp. 24185–24190.
[94] Yu, X., Chang, Z., Corkum, P. B., and Lei, S., 2014, "Fabricating Nanostructures on Fused Silica Using Femtosecond Infrared Pulses Combined With Sub-Nanojoule Ultraviolet Pulses," Opt. Lett., **39**(19), pp. 5638–5640.
[95] Götte, N., Winkler, T., Meinl, T., Kusserow, T., Zielinski, B., Sarpe, C., Senftleben, A., Hillmer, H., and Baumert, T., 2016, "Temporal Airy Pulses for Controlled High Aspect Ratio Nanomachining of Dielectrics," Opt. Mater. Express, **3**(4), pp. 389–395.
[96] Chimmalgi, A., Choi, T. Y., Grigoropoulos, C. P., and Komvopoulos, K., 2003, "Femtosecond Laser Aperturless Near-Field Nanomachining of Metals Assisted by Scanning Probe Microscopy," Appl. Phys. Lett., **82**(8), pp. 1146–1148.
[97] Lin, Y., Hong, M. H., Wang, W. J., Law, Y. Z., and Chong, T. C., 2005, "Sub-30 Nm Lithography With Near-Field Scanning Optical Microscope Combined With Femtosecond Laser," Appl. Phys. A, **80**(3), pp. 461–465.
[98] Chen, C. Y., Tsai, M. W., Chuang, T. H., Chang, Y. T., and Lee, S. C., 2007, "Extraordinary Transmission Through a Silver Film Perforated With Cross Shaped Hole Arrays in a Square Lattice," Appl. Phys. Lett., **91**(6), p. 063108.
[99] Srituravanich, W., Fang, N., Sun, C., Luo, Q., and Zhang, X., 2004, "Plasmonic Nanolithography," Nano Lett., **4**(6), pp. 1085–1088.
[100] Genet, C., and Ebbesen, T. W., 2007, "Light in Tiny Holes," Nature Mater., **445**(7123), pp. 39–46.
[101] Kato, J. I., Takeyasu, N., Adachi, Y., Sun, H.-B., and Kawata, S., 2005, "Multiple-Spot Parallel Processing for Laser Micronanofabrication," Appl. Phys. Lett., **86**(4), p. 044102.
[102] Lim, C. S., Hong, M. H., Lin, Y., Xie, Q., Luk'Yanchuk, B. S., Senthil Kumar, A., and Rahman, M., 2006, "Microlens Array Fabrication by Laser Interference Lithography for Super-Resolution Surface Nanopatterning," Appl. Phys. Lett., **89**(19), p. 191125.
[103] Choi, W. K., Liew, T. H., Dawood, M. K., Smith, H. I., Thompson, C. V., and Hong, M. H., 2008, "Synthesis of Silicon Nanowires and Nanofin Arrays Using Interference Lithography and Catalytic Etching," Nano Lett., **8**(11), pp. 3799–3802.
[104] Liao, Y., Cheng, Y., Liu, C., Song, J., He, F., Shen, Y., Chen, D., Xu, Z., Fan, Z., Wei, X., Sugioka, K., and Midorikawa, K., 2013, "Direct Laser Writing of Sub-50 Nm Nanofluidic Channels Buried in Glass for Three-Dimensional Micro-Nanofluidic Integration," Lab Chip, **13**(8), pp. 1626–1631.
[105] Shimotsuma, Y., Kazansky, P. G., Qiu, J., and Hirao, K., 2003, "Self-Organized Nanogratings in Glass Irradiated by Ultrashort Light Pulses," Phys. Rev. Lett., **91**(24), p. 247405.
[106] Liao, Y., Shen, Y., Qiao, L., Chen, D., Cheng, Y., Sugioka, K., and Midorikawa, K., 2013, "Femtosecond Laser Nanostructuring in Porous Glass With Sub-50 Nm Feature Sizes," Opt. Lett., **38**(2), pp. 187–189.
[107] Buividas, R., Rekštytė, S., Malinauskas, M., and Juodkazis, S., 2013, "Nano-Groove and 3D Fabrication by Controlled Avalanche Using Femtosecond Laser Pulses," Opt. Mater. Express, **3**(10), pp. 1674–1686.
[108] Birnbaum, M., 1965, "Semiconductor Surface Damage Produced by Ruby Lasers," J. Appl. Phys., **36**(11), pp. 3688–3689.
[109] Isenor, N. R., 1977, "CO2 Laser-Induced Ripple Patterns on NixP1-x Surfaces," Appl. Phys. Lett., **31**(3), pp. 148–150.
[110] Maracas, G. N., Harris, G. L., Lee, C. A., and McFarlane, R. A., 1978, "On the Origin of Periodic Surface Structure of Laser-Annealed Semiconductors," Appl. Phys. Lett., **33**(5), pp. 453–455.
[111] Oron, M., and Sørensen, G., 1979, "New Experimental Evidence of the Periodic Surface Structure in Laser Annealing," Appl. Phys. Lett., **35**(10), pp. 782–784.
[112] Ionin, A. A., Kudryashov, S. I., Makarov, S. V., Rudenko, A. A., Seleznev, L. V., Sinitsyn, D. V., Golosov, E. V., Kolobov, Y. R., and Ligachev, A. E., 2013, "Beam Spatial Profile Effect on Femtosecond Laser Surface Structuring of Titanium in Scanning Regime," Appl. Surf. Sci., **284**, pp. 634–637.
[113] Hwang, T. Y., and Guo, C., 2011, "Femtosecond Laser-Induced Blazed Periodic Grooves on Metals," Opt. Lett., **36**(13), pp. 2575–2577.
[114] Vorobyev, A. Y., and Guo, C., 2008, "Femtosecond Laser Blackening of Platinum," J. Appl. Phys., **104**(5), p. 053516.
[115] Lim, H. U., Kang, J., Guo, C., and Hwang, T. Y., 2018, "Manipulation of Multiple Periodic Surface Structures on Metals Induced by Femtosecond Lasers," Appl. Surf. Sci., **454**, pp. 327–333.
[116] Nivas, J. J., Anoop, K. K., Bruzzese, R., Philip, R., and Amoruso, S., 2018, "Direct Femtosecond Laser Surface Structuring of Crystalline Silicon at 400 nm," Appl. Phys. Lett., **112**(12), p. 121601.
[117] Austin, D. R., Kafka, K. R. P., Trendafilov, S., Shvets, G., Li, H., Yi, A. Y., Szafruga, U. B., Wang, Z., Lai, Y. H., Blaga, C. I., DiMauro, L. F., and

Chowdhury, E. A., 2015, "Laser Induced Periodic Surface Structure Formation in Germanium by Strong Field Mid IR Laser Solid Interaction at Oblique Incidence," Optics Express, **23**(15), pp. 19522–19534.
[118] Abere, M. J., Chen, C., Rittman, D. R., Kang, M., Goldman, R. S., Phillips, J. D., Torralva, B., and Yalisove, S. M., 2014, "Nanodot Formation Induced by Femtosecond Laser Irradiation," Appl. Phys. Lett., **105**(16), p. 163103.
[119] Rebollar, E., Vázquez De Aldana, J. R., Pérez-Hernández, J. A., Ezquerra, T. A., Moreno, P., and Castillejo, M., 2012, "Ultraviolet and Infrared Femtosecond Laser Induced Periodic Surface Structures on Thin Polymer Films," Appl. Phys. Lett., **100**(4), p. 041106.
[120] Höhm, S., Rohloff, M., Rosenfeld, A., Krüger, J., and Bonse, J., 2013, "Dynamics of the Formation of Laser-Induced Periodic Surface Structures on Dielectrics and Semiconductors Upon Femtosecond Laser Pulse Irradiation Sequences," Appl. Phys. A, **110**(3), pp. 553–557.
[121] Dufft, D., Rosenfeld, A., Das, S. K., Grunwald, R., and Bonse, J., 2009, "Femtosecond Laser Induced Periodic Surface Structures Revisited: A Comparative Study on ZnO," J. Appl. Phys., **105**(3), p. 034908.
[122] Huang, M., Zhao, F., Cheng, Y., Xu, N., and Xu, Z., 2009, "Mechanisms of Ultrafast Laser Induced Deep Subwavelength Grating on Graphite and Diamond," Phys. Rev. B, **79**(12), p. 125436.
[123] Gnilitskyi, I., Derrien, T. J.-Y., Levy, Y., Bulgakova, N. M., Mocek, T., and Orazi, L., 2017, "High-Speed Manufacturing of Highly Regular Femtosecond Laser Induced Periodic Surface Structures: Physical Origin of Regularity," Sci. Rep., **7**(1), p. 8485.
[124] Reif, J., Costache, F., Henyk, M., and Pandelov, S. V., 2002, "Ripples Revisited: Non-Classical Morphology at the Bottom of Femtosecond Laser Ablation Craters in Transparent Dielectrics," Appl. Surf. Sci., **197–198**, pp. 891–895.
[125] Fraggelakis, F., Stratakis, E., and Loukakos, P. A., 2018, "Control of Periodic Surface Structures on Silicon by Combined Temporal and Polarization Shaping of Femtosecond Laser Pulses," Appl. Surf. Sci., **444**, pp. 154–160.
[126] Bonse, J., Rosenfeld, A., and Krüger, J., 2009, "On the Role of Surface Plasmon Polaritons in the Formation of Laser-Induced Periodic Surface Structures Upon Irradiation of Silicon by Femtosecond Laser Pulses," J. Appl. Phys., **106**(10), p. 104910.
[127] Nivas, J. J. J., Gesuele, F., Allahyari, E., Oscurato, S. L., Fittipaldi, R., Vecchione, A., Bruzzese, R., and Amoruso, S., 2017, "Effects of Ambient Air Pressure on Surface Structures Produced by Ultrashort Laser Pulse Irradiation," Opt. Lett., **42**(14), pp. 2710–2713.
[128] Höhm, S., Rosenfeld, A., Krüger, J., and Bonse, J., 2015, "Laser-Induced Periodic Surface Structures on Titanium Upon Single- and Two-Color Femtosecond Double-Pulse Irradiation," Opt. Express, **23**(20), pp. 25959–25971.
[129] Bonse, J., Munz, M., and Sturm, H., 2005, "Structure Formation on the Surface of Indium Phosphide Irradiated by Femtosecond Laser Pulses," J. Appl. Phys., **97**(1), p. 013538.
[130] Beltaos, A., Kovačević, A. G., Matković, A., Ralević, U., Savić-Šević, S., Jovanovi, D., Jovanović, B. M., and Gajić, R., 2014, "Femtosecond Laser Induced Periodic Surface Structures on Multi-Layer Graphene," J. Appl. Phys., **116**(20), p. 204306.
[131] Sipe, J. E., Young, J. F., Preston, J. S., and Van Driel, H. M., 1983, "Laser-Induced Surface Structure. I Theory," Phys. Rev. B, **27**(2), pp. 1141–1154.
[132] Jost, D., Lüthy, W., and Weber, H. P., 1986, "Recording a Surface Acoustic Wave on the Surface of Silicon," Laser Process. Diagonstics, **2**, pp. 215–219.
[133] Costache, F., Henyk, M., and Reif, J., 2003, "Surface Patterning on Insulators Upon Femtosecond Laser Ablation," Appl. Surf. Sci., **208–209**, pp. 486–491.
[134] He, S., Nivas, J. J. J., Anoop, K. K., Vecchione, A., Hu, M., Bruzzese, R., and Amoruso, S., 2015, "Surface Structures Induced by Ultrashort Laser Pulses: Formation Mechanisms of Ripples and Grooves," Appl. Surf. Sci., **353**, pp. 1214–1222.
[135] Jia, T. Q., Chen, H. X., Huang, M., Zhao, F. L., Qiu, J. R., Li, R. X., Xu, Z. Z., He, X. K., Zhang, J., and Kuroda, H., 2005, "Formation of Nanogratings on the Surface of a ZnSe Crystal Irradiated by Femtosecond Laser Pulses," Phys. Rev. B, **72**(12), p. 125429.
[136] Carey, J. E., Crouch, C. H., and Mazur, E., 2003, "Femtosecond-Laser-Assisted Microstructuring of Silicon Surfaces," Opt. Photonics News, **14**(2), pp. 32–36.
[137] Shen, M. Y., Crouch, C. H., Carey, J. E., and Mazur, E., 2004, "Femtosecond Laser Induced Formation of Submicrometer Spikes on Silicon in Water," Appl. Phys. Lett., **85**(23), pp. 5694–5696.
[138] Nayak, B. K., Gupta, M. C., and Kolasinski, K. W., 2008, "Formation of Nano-Textured Conical Microstructures in Titanium Metal Surface by Femtosecond Laser Irradiation," Appl. Phys. A: Mater. Sci. Process., **90**(3), pp. 399–402.
[139] Li, Y., Cui, Z., Wang, W., Lin, C., and Tsai, H. L., 2015, "Formation of Linked Nanostructure-Textured Mound-Shaped Microstructures on Stainless Steel Surface via Femtosecond Laser Ablation," Appl. Surf. Sci., **324**, pp. 775–783.
[140] Bonse, J., Baudach, S., Krüger, J., Kautek, W., and Lenzner, M., 2002, "Femtosecond Laser Ablation of Silicon–Modification Thresholds and Morphology," Appl. Phys. A: Mater. Sci. Process., **74**(1), pp. 19–25.
[141] Cong, J., Yang, J., Zhao, B., and Xu, X., 2015, "Fabricating Subwavelength Dot-Matrix Surface Structures of Molybdenum by Transient Correlated Actions of Two-Color Femtosecond Laser Beams," Opt. Express, **23**(4), pp. 5357–5367.
[142] Skoulas, E., Manousaki, A., Fotakis, C., and Stratakis, E., 2017, "Biomimetic Surface Structuring Using Cylindrical Vector Femtosecond Laser Beams," Sci. Rep., **7**(1), p. 45114.
[143] Liu, Q., Zhang, N., Yang, J., Qiao, H., and Guo, C., 2018, "Direct Fabricating Large-Area Nanotriangle Structure Arrays on Tungsten Surface by Nonlinear Lithography of Two Femtosecond Laser Beams," Opt. Express, **26**(9), pp. 11718–11727.
[144] Nakata, Y., Okada, T., and Maeda, M., 2003, "Nano-Sized Hollow Bump Array Generated by Single Femtosecond Laser Pulse," Jpn. J. Appl. Phys., **42**(Part 2), pp. L1452–1454.
[145] Nivas, J. J. J., He, S., Song, Z., Rubano, A., Vecchione, A., Paparo, D., Marrucci, L., Bruzzese, R., and Amoruso, S., 2017, "Femtosecond Laser Surface Structuring of Silicon With Gaussian and Optical Vortex Beams," Appl. Surf. Sci., **418**, pp. 565–571.
[146] Oliveira, V., Moreira, R. D. F., de Moura, M. F. S. F., and Vilar, R., 2018, "Surface Patterning of CFRP Composites Using Femtosecond Laser Interferometry," Appl. Phys. A: Mater. Sci. Process., **124**(3), p. 231.
[147] Tan, Y., Chu, W., Lin, J., Fang, Z., Liao, Y., and Cheng, Y., 2018, "Metal Surface Structuring With Spatiotemporally Focused Femtosecond Laser Pulses," J. Opt., **20**(1), p. 014010.
[148] Almeida, G. F. B., Martins, R. J., Otuka, A. J. G., Siqueira, J. P., and Mendonca, C. R., 2015, "Laser Induced Periodic Surface Structuring on Si by Temporal Shaped Femtosecond Pulses," Opt. Express, **23**(21), pp. 27597–27605.
[149] Kuang, Z., Liu, D., Perrie, W., Edwardson, S., Sharp, M., Fearon, E., Dearden, G., and Watkins, K., 2009, "Fast Parallel Diffractive Multi-Beam Femtosecond Laser Surface Micro-Structuring," Appl. Surf. Sci., **255**(13–14), pp. 6582–6588.
[150] Younkin, R., Carey, J. E., Mazur, E., Levinson, J. A., and Friend, C. M., 2003, "Infrared Absorption by Conical Silicon Microstructures Made in a Variety of Background Gases Using Femtosecond-Laser Pulses," J. Appl. Phys., **93**(5), pp. 2626–2629.
[151] Parmar, V., and Shin, Y. C., 2018, "Wideband Anti-Reflective Silicon Surface Structures Fabricated by Femtosecond Laser Texturing," Appl. Surf. Sci., **459**, pp. 86–91.
[152] Vorobyev, A. Y., and Guo, C., 2011, "Direct Creation of Black Silicon Using Femtosecond Laser Pulses," Appl. Surf. Sci., **257**(16), pp. 7291–7294.
[153] Yang, J., Yang, Y., Zhao, B., Wang, Y., and Zhu, X., 2012, "Femtosecond Laser-Induced Surface Structures to Significantly Improve the Thermal Emission of Light From Metals," Appl. Phys. B, **106**(2), pp. 349–355.
[154] Vorobyev, A. Y., and Guo, C., 2010, "Laser Turns Silicon Superwicking," Optics Express, **18**(7), pp. 6455–6460.
[155] Vorobyev, A. Y., and Guo, C., 2013, "Femtosecond Laser Surface Structuring Technique for Making Human Enamel and Dentin Surfaces Superwetting," Appl. Phys. B, **113**(3), pp. 423–428.
[156] Vorobyev, A. Y., and Guo, C., 2015, "Multifunctional Surfaces Produced by Femtosecond Laser Pulses," J. Appl. Phys., **117**(3), p. 033103.
[157] Huang, C., Bell, R., Tsubaki, A., Zuhlke, C. A., and Alexander, D. R., 2018, "Condensation and Subsequent Freezing Delays as a Result of Using Femtosecond Laser Functionalized Surfaces," J. Laser Appl., **30**(1), p. 011501.
[158] Kostal, E., Stroj, S., Kasemann, S., Matylitsky, V., and Domke, M., 2018, "Fabrication of Biomimetic Fog-Collecting Superhydrophilic-Superhydrophobic Surface Micropatterns Using Femtosecond Lasers," Langmuir, **34**(9), pp. 2933–2941.
[159] Kunz, C., Müller, F. A., and Gräf, S., 2018, "Multifunctional Hierarchical Surface Structures by Femtosecond Laser Processing," Materials, **11**(5), p. 789.
[160] Sarbada, S., and Shin, Y. C., 2017, "Superhydrophobic Contoured Surfaces Created on Metal and Polymer Using a Femtosecond Laser," Appl. Surf. Sci., **405**, pp. 465–475.
[161] Yong, J., Chen, F., Yang, Q., Jiang, Z., and Hou, X., 2018, "A Review of Femtosecond-Laser-Induced Underwater Superoleophobility Surfaces," Adv. Mater. Interfaces, **5**, p. 1701370.
[162] Bonse, J., Kirner, S. V., Griepentrog, M., Spaltmann, D., and Krüger, J., 2018, "Femtosecond Laser Texturing of Surfaces for Tribological Applications," Materials, **11**(5), p. 801.
[163] Kawasegi, N., Sugimori, H., Morimoto, H., Morita, N., and Hori, I., 2009, "Development of Cutting Tools With Microscale and Nanoscale Textures to Improve Frictional Behavior," Precis. Eng., **33**(3), pp. 248–254.
[164] Sugihara, T., and Enomoto, T., 2009, "Development of a Cutting Tool With a Nano/Micro-Textured Surface-Improvement of Anti-Adhesive Effect by Considering the Texture Patterns," Precis. Eng., **33**(4), pp. 425–429.
[165] Bonse, J., Höhm, S., Koter, R., Hartelt, M., Spaltmann, D., Pentzien, S., Rosenfeld, A., and Krüger, J., 2016, "Tribological Performance of Sub-100-nm Femtosecond Laser-Induced Periodic Surface Structures on Titanium," Appl. Surf. Sci., **374**, pp. 190–196.
[166] Lei, S., Devarajan, S., and Chang, Z., 2009, "A Study of Micropool Lubricated Cutting Tool in Machining of Mild Steel," J. Mater. Process. Technol., **209**(3), pp. 1612–1620.
[167] Zhang, K., Deng, J., Sun, J., Jiang, C., Liu, Y., and Chen, S., 2015, "Effect of Micro/Nano-Scale Textures on Anti-Adhesive Wear Properties of WC/Co-Based TiAlN Coated Tools in AISI 316 Austenitic Stainless Steel Cutting," Appl. Surf. Sci., **355**, pp. 602–614.
[168] Zhang, K., Deng, J., Ding, Z., Guo, X., and Sun, L., 2017, "Improving Dry Machining Performance of TiAlN Hard-Coated Tools Through Combined Technology of Femtosecond Laser-Textures and WS2 Soft-Coatings," J. Manuf. Processes, **30**, pp. 492–501.
[169] Ling, T. D., Liu, P., Xiong, S., Grzina, D., Cao, J., Wang, Q. J., Xia, Z. C., and Talwar, R., 2013, "Surface Texturing of Drill Bits for Adhesion Reduction and Tool Life Enhancement," Tribol. Lett., **52**(1), pp. 113–122.
[170] Hermann, J., Benfarah, M., Coustillier, G., Bruneau, S., Axente, E., Guillemoles, J.-F., Sentis, M., Alloncle, P., and Itina, T., 2006, "Selective Ablation of Thin Films With Short and Ultrashort Laser Pulses," Appl. Surf. Sci., **252**(13), pp. 4814–4818.

[171] Kim, T. W., Pahk, H. J., Park, H. K., Hwang, D. J., and Grigoropoulos, C. P., 2009, "Comparison of Multilayer Laser Scribing of Thin Film Solar Cells With Femto, Pico and Nanosecond Pulse Durations. Thin Film Solar Technology," Proc. SPIE, A. E. Delahoy and L. A. Eldada, eds., 7409, p. 74090A.
[172] Gečys, P., Raciukaitis, G., Wehrmann, A., Zimmer, K., Braun, A., and Ragnow, S., 2012, "Scribing of Thin-Film Solar Cells With Picosecond and Femtosecond Lasers," J. Laser Micro/Nanoeng., **7**(1), pp. 33–37.
[173] Zhao, X., Cao, Y., Shin, Y. C., Cheng, G., and Nian, Q., 2014, "Precise Selective Scribing of Thin Film Solar Cells by A Picoseconds Laser," Appl. Phys. A: Mater. Sci. Process., **116**(2), pp. 671–681.
[174] Zhao, X., Cao, Y., Nian, Q., Cheng, G., and Shin, Y. C., 2014, "Control of Ablation Depth and Surface Structure in P3 Scribing of Thin-Film Solar Cells by A Picosecond Laser," ASME J. Micro Nano Manuf., **2**(3), p. 031007.
[175] Bayer, L., Ye, X., Lorenz, P., and Zimmer, K., 2017, "Studies on Perovskite Film Ablation and Scribing With ns-, ps- and fs-Laser Pulses," Appl. Phys. A: Mater. Sci. Process., **123**(10), p. 619.
[176] Gečys, P., Markauskas, E., Dudutis, J., and Račiukaitis, G., 2014, "Interaction of Ultrashort Laser Pulses With CIGS and CZTSe Thin Films," Appl. Phys. A: Mater. Sci. Process., **114**(1), pp. 231–241.
[177] Markauskas, E., Geys, P., Repins, I., Beall, C., and Raiukaitis, G., 2017, "Laser Lift-off Scribing of the CZTSe Thin-Film Solar Cells at Different Pulse Durations," Sol. Energy, **150**, pp. 246–254.
[178] Krause, S., Miclea, P. T., and Seifert, G., 2015, "Selective Femtosecond Laser Lift-off Process for Scribing in Thin-Film Photovoltaics," J. Laser Micro/Nanoeng., **10**(3), pp. 274–278.
[179] Wang, H., Yao, Y. L., and Chen, H., 2015, "Removal Mechanism and Defect Characterization for Glass-Side Laser Scribing of CdTe/CdS Multilayer in Solar Cells," ASME J. Manuf. Sci. Eng., **137**(6), p. 061006.
[180] Jeoung, S. C., Lee, H. S., Yahng, J. S., Lee, H. K., Moon, H. Y., Kim, K. J., Lee, D. G., Park, D. H., Yu, Y. S., and Ji, S. J., 2011, "Microstructuring of CIGS Thin Film Coated on Mo Back Contact by Ultrafast Laser 'Rail-Roading' Patterning," Opt. Express, **19**(28), p. 16730.
[181] Zoppel, S., Huber, H., and Reider, G. A., 2007, "Selective Ablation of Thin Mo and TCO Films With Femtosecond Laser Pulses for Structuring Thin Film Solar Cells," Appl. Phys. A: Mater. Sci. Process., **89**(1), pp. 161–163.
[182] Bian, Q., Yu, Y., Zhao, B., Chang, Z., and Lei, S., 2013, "Femtosecond Laser Ablation of Indium Tin-Oxide Narrow Grooves for Thin Film Solar Cells," Opt. Laser Technol., **45(1)**, pp. 395–401.
[183] Krause, S., Miclea, P. T., Steudel, F., Schweizer, S., and Seifert, G., 2014, "Few Micrometers Wide, Perfectly Isolating Scribes in Transparent Conductive Oxide Layers Prepared by Femtosecond Laser Processing," J. Renewable Sustainable Energy, **6**(6), p. 011402.
[184] Yu, X., Ma, J., and Lei, S., 2015, "Femtosecond Laser Scribing of Mo Thin Film on Flexible Substrate Using Axicon Focused Beam," J. Manuf. Processes, **20**, pp. 349–355.
[185] Sahin, R., and Kabacelik, I., 2016, "Nanostructuring of ITO Thin Films Through Femtosecond Laser Ablation," Appl. Phys. A: Mater. Sci. Process., **122**(4), p. 314.
[186] Yu, X., Trallero-Herrero, C. A., and Lei, S., 2016, "Materials Processing With Superposed Bessel Beams," Appl. Surf. Sci., **360**, pp. 833–839.
[187] Chang, T. L., Chen, C. Y., and Wang, C. P., 2013, "Precise Ultrafast Laser Micromachining in Thin-Film CIGS Photovoltaic Modules," Microelectron. Eng., **110**, pp. 381–385.
[188] Chen, C. Y., and Chang, T. L., 2015, "Multilayered Structuring of Thin-Film PV Modules by Ultrafast Laser Ablation," Microelectron. Eng., **143**, pp. 41–47.
[189] Pecholt, B., Vendan, M., Dong, Y., and Molian, P., 2008, "Ultrafast Laser Micromachining of 3C-SiC Thin Films for MEMS Device Fabrication," Int. J. Adv. Manuf. Technol., **39**(3–4), pp. 239–250.
[190] Yuan, D. Q., Zhou, M., Cai, L., and Xu, J. T., 2009, "Processing Microstructure on Film by Femtosecond Laser," Optica Applicata, **39**(3), pp. 629–635.
[191] Halstuch, A., Westreich, O., Sicron, N., and Ishaaya, A., 2018, "Femtosecond Laser Inscription of Bragg Gratings on a Thin GaN Film Grown on a Sapphire Substrate," Opt. Lasers Eng., **109**, pp. 68–72.
[192] Rapp, S., Rosenberger, J., Domke, M., Heise, G., Huber, H. P., and Schmidt, M., 2014, "Ultrafast Pump-Probe Microscopy Reveals the Mechanism of Selective fs Laser Structuring of Transparent Thin Films for Maskless Micropatterning," Appl. Surf. Sci., **290**, pp. 368–372.
[193] Lee, S., Yang, D., and Nikumb, S., 2007, "Femtosecond Laser Patterning of Ta0.1W0.9Ox/ITO Thin Film Stack," Appl. Surf. Sci., **253**(10), pp. 4740–4747.
[194] Venkatakrishnan, K., Tan, B., and Sivakumar, N. R., 2002, "Sub-Micron Ablation of Metallic Thin Film by Femtosecond Pulse Laser," Opt.Laser Technol., **34**(7), pp. 575–578.
[195] Tan, B., Dalili, A., and Venkatakrishnan, K., 2009, "High Repetition Rate Femtosecond Laser Nano-Machining of Thin Films," Appl. Phys. A: Mater. Sci. Process., **95**(2), pp. 537–545.
[196] Kim, J., and Na, S., 2007, "Metal Thin Film Ablation With Femtosecond Pulsed Laser," Opt. Laser Technol., **39**(7), pp. 1443–1448.
[197] Tan, B., Venkatakrishnan, K., and Tok, K. G., 2003, "Selective Surface Texturing Using Femtosecond Pulsed Laser Induced Forward Transfer," Appl. Surf. Sci., **207**(1–4), pp. 365–371.
[198] Nakata, Y., Tatsuo, O., and Mitsuo, M., 2004, "Micromachining of a Thin Film by Laser Ablation Using Femtosecond Laser With Masks," Opt. Lasers Eng., **42**(4), pp. 389–393.
[199] Watanabe, W., Li, Y., and Itoh, K., 2016, "[INVITED] Ultrafast Laser Micro-Processing of Transparent Material," Opt. Laser Technol., **78**(Part A), pp. 52–61.
[200] Tan, D., Sharafudeen, K. N., Yue, Y., and Qiu, J., 2016, "Femtosecond Laser Induced Phenomena in Transparent Solid Materials: Fundamentals and Applications," Prog. Mater. Sci., **76**, pp. 154–228.
[201] Jiang, L. J., Maruo, S., Osellame, R., Xiong, W., Campbell, J. H., and Lu, Y. F., 2016, "Femtosecond Laser Direct Writing in Transparent Materials Based on Nonlinear Absorption," MRS Bull., **41**(12), pp. 975–983.
[202] Veiko, V. P., Kudryashov, S. I., Sergeev, M. M., Zakoldaev, R. A., Danilov, P. A, Ionin, A. A., Antropova, T. V., and Anfimova, I. N., 2016, "Femtosecond Laser-Induced Stress-Free Ultra-Densification Inside Porous Glass," Laser Phys. Lett., **13**(5), p. 055901.
[203] Cao, J., Mazerolles, L., Lancry, M., Brisset, F., and Poumellec, B., 2017, "Modifications in Lithium Niobium Silicate Glass by Femtosecond Laser Direct Writing: Morphology, Crystallization, and Nanostructure," J. Opt. Soc. Am. B, **34**(1), pp. 160–168.
[204] Hnatovsky, C., Grobnic, D., Coulas, D., Barnes, M., and Mihailov, S. J., 2017, "Self-Organized Nanostructure Formation During Femtosecond-Laser Inscription of Fiber Bragg Gratings," Opt. Lett., **42**(3), pp. 399–402.
[205] Hnatovskya, C., Taylor, R. S., Rajeev, P. P., Simova, E., Bhardwaj, V. R., Rayner, D. M., and Corkum, P. B., 2005, "Pulse Duration Dependence of Femtosecond-Laser-Fabricated Nanogratings in Fused Silica," Appl. Phys. Lett., **87**(1), p. 014104.
[206] Poumellec, B., Lancry, M., Chahid-Erraji, A., and Kazansky, P. G., 2011, "Modification Thresholds in Femtosecond Laser Processing of Pure Silica: Review of Dependencies on Laser Parameters [Invited]," Opt. Mater. Express, **1**(4), pp. 766–782.
[207] Bérubé, J.-P., and Vallée, R., 2016, "Femtosecond Laser Direct Inscription of Surface Skimming Waveguides in Bulk Glass," Opt. Lett., **41**(13), pp. 3074–3077.
[208] Grobnic, D., Mihailov, S. J., Ballato, J., and Dragic, P. D., 2015, "Type I and II Bragg Gratings Made With Infrared Femtosecond Radiation in High and Low Alumina Content Aluminosilicate Optical Fibers," Opt. Mater. Express, **2**(4), pp. 313–322.
[209] Sima, F., Sugioka, K., Vázquez Rebeca, M., Osellame, R., Kelemen, L., and Ormos, P., 2018, "Three-Dimensional Femtosecond Laser Processing for Lab-on-a-Chip Applications," Nanophotonics, **7**(3), p. 613–634.
[210] Abou Khalil, A., Bérubé, J.-P., Danto, S., Desmoulin, J.-C., Cardinal, T., Petit, Y., Vallée, R., and Canioni, L., 2017, "Direct Laser Writing of a New Type of Waveguides in Silver Containing Glasses," Sci. Rep., **7**(1), p. 11124.
[211] Morris, J., Stevenson, N. K., Bookey, H. T., Kar, A. K., Brown, C. T. A., Hopkins, J. M., Dawson, M. D., and Lagatsky, A. A.,, 2017, "1.9 μm Waveguide Laser Fabricated by Ultrafast Laser Inscription in Tm:Lu2O3 Ceramic," Opt. Express, **25**(13), pp. 14910–14917.
[212] Pätzold, W. M., Demircan, A., and Morgner, U., 2017, "Low-Loss Curved Waveguides in Polymers Written With a Femtosecond Laser," Opt. Express, **25**(1), pp. 263–270.
[213] Ams, M., Dekker, P., Gross, S., and Withford Michael, J., 2017, "Fabricating Waveguide Bragg Gratings (WBGs) in Bulk Materials Using Ultrashort Laser Pulses," Nanophotonics, **6**(5), p. 743–763.
[214] Mihailov, S., Grobnic, D., Hnatovsky, C., Walker, R., Lu, P., Coulas, D., and Ding, H., 2017, "Extreme Environment Sensing Using Femtosecond Laser-Inscribed Fiber Bragg Gratings," Sensors, **17**(12), p. 2909.
[215] Chen, P., and Shu, X., 2018, "Refractive-Index-Modified-Dot Fabry-Perot Fiber Probe Fabricated by Femtosecond Laser for High-Temperature Sensing," Opt. Express, **26**(5), pp. 5292–5299.
[216] Joe, H.-E., Yun, H., Jo, S.-H., Jun, M. B. G., and Min, B.-K., 2018, "A Review on Optical Fiber Sensors for Environmental Monitoring," Int. J. Precis. Eng. Manuf.-Green Technol., **5**(1), pp. 173–191.
[217] Bharadwaj, V., Courvoisier, A., Fernandez, T. T., Ramponi, R., Galzerano, G., Nunn, J., Booth, M. J., Osellame, R., Eaton, S. M., and Salter, P. S., 2017, "Femtosecond Laser Inscription of Bragg Grating Waveguides in Bulk Diamond," Opt. Lett., **42**(17), pp. 3451–3453.
[218] Matushiro, Y., Juodkazis, S., Hatanaka, K., and Watanabe, W., 2017, "Regenerated Volume Gratings in PMMA After Femtosecond Laser Writing," Opt. Lett., **42**(8), pp. 1632–1635.
[219] Ahmed, F., Joe, H.-E., Min, B.-K., and Jun, M. B. G., 2015, "Characterization of Refractive Index Change and Fabrication of Long Period Gratings in Pure Silica Fiber by Femtosecond Laser Radiation," Opt. Laser Technol., **74**, pp. 119–124.
[220] Heck, M., Nolte, S., Tünnermann, A., Vallée, R., and Bernier, M., 2018, "Femtosecond-Written Long-Period Gratings in Fluoride Fibers," Opt. Lett., **43**(9), pp. 1994–1997.
[221] Theodosiou, A., Lacraz, A., Stassis, A., Koutsides, C., Komodromos, M., and Kalli, K., 2017, "Plane-by-Plane Femtosecond Laser Inscription Method for Single-Peak Bragg Gratings in Multimode CYTOP Polymer Optical Fiber," J. Lightwave Technol., **35**(24), pp. 5404–5410.
[222] Hu, X., Kinet, D., Chah, K., Pun, C.-F. J., Tam, H.-Y., and Caucheteur, C., 2017, "Bragg Grating Inscription in PMMA Optical Fibers Using 400-nm Femtosecond Pulses," Opt. Lett., **42**(14), pp. 2794–2797.
[223] Ishikawa, R., Lee, H., Lacraz, A., Theodosiou, A., Kalli, K., Mizuno, Y., and Nakamura, K., 2017, "Pressure Dependence of Fiber Bragg Grating Inscribed in Perfluorinated Polymer Fiber," IEEE Photonics Technol. Lett., **29**(24), pp. 2167–2170.
[224] Donko, A., Beresna, M., Jung, Y., Hayes, J., Richardson, D. J., and Brambilla, G., 2018, "Point-by-Point Femtosecond Laser Micro-Processing of Independent Core-Specific Fiber Bragg Gratings in a Multi-Core Fiber," Opt. Express, **26**(2), pp. 2039–2044.
[225] Fuerbach, A., Bharathan, G., Antipov, S., Ams, M., Williams, R. J., Hudson, D. D., Woodward, R. I., Jackson, S. D., 2018, "Line-by-line Femtosecond

FBG Inscription for Innovative Fiber Lasers," Advanced Photonics 2018 (BGPP, IPR, NP, NOMA, Sensors, Networks, SPPCom, SOF), Zurich, Paper No. BW3A.6.
[226] Ertorer, E., Haque, M., Li, J., and Herman, P. R., 2018, "Femtosecond Laser Filaments for Rapid and Flexible Writing of Fiber Bragg Grating," Opt. Express, **26**(7), pp. 9323–9331.
[227] Sugioka, K., and Cheng, Y., 2014, "Fabrication of 3D Microfluidic Structures Inside Glass by Femtosecond Laser Micromachining," Appl. Phys. A: Mater. Sci. Process., **114**(1), pp. 215–221.
[228] Sima, F., Xu, J., Wu, D., and Sugioka, K., 2017, "Ultrafast Laser Fabrication of Functional Biochips: New Avenues for Exploring 3D Micro- and Nano-Environments," Micromachines, **8**(2), p. 40.
[229] Sugioka, K., Xu, J., Wu, D., Hanada, Y., Wang, Z., Cheng, Y., and Midorikawa, K., 2014, "Femtosecond Laser 3D Micromachining: A Powerful Tool for the Fabrication of Microfluidic, Optofluidic, and Electrofluidic Devices Based on Glass," Lab Chip, **14**(18), pp. 3447–3458.
[230] Shan, C., Chen, F., Yang, Q., Jiang, Z., and Hou, X., 2018, "3D Multi-Microchannel Helical Mixer Fabricated by Femtosecond Laser Inside Fused Silica," Micromachines, **9**(1), p. 29.
[231] Wang, Z., Jiang, L., Li, X., Wang, A., Yao, Z., Zhang, K., and Lu, Y., 2018, "High-Throughput Microchannel Fabrication in Fused Silica by Temporally Shaped Femtosecond Laser Bessel-Beam-Assisted Chemical Etching," Opt. Lett., **43**(1), pp. 98–101.
[232] Roth, G.-L., Esen, C., and Hellmann, R., 2017, "Femtosecond Laser Direct Generation of 3D-Microfluidic Channels Inside Bulk PMMA," Opt. Express, **25**(15), pp. 18442–18450.
[233] Martínez Vázquez, R., Trotta, G., Volpe, A., Bernava, G., Basile, V., Paturzo, M., Ferraro, P.o, Ancona, A., Fassi, I., and Osellame, R., 2017, "Rapid Prototyping of Plastic Lab-on-a-Chip by Femtosecond Laser Micromachining and Removable Insert Microinjection Molding," Micromachines, **8**(11), p. 328.
[234] Ma, H., Zakoldaev, R. A., Rudenko, A., Sergeev, M. M., Veiko, V. P., and Itina, T. E., 2017, "Well-Controlled Femtosecond Laser Inscription of Periodic Void Structures in Porous Glass for Photonic Applications," Opt. Express, **25**(26), pp. 33261–33270.
[235] Teng, Y., Zhou, J., Sharafudeen, K., Zhou, S., Miura, K., and Qiu, J., 2014, "Space-Selective Crystallization of Glass Induced by Femtosecond Laser Irradiation," J. Non-Cryst. Solids, **383**, pp. 91–96.
[236] Podlipensky, A., Abdolvand, A., Seifert, G., and Graener, H., 2005, "Femtosecond Laser Assisted Production of Dichroitic 3D Structures in Composite Glass Containing Ag Nanoparticles," Appl. Phys. A: Mater. Sci. Process., **80**(8), pp. 1647–1652.
[237] Sotillo, B., Bharadwaj, V., Hadden, J. P., Sakakura, M., Chiappini, A., Fernandez, T. T., Longhi, S., Jedrkiewicz, O., Shimotsuma, Y., Criante, L., Osellame, R., Galzerano, G., Ferrari, M., Miura, K., Ramponi, R., Barclay, P. E., and Eaton, S. M.l, 2016, "Diamond Photonics Platform Enabled by Femtosecond Laser Writing," Sci. Rep., **6**(1), p. 35566.
[238] Sotillo, B., Bharadwaj, V., Hadden, J., Rampini, S., Chiappini, A., Fernandez, T., Armellini, C., Serpengüzel, A., Ferrari, M., Barclay, P., Ramponi, R., and Eaton, S., 2017, "Visible to Infrared Diamond Photonics Enabled by Focused Femtosecond Laser Pulses," Micromachines, **8**(2), p. 60.
[239] Hadden, J. P., Bharadwaj, V., Sotillo, B., Rampini, S., Osellame, R., Witmer, J. D., Jayakumar, H., Fernandez, T. T., Chiappini, A., Armellini, C., Ferrari, M., Ramponi, R., Barclay, P. E., and Eaton S. M., 2018, "Integrated Waveguides and Deterministically Positioned Nitrogen Vacancy Centers in Diamond Created by Femtosecond Laser Writing," Opt. Lett., **43**(15), pp. 3586–3589.
[240] Ashikkalieva, K. K., Kononenko, T. V., Obraztsova, E. A., Zavedeev, E. V., Khomich, A. A., Ashkinazi, E. E., and Konov, V. I., 2016, "Direct Observation of Graphenic Nanostructures Inside Femtosecond-Laser Modified Diamond," Carbon, **102**, pp. 383–389.
[241] Kononenko, V. V., Vlasov, I. I., Gololobov, V. M., Kononenko, T. V., Semenov, T. A., Khomich, A. A., Shershulin, V. A., Krivobok, V. S., and Konov, V. I., 2017, "Nitrogen-Vacancy Defects in Diamond Produced by Femtosecond Laser Nanoablation Technique," Appl. Phys. Lett., **111**(8), p. 081101.
[242] Fukuyo, F., Fukumitsu, K., Uchiyama, N., and Wakuda, T., 2006, "Laser Processing Method and Laser Processing Apparatus," U.S. Patent No. 6992026.
[243] Ohmura, E., Fukuyo, F., Fukumitsu, K., and Morita, H., 2006, "Internal Modified-Layer Formation Mechanism Into Silicon With Nanosecond Laser," J. Achiev. Mater. Manuf. Eng., **17**, pp. 381–384.
[244] Nara, Y., and Kiyota, H., 2018, "Direct Observation of Internal Void-Formation in Stealth Dicing," Proceedings of SPIE, Laser-Based Micro-Nanoprocessing XII, San Francisco, CA, Jan. 27-Feb. 1.
[245] Verburg, P. C., Smillie, L. A., Römer, G. R. B. E., Haberl, B., Bradby, J. E., Williams, J. S., and Huis in 't Veld, A. J., 2015, "Crystal Structure of Laser-Induced Subsurface Modifications in Si," Appl. Phys. A, **120**(2), pp. 683–691.
[246] Ohmura, E., Kawahito, Y., Fukumitsu, K., Okuma, J., and Morita, H., 2011, "Analysis of Internal Crack Propagation in Silicon Due to Permeable Pulse Laser Irradiation: Study on Processing Mechanism of Stealth Dicing," Proc. SPIE 7996, Fundamentals of Laser-Assisted Micro- and Nanotechnologies 2010, 799603 (28 February 2011); https://doi.org/10.1117/12.887431, St. Petersburg, July 5–8.
[247] Verburg, P. C., Römer, G. R. B. E., and Huis in 't Veld, A. J., 2014, "Two-Photon–induced Internal Modification of Silicon by Erbium-Doped Fiber Laser," Opt. Express, **22**(18), pp. 21958–21971.
[248] Li, Q., Chambonneau, M., Chanal, M., and Grojo, D., 2016, "Quantitative-Phase Microscopy of Nanosecond Laser-Induced Micro-Modifications Inside Silicon," **55**, pp. 2–8.
[249] Chambonneau, M., Li, Q., Chanal, M., Sanner, N., and Grojo, D., 2016, "Writing Waveguides Inside Monolithic Crystalline Silicon With Nanosecond Laser Pulses," Opt. Lett., **41**(21), pp. 4875–4878.
[250] Nejadmalayeri, A. H., Herman, P. R., Burghoff, J., Will, M., Nolte, S., and Tünnermann, A., 2005, "Inscription of Optical Waveguides in Crystalline Silicon by Mid-Infrared Femtosecond Laser Pulses," Opt. Lett., **30**(9), pp. 964–966.
[251] Pavlov, I., Tokel, O., Pavlova, S., Kadan, V., Makey, G., Turnali, A., Yavuz, Ö, and Ilday, FÖ, 2017, "Femtosecond Laser Written Waveguides Deep Inside Silicon," Opt. Lett., **42**(15), p. 3028.
[252] Mori, M., Shimotsuma, Y., Sei, T., Sakakura, M., Miura, K., and Udono, H., 2015, "Tailoring Thermoelectric Properties of Nanostructured Crystal Silicon Fabricated by Infrared Femtosecond Laser Direct Writing," Phys. Status Solidi A, **212**(4), pp. 715–721.
[253] Bhardwaj, V. R., Simova, E., Rajeev, P. P., Hnatovsky, C., Taylor, R. S., Rayner, D. M., and Corkum, P. B., 2006, "Optically Produced Arrays of Planar Nanostructures Inside Fused Silica," Phys. Rev. Lett., **96**(5), p. 57404.
[254] Liao, Y., Cheng, Y., Liu, C., Song, J., He, F., Shen, Y., Chen, D., Xu, Z., Fan, Z., Wei, X., Sugioka, K., and Midorikawa, K., 2013, "Direct Laser Writing of Sub-50 nm Nanofluidic Channels Buried in Glass for Three-Dimensional Micro-Nanofluidic Integration," Lab Chip, **13**(8), pp. 1626–1631.
[255] Grojo, D., Mouskeftaras, A., Delaporte, P., and Lei, S., 2015, "Limitations to Laser Machining of Silicon Using Femtosecond Micro-Bessel Beams in the Infrared," J. Appl. Phys., **117**(15), p. 153105.
[256] Chanal, M., Fedorov, V. Y., Chambonneau, M., Clady, R., Tzortzakis, S., and Grojo, D., 2017, "Crossing the Threshold of Ultrafast Laser Writing in Bulk Silicon," Nat. Commun., **8**(1), pp. 1–6.
[257] Mingareev, I., Gehlich, N., Bonhoff, T., Abdulfattah, A., Sincore, A. M., Kadwani, P., Shah, L., and Richardson, M., 2016, "Principles and Applications of Trans-Wafer Processing Using a 2-μm Thulium Fiber Laser," Int. J. Adv. Manuf. Technol., **84**(9–12), pp. 2567–2578.
[258] Lei, S., Grojo, D., Ma, J., Yu, X., and Wu, H., 2016, "Femtosecond Laser Backside Ablation of Gold Film on Silicon Substrate," Procedia Manuf., **5**, pp. 594–608.
[259] Ito, Y., Sakashita, H., Suzuki, R., Uewada, M., Luong, K. P., and Tanabe, R., 2014, "Modification and Machining on Back Surface of a Silicon Substrate by Femtosecond Laser Pulses at 1552 nm," J. Laser Micro/Nanoeng., **9**(2), pp. 98–102.
[260] Kadan, V., Pavlova, S., Pavlov, I., Rezaei, H., Ilday, Ö, and Blonskyi, I., 2018, "Spatio-Temporal Dynamics of Femtosecond Laser Pulses at 1550 nm Wavelength in Crystal Silicon," Appl. Phys. A, **124**(8), p. 560.
[261] Zavedeev, E. V., Kononenko, V. V., and Konov, V. I., 2016, "Delocalization of Femtosecond Laser Radiation in Crystalline Si in the Mid-IR Range," Laser Phys., **26**(1), p. 16101.
[262] He, F., Yu, J., Tan, Y., Chu, W., Zhou, C., Cheng, Y., and Sugioka, K., 2017, "Tailoring Femtosecond 1.5-μm Bessel Beams for Manufacturing High-Aspect-Ratio Through-Silicon Vias," Sci. Rep., **7**, pp. 1–9.
[263] Kämmer, H., Matthäus, G., Nolte, S., Chanal, M., Utéza, O., and Grojo, D., 2018, "In-Volume Structuring of Silicon Using Picosecond Laser Pulses," Appl. Phys. A, **124**(4), p. 302.
[264] Sun, H.-B., and Kawata, S., 2004, "Two-Photon Photopolymerization and 3D Lithographic Microfabrication," Adv. Polym. Sci., **170**, pp. 169–273.
[265] Malinauskas, M., Farsari, M., Piskarskas, A., and Juodkazis, S., 2013, "Ultrafast Laser Nanostructuring of Photopolymers: A Decade of Advances," Phys. Rep., **533**(1), pp. 1–31.
[266] Hohmann, J. K., Renner, M., Waller, E. H., and von Freymann, G., 2015, "Three-Dimensional μ-Printing: An Enabling Technology," Adv. Opt. Mater., **3**(11), pp. 488–1507.
[267] Xing, J.-F., Zheng, M.-L., and Duan, X.-M., 2015, "Two-Photon Polymerization Microfabrication of Hydrogels: An Advanced 3D Printing Technology for Tissue Engineering and Drug Delivery," Chem. Soc. Rev., **44**(15), pp. 5031–5039.
[268] LaFratta, C. N., and Baldacchini, T., 2017, "Two-Photon Polymerization Metrology: Characterization Methods of Mechanisms and Microstructures," Micromachines, **8**(4), p. 101.
[269] Li, L., and Fourkas, J., 2007, "The Inherent Optical Nonlinearity of Multiphoton Absorption Allows Such Polymerization," Mater. Today, **10**(6), pp. 30–37.
[270] LaFratta, C. N., Fourkas, J. T., Baldacchini, T., and Farrer, R. A., 2007, "Multiphoton Fabrication," Angew. Chem. Int. Ed., **46**(33), pp. 6238–6258.
[271] Williams, H. E., Diaz, C., Padilla, G., Hernandez, F. E., and Kuebler, S. M., 2017, "Order of Multiphoton Excitation of Sulfonium Photo-Acid Generators Used in Photoresists Based on SU-8," J. Appl. Phys., **121**(22), p. 223104.
[272] Malinauskas, M., Danilevičius, P., and Juodkazis, S., 2011, "Three-Dimensional Micro-/Nano-Structuring via Direct Write Polymerization With Picosecond Laser Pulses," Opt. Express, **19**(6), p. 5602.
[273] Göppert-Mayer, M., 1931, "Über Elementarakte Mit Zwei Quantensprüngen," Ann. Phys., **9**(3), pp. 273–294.
[274] Kaiser, W., and Garrett, C. G. B., 1961, "Two-Photon Excitation in CaF2: Eu2 + ," Phys. Rev. Lett., **7**(6), pp. 229–231.
[275] Cabrera, M., Jezequel, J. Y., and Andre, J. C., 1990, *Lasers in Polymer Science and Technology: Applications*, Ed. Fouassier, J.P. and Rabek, J.F, Vol. 3, CRC Press, Boca Raton, Florida, p. 73.
[276] Strickler, J. H., and Webb, W. W., 1991, "Two-Photon Excitation in Laser Scanning Fluorescence Microscopy," Proceedings of SPIE 1398, CAN-AM Eastern '90, Rochester, NY, Oct. 4–5.
[277] Maruo, S., Nakamura, O., and Kawata, S., 1997, "Three-Dimensional Microfabrication With Two-Photon-Absorbed Photopolymerization," Opt. Lett., **22**(2), pp. 132–134.

[278] Kawata, S., Sun, H. B., Tanaka, T., and Takada, K., 2001, "Finer Features for Functional Microdevices," Nature Comm., **412**(6848), pp. 697–698.
[279] Stuart, B. C., Feit, M. D., Rubenchik, A. M., Shore, B. W., and Perry, M. D., 1995, "Laser-Induced Damage in Dielectrics With Nanosecond to Subpicosecond Pulses," Phys. Rev. Lett., **74**(12), pp. 2248–2251.
[280] Grojo, D., Gertsvolf, M., Lei, S., Barillot, T., Rayner, D. M., and Corkum, P. B., 2010, "Exciton-Seeded Multiphoton Ionization in Bulk SiO2," Phys. Rev. B, **81**(21), pp. 3–6.
[281] Malinauskas, M., Žukauskas, A., Bičkauskaitė, G., Gadonas, R., and Juodkazis, S., 2010, "Mechanisms of Three-Dimensional Structuring of Photo-Polymers by Tightly Focussed Femtosecond Laser Pulses," Opt. Express, **18**(10), p. 10209.
[282] Liaros, N., and Fourkas, J. T., 2017, "The Characterization of Absorptive Nonlinearities," Laser Photonics Rev., **11(5)**, pp. 1–21.
[283] Tomova, Z., Liaros, N., Gutierrez Razo, S. A., Wolf, S. M., and Fourkas, J. T., 2016, "In Situ Measurement of the Effective Nonlinear Absorption Order in Multiphoton Photoresists," Laser Photonics Rev., **10**(5), pp. 849–854.
[284] Vizsnyiczai, G., Kelemen, L., and Ormos, P., 2014, "Holographic Multi-Focus 3D Two-Photon Polymerization With Real-Time Calculated Holograms," Opt. Express, **22**(20), pp. 24217–24223.
[285] Yu, X., Zhang, M., and Lei, S., 2017, "Multiphoton Polymerization Using Femtosecond Bessel Beam for Layerless Three-Dimensional Printing," J. Micro Nano-Manuf., **6**(1), pp. 10901–10908.
[286] Yu, X., Todi, A., and Tang, H., 2018, "Bessel Beam Generation Using a Segmented Deformable Mirror," Appl. Opt., **57**(16), p. 4677.
[287] Jiang, L., Xiong, W., Zhou, Y., Liu, Y., Huang, X., Li, D., Baldacchini, T., Jiang, L., and Lu, Y., 2016, "Performance Comparison of Acrylic and Thiol-Acrylic Resins in Two-Photon Polymerization," Opt. Express, **24**(12), pp. 13687–13701.
[288] Barner-Kowollik, C., Bastmeyer, M., Blasco, E., Patrick, M., Delaittre, G., Richter, B., Müller, P., Richter, B., and Wegener, M., 2017, "3D Laser Micro- and Nano-Printing: Challenges for Chemistry," Angew. Chem. Int. Ed., **56**(50), pp. 15828–15845.
[289] Xiong, W., Zhou, Y. S., He, X. N., Gao, Y., Mahjouri-Samani, M., Jiang, L., Baldacchini, T., and Lu, Y. F., 2012, "Simultaneous Additive and Subtractive Three-Dimensional Nanofabrication Using Integrated Two-Photon Polymerization and Multiphoton Ablation," Light Sci. Appl., **1**(4), p. e6.
[290] Nie, B., Yang, L., Huang, H., Bai, S., Wan, P., and Liu, J., 2015, "Femtosecond Laser Additive Manufacturing of Iron and Tungsten Parts," Appl. Phys. A Mater. Sci. Process., **119**(3), pp. 1075–1080.
[291] Kaden, L., Matthäus, G., Ullsperger, T., Engelhardt, H., Rettenmayr, M., Tünnermann, A., and Nolte, S., 2017, "Selective Laser Melting of Copper Using Ultrashort Laser Pulses," Appl. Phys. A, **123**(9), p. 596.
[292] Kaden, L., Seyfarth, B., Ullsperger, T., Matthäus, G., and Nolte, S., 2018, "Selective Laser Melting of Copper Using Ultrashort Laser Pulses at Different Wavelengths," Proceedings of SPIE 10523, Laser 3D Manufacturing V, San Francisco, CA, Jan. 29–Feb. 1, p. 1052312.
[293] Ovsianikov, A., Chichkov, B., Mente, P., Monteiro-Riviere, N. A., Doraiswamy, A., and Narayan, R. J., 2007, "Two Photon Polymerization of Polymer Ceramic Hybrid Materials for Transdermal Drug Delivery," Int. J. Appl. Ceram. Technol., **4**(1), pp. 22–29.
[294] Mingareev, I., Bonhoff, T., El-Sherif, A. F., Meiners, W., Kelbassa, I., Biermann, T., and Richardson, M., 2013, "Femtosecond Laser Post-Processing of Metal Parts Produced by Laser Additive Manufacturing," J. Laser Appl., **25**(5), p. 52009.
[295] Hubler, G. K., 1992, "Pulsed Laser Deposition," MRS Bull., **17**(2), pp. 26–29.
[296] Piqué, A., Auyeung, R. C. Y., Kim, H., Charipar, N. A., and Mathews, S. A., 2016, "Laser 3D Micro-Manufacturing," J. Phys. D: Appl. Phys., **49**(22), p. 223001.
[297] Yanik, M. F., Cinar, H., Cinar, H. N., Chisholm, A. D., Jin, Y. S., and Ben-Yakar, A., 2004, "Neurosurgery—Functional Regeneration After Laser Axotomy," Nature Comm., **432**(7019), pp. 822–822.
[298] Watanabe, W., Arakawa, N., Matsunaga, S., Higashi, T., Fukui, K., Isobe, K., and Itoh, K., 2004, "Femtosecond Laser Disruption of Subcellular Organelles in a Living Cell," Opt. Express, **12**(18), pp. 4203–4213.
[299] Heisterkamp, A., Ripken, T., Mamom, T., Drommer, W., Welling, H., Ertmer, W., and Lubatschowski, H., 2002, "Nonlinear Side Effects of fs Pulses Inside Corneal Tissue During Photodisruption," Appl. Phys. B, **74**(4–5), pp. 419–425.
[300] Shen, N., Datta, D., Schaffer, C. B., LeDuc, P., Ingber, D. E., and Mazur, E., 2005, "Ablation of Cytoskeletal Filaments and Mitochondria in Live Cells Using a Femtosecond Laser Nanoscissor," Mech. Chem. Biosyst., **2**(1), pp. 17–25.
[301] Guo, Y., and Vukelić, S., 2015, "Evolution of Cavitation Bubbles in Corneal Stroma Subject to Micro-Joule Femtosecond Laser Pulses," Proceedings of SPIE Optical Interactions With Tissue and Cells, San Francisco, CA, Feb. 8–10, p. 932106.
[302] König, K., 2000, "Robert Feulgen Prize Lecture. Laser Tweezers and Multiphoton Microscopes in Life Sciences," Histochem. Cell Biol., **114**(2), pp. 79–92.
[303] Tirlapur, U. K., and König, K., 2002, "Cell Biology—Targeted Transfection by Femtosecond Laser," Nature Comm., **418**(6895), pp. 290–291.
[304] Zeira, E., Manevitch, A., Khatchatouriants, A., Pappo, O., Hyam, E., Darash-Yahana, M., Tavor, E., Honigman, A., Lewis, A., and Galun, E., 2003, "Femtosecond Infrared Laser-an Efficient and Safe in Vivo Gene Delivery System for Prolonged Expression," Mol. Ther., **8**(2), pp. 342–350.
[305] Smith, N. I., Fujita, K., Kaneko, T., Katoh, K., Nakamura, O., Kawata, S., and Takamatsu, T., 2001, "Generation of Calcium Waves in Living Cells by Pulsed-Laser-Induced Photodisruption," Appl. Phys. Lett., **79**(8), pp. 1208–1210.
[306] Oraevsky, A. A., Da Silva, L. B., Rubenchik, A. M., Feit, M. D., Glinsky, M. E., Perry, M. D., Mammini, B. M., Small, W., and Stuart, B. C., 1996, "Plasma Mediated Ablation of Biological Tissues With Nanosecond-to-Femtosecond Laser Pulses: Relative Role of Linear and Nonlinear Absorption," IEEE J. Sel. Top. Quantum Electron., **2**(4), pp. 801–809.
[307] Oraevsky, A. A., Jacques, S. L., Esenaliev, R. O., and Tittel, F. K., 1996, "Pulsed Laser Ablation of Soft Tissues, Gels, and Aqueous Solutions at Temperatures Below 100 Degrees C," Lasers Surg. Med., **18**(3), pp. 231–240.
[308] Esenaliev, R. O., Oraevsky, A. A., Jacques, S. L., and Tittel, F. K., 1996, "Effect of Tensile Stress Amplitude and Temporal Characteristics on Threshold of Cavitation-Driven Ablation," Proceedings of, 2681, Laser-Tissue Interaction Vii, San Jose, CA, May 7, pp. 326–333.
[309] Chung, S. H., and Mazur, E., 2009, "Surgical Applications of Femtosecond Lasers," J. Biophotonics, **2**(10), pp. 557–572.
[310] Chung, S. H., Schmalz, A., Ruiz, R. C., Gabel, C. V., and Mazur, E., 2013, "Femtosecond Laser Ablation Reveals Antagonistic Sensory and Neuroendocrine Signaling That Underlie C. Elegans Behavior and Development," Cell Rep., **4**(2), pp. 316–326.
[311] König, K., Riemann, I., and Fritzsche, W., 2001, "Nanodissection of Human Chromosomes With Near-Infrared Femtosecond Laser Pulses," Opt. Lett., **26**(11), pp. 819–821.
[312] Konig, K., Riemann, I., Krauss, O., and Fritzsche, W., 2002, "Nanodissection of Human Chromosomes and Ultraprecise Eye Surgery With Nanojoule Near Infrared Femtosecond Laser Pulses," Commercial and Biomedical Applications of Ultrafast and Free-Electron Lasers, San Jose, CA, Jan. 20–25, pp. 11–22.
[313] Vogel, A., Noack, J., Hüttman, G., and Paltauf, G., 2005, "Mechanisms of Femtosecond Laser Nanosurgery of Cells and Tissues," Appl. Phys. B, **81**(8), pp. 1015–1047.
[314] Juhasz, T., Kurtz, R., Raksi, F., Suarez, C., Horvath, C., and Spooner, G., 2002, "The Femtosecond Blade: Applications in Corneal Surgery," Opt. Photonics News, **13**(1), pp. 24–29.
[315] Soong, H. K., and Malta, J. B., 2009, "Femtosecond Lasers in Ophthalmology," Am. J. Ophthalmol., **147**(2), pp. 189–197.
[316] Wei, S., and Wang, Y., 2013, "Comparison of Corneal Sensitivity Between FS-LASIK and Femtosecond Lenticule Extraction (ReLEx Flex) or Small-Incision Lenticule Extraction (ReLEx Smile) for Myopic Eyes," Graefes Archive Clin. Exp. Ophthalmol., **251**(10), pp. 1645, 2495–2497.
[317] Sidhu, M. S., Choi, M. Y., Woo, S. Y., Lee, H. K., Lee, H. S., Kim, K. J., Jeoung, S. C., Choi, J. S., Joo, C. K., and Park, I. H., 2014, "Femtosecond Laser-Assisted Selective Reduction of Neovascularization in Rat Cornea," Lasers Med. Sci., **29**(4), pp. 1417–1427.
[318] Demirok, A., Ozgurhan, E. B., Agca, A., Kara, N., Bozkurt, E., Cankaya, K. I., and Yilmaz, O. F., 2013, "Corneal Sensation After Corneal Refractive Surgery With Small Incision Lenticule Extraction," Optom. Vis. Sci., **90**(10), pp. 1040–1047.
[319] Juhasz, T., Kastis, G. A., Suárez, C., Bor, Z., and Bron, W. E., 1996, "Time-Resolved Observations of Shock Waves and Cavitation Bubbles Generated by Femtosecond Laser Pulses in Corneal Tissue and Water," Lasers Surg. Med., **19**(1), pp. 23–31.
[320] Juhasz, E., Filkorn, T., Kranitz, K., Sandor, G. L., Gyenes, A., and Nagy, Z. Z., 2014, "Analysis of Planned and Postoperatively Measured Flap Thickness After LASIK Using the LenSx Multifunctional Femtosecond Laser System," J. Refract. Surg., **30**(9), pp. 622–626.
[321] Lubatschowski, H., 2008, "Overview of Commercially Available Femtosecond Lasers in Refractive Surgery," J. Refract. Surg., **24**(1), pp. S102–7.
[322] Netto, M. V., Mohan, R. R., Medeiros, F. W., Dupps, W. J., Jr., Sinha, S., Krueger, R. R., Stapleton, W. M., Rayborn, M., Suto, C., and Wilson, S. E., 2007, "Femtosecond Laser and Microkeratome Corneal Flaps: Comparison of Stromal Wound Healing and Inflammation," J. Refract. Surg., **23**(7), pp. 667–676.
[323] Wang, C., Fomovsky, M., Miao, G., Zyablitskaya, M., and Vukelic, S., 2018, "Femtosecond Laser Crosslinking of the Cornea for Noninvasive Vision Correction," Nat. Photonics, **12**(7), pp. 416–422.
[324] Fomovsky, M., Wang, C., Roland-Hall, J., Paik, D. C., Trokel, S. L., and Vukelic, S., 2017, "A New Paradigm for Use of Ultrafast Lasers in Ophthalmology for Enhancement of Corneal Mechanical Properties and Permanent Correction of Refractive Errors," Proc. SPIE, **10066**, p. 100660Y.
[325] Durney-Antonelli, K., Wang, C., Zimmerman, B., Sonar, S., Montegut, L., Bolene, M. A., Guan, K., Hung, C. T., Ateshian, G. A., and Vukelić, S., 2018, "Novel Laser Treatment Modality for Crosslinking and Strengthening Early-Stage Osteoarthritic Cartilage," 8th World Congress of Biomechanics, Dublin, Ireland, July 8–12, p. 00400.
[326] Wang, C., Durney, K. M., Fomovsky, M., Yu, J., Roland-Hall, J., Ateshian, G. A., and Vukelić, S., 2017, "Femtosecond Laser Irradiation as Novel Paradigm for Treatment of Early Osteoarthritis," Annual Meeting of the Orthopaedic Research Society (ORS), San Diego, CA, Mar. 19–22.
[327] Engstrom, D. S., Porter, B., Pacios, M., and Bhaskaran, H., 2014, "Additive Nanomanufacturing—A Review," J. Mater. Res., **29**(17), p. 1792–1816.
[328] Liddle, J. A., and Gallatin, G. M., 2016, "Nanomanufacturing: A Perspective," ACS Nano, **10**(3), p. 2995–3014.
[329] Chong, T. C., Hong, M. H., and Shi, L. P., 2010, "Laser Precision Engineering: From Microfabrication to Nanoprocessing," Laser Photonics Rev., **4**(1), p. 123–143.
[330] Huber, C., Trügler, A., Hohenester, U., Prior, Y., and Kautek, W., 2014, "Optical Near-Field Excitation at Commercial Scanning Probe Microscopy

Tips: A Theoretical and Experimental Investigation," Phys. Chem. Chem. Phys., **16**(6), p. 2289–2296.
[331] Grigoropoulos, C. P., Hwang, D. J., and Chimmalgi, A., 2007, "Nanometer-Scale Laser Direct-Write Using Near-Field Optics," MRS Bull., **32**(1), pp. 16–22.
[332] Fischer, J., and Wegener, M., 2013, "Three-Dimensional Optical Laser Lithography Beyond the Diffraction Limit," Laser Photonics Rev., **7**(1), pp. 22–44.
[333] Serbin, J., Ovsianikov, A., and Chichkov, B., 2004, "Fabrication of Woodpile Structures by Two-Photon Polymerization and Investigation of Their Optical Properties," Opt. Exp., **12**(21), p. 5221.
[334] Tian, Y., Kwon, H. J., Shin, Y. C., and King, G. B., 2014, "Fabrication and Characterization of Photonic Crystals by Two-Photon Polymerization Using a Femtosecond Laser," ASME J. Micro Nano-Manuf., **2**(3), p. 034501.
[335] Zheng, C., Hu, A., Chen, T., Oakes, K., and Liu, S., 2015, "Femtosecond Laser Internal Manufacturing of Three-Dimensional Microstructure Devices," Appl. Phys. A, **121**(1), p. 163–177.
[336] Fischer, J., von Freymann, G., and Wegener, M., 2010, "The Materials Challenge in Diffraction-Unlimited Direct-Laser-Writing Optical Lithography," Adv. Mater., **22**(32), pp. 3578–3582.
[337] Fischer, J., and Wegener, M., 2012, "Ultrafast Polymerization Inhibition by Stimulated Emission Depletion for Three-Dimensional Nanolithography," Adv. Opt. Mater., **24(10)**, p. OP65.
[338] Li, L., Gattass, R. G., Gershgoren, E., Hwang, H., and Fourkas, J., 2009, "Achieving 1/20 Resolution by One-Color Initiation and Deactivation of Polymerization," Science, **324**(5929), pp. 910–913.
[339] Scott, T., Kowalski, B. A., Sullivan, A. C., Bowman, C. N., and McLeod, R. R., 2009, "Two-Color Single Photon Photoinitiation and Photoinhibition for Subdiffraction Photolithography," Science, **324**(5929), pp. 913–917.
[340] Harke, B., Keller, J., Ullal, C. K., Westphal, V., Schönle, A., and Hell, S. W., 2008, "Resolution Scaling in STED Microscopy," Opt. Exp., **16**(6), p. 4154.
[341] Harke, B., Bianchini, P., Brandi, F., and Diaspro, A., 2012, "Photopolymerization Inhibition Dynamics for sub-Diffraction Direct Laser Writing Lithography," ChemPhysChem, **13**(6), pp. 1429–1434.
[342] Gan, Z., Cao, Y., Evans, R. A., and Gu, M., 2013, "Three-Dimensional Deep Sub-Diffraction Optical Beam Lithography With 9 nm Feature Size," Nature Comm., **4**(1), p. 2061.
[343] Fischer, J., Ergin, T., and Wegener, M., 2011, "Three-Dimensional Polarization—Independent Visible-Frequency Carpet Invisibility Cloak," Opt. Lett., **36**(11), p. 2059.
[344] Cao, Y., Li, X., and Gu, M., 2011, "Super-Resolution Nanofabrication Either Metal-Ion Doped Hybrid Material Through an Optical Dual-Beam Approach," Appl. Phys. Lett., **105**(26), p. 263102.
[345] Frölich, A., Fischer, J., Zebrowski, T., Busch, K., and Wegener, M., 2013, "Titania Woodpiles With Compete Three-Dimensional Photonic Bandgaps in the Visible," Adv. Mater., **25**(26), pp. 3588–3592.
[346] Bechtel, J. H., Lee Smith, W., and Bloembergen, N., 1977, "Two-Photon Photoemission From Metals Induced by Picosecond Laser Pulses," Phys. Rev. B, **15**(10), pp. 4557–4563.
[347] Mao, S. S., Mao, X. L., Greif, R., and Russo, R. E., 1998, "Simulation of Infrared Picosecond Laser-Induced Electron Emission From Semiconductors," Appl. Surf. Sci., **127–129**, pp. 206–211.
[348] Rethfeld, B., Sokolowski-Tinten, K., Von Der Linde, D., and Anisimov, S. I., 2004, "Timescales in the Response of Materials to Femtosecond Laser Excitation," Appl. Phys. A, **79**(4–6), pp. 767–769.
[349] Zhao, X., and Shin, Y. C., 2012, "A Two-Dimensional Comprehensive Hydrodynamic Model for Femtosecond Laser Pulse Interaction With Metals," J. Phys. D: Appl. Phys., **45**(10), p. 105201.
[350] Hu, W., Shin, Y. C., and King, G., 2011, "Early-Stage Plasma Dynamics With Air Ionization During Ultrashort Laser Ablation of Metal," Phys. Plasmas, **18**(9), p. 093302.
[351] Anisimov, S. I., Kapeliovich, B. L., and Perel-man, T. L., 1974, "Electron Emission From Metal Surfaces Exposed to Ultrashort Laser Pulses," J. Exp. Theor. Phys., **39(2)**, pp. 375–377.
[352] Qiu, T. Q., and Tien, C. L., 1993, "Heat Transfer Mechanisms During Short-Pulse Laser Heating of Metals," ASME J. Heat Transfer, **115**(4), pp. 835–841.
[353] Tzou, D. Y., 1995, "A Unified Field Approach for Heat Conduction From Macro- to Micro-Scales," ASME J. Heat Transfer, **117**(1), pp. 8–16.
[354] Chen, J. K., Tzou, D. Y., and Beraun, J. E., 2006, "A Semiclassical Two-Temperature Model for Ultrafast Laser Heating," Int. J. Heat Mass Transfer, **49**(1–2), pp. 307–316.
[355] Bulgakova, N. M., Stoian, R., Rosenfeld, A., Hertel, I. V., Marine, W., and Campbell, E. E. B., 2005, "A General Continuum Approach to Describe Fast Electronic Transport in Pulsed Laser Irradiated Materials: The Problem of Coulomb Explosion," Appl. Phys. A, **81**(2), pp. 345–356.
[356] Wu, B., and Shin, Y. C., 2007, "A Simple Model for High Fluence Ultra-Short Pulsed Laser Metal Ablation," Appl. Surf. Sci., **253**(8), pp. 4079–4084.
[357] Wu, B., and Shin, Y. C., 2009, "A Simplified Model for High Fluence Ultra-Short Pulsed Laser Ablation of Semiconductors and Dielectrics," Appl. Surf. Sci., **255**(9), pp. 4996–5002.
[358] Chen, J. K., and Beraun, J. E., 2003, "Modelling of Ultrashort Laser Ablation of Gold Films in Vacuum," J. Opt. A: Pure Appl. Opt., **5**(3), pp. 168–173.
[359] Jia, X., and Zhao, X., 2019, "Numerical Study of Material Decomposition in Ultrafast Laser Interaction With Metals," Appl. Surf. Sci., **463**, pp. 781–790.
[360] Larsen, J. T., and Lane, S. M., 1994, "HYADES—A Plasma Hydrodynamics Code for Dense Plasma Studies," J. Quant. Spectrosc. Radiat. Transfer, **51**(1–2), pp. 179–186.
[361] Spitzer, L., and Härm, R., 1953, "Transport Phenomena in a Completely Ionized Gas," Phys. Rev., **89**(5), pp. 977–981.
[362] Eidmann, K., Meyer-ter-Vehn, J., Schlegel, T., and Hüller, S., 2000, "Hydrodynamic Simulation of Subpicosecond Laser Interaction With Solid-Density Matter," Phys. Rev. E, **62**(1), pp. 1202–1214.
[363] Colombier, J. P., Combis, P., Bonneau, F., Le Harzic, R., and Audouard, E., 2005, "Hydrodynamic Simulations of Metal Ablation by Femtosecond Laser Irradiation," Phys. Rev. B, **71**(16), p. 165406.
[364] Wu, B., and Shin, Y. C., 2007, "A One-Dimensional Hydrodynamic Model for Pressures Induced Near the Coating-Water Interface During Laser Shock Peening," J. Appl. Phys., **101**(2), p. 023510.
[365] Wu, B., and Shin, Y. C., 2007, "Two Dimensional Hydrodynamic Simulation of High Pressures Induced by High Power Nanosecond Laser-Matter Interactions Under Water," J. Appl. Phys., **101**(10), p. 103514.
[366] Veysman, M. E., Agranat, M. B., Andreev, N. E., Ashitkov, S. I., Fortov, V. E., Khishchenko, K. V., Kostenko, O. F., Levashov, P. R., Ovchinnikov, A. V., and Sitnikov, D. S., 2008, "Femtosecond Optical Diagnostics and Hydrodynamic Simulation of Ag Plasma Created by Laser Irradiation of a Solid Target," J. Phys. B: At. Mol. Opt. Phys., **41**(12), p. 125704.
[367] Wu, B., Shin, Y. C., Pakhal, H., Laurendeau, N. M., and Lucht, R. P., 2007, "Modeling and Experimental Verification of Plasmas Induced by High-Power Nanosecond Laser-Aluminum Interactions in Air," Phys. Rev. E, **76**(2), p. 026405.
[368] Bulgakova, N. M., Rosenfeld, A., Ehrentraut, L., Stoian, R., and Hertel, I. V., 2007, "Modeling of Electron Dynamics in Laser-Irradiated Solids: Progress Achieved Through a Continuum Approach and Future Prospects," Proc. SPIE, **6732**, p. 673208.
[369] Chen, Z., and Mao, S. S., 2008, "Femtosecond Laser-Induced Electronic Plasma at Metal Surface," Appl. Phys. Lett., **93**(5), p. 051506.
[370] Zhigilei, L. V., and Ivanov, D. S., 2005, "Channels of Energy Redistribution in Short-Pulse Laser Interactions With Metal Targets," Appl. Surf. Sci., **248**(1–4), pp. 433–439.
[371] Zhigilei, L. V., and Garrison, B. J., 2000, "Microscopic Mechanisms of Laser Ablation of Organic Solids in the Thermal and Stress Confinement Irradiation Regimes," J. Appl. Phys., **88**(3), pp. 1281–1298.
[372] Perez, D., and Lewis, L. J., 2004, "Thermodynamic Evolution of Materials During Laser Ablation Under Pico and Femtosecond Pulses," Appl. Phys. A, **79**(4–6), pp. 987–990.
[373] Schäfer, C., Urbassek, H. M, and Zhigilei, L. V., 2002, "Metal Ablation by Picosecond Laser Pulses: A Hybrid Simulation," Phys. Rev. B, **66**(11), p. 115404.
[374] Lorazo, P., Lewis, L. J., and Meunier, M., 2006, "Thermodynamic Pathways to Melting, Ablation, and Solidification in Absorbing Solids Under Pulsed Laser Irradiation," Phys. Rev. B, **73**(13), p. 134108.
[375] Hu, W., Shin, Y. C., and King, G., 2010, "Energy Transport Analysis in Ultrashort Pulse Laser Ablation Through Combined Molecular Dynamics and Monte Carlo Simulation," Phys. Rev. B, **82**(9), p. 094111.
[376] Inogamov, N. A., Anisimov, S. I., Petrov, Y. V., Khokhlov, V. A., Zhakhovskii, V. V., Nishihara, K., Agranat, M. B., Ashitkov, S. I., and Komarov, P. S., 2008, "Theoretical and Experimental Study of Hydrodynamics of Metal Target Irradiated by Ultrashort Laser Pulse," Proc. SPIE, **7005**, p. 70052F.
[377] Balling, P., and Schou, J., 2013, "Femtosecond-Laser Ablation Dynamics of Dielectrics: Basics and Applications for Thin Films," Rep. Prog. Phys., **76**(3), p. 36502.
[378] Gamaly, E. G., and Rode, A. V., 2013, "Physics of Ultra-Short Laser Interaction With Matter: From Phonon Excitation to Ultimate Transformations," Prog. Quantum Electron., **37**(5), pp. 215–323.
[379] Gamaly, E. G., and Rode, A. V., 2014, "Transient Optical Properties of Dielectrics and Semiconductors Excited by an Ultrashort Laser Pulse," J. Opt. Soc. Am. B, **31**(11), p. C36.
[380] Mouskeftaras, A., Guizard, S., Fedorov, N., and Klimentov, S., 2013, "Mechanisms of Femtosecond Laser Ablation of Dielectrics Revealed by Double Pump-Probe Experiment," Appl. Phys. A Mater. Sci. Process., **110**(3), pp. 709–715.
[381] Mauclair, C., Mermillod-Blondin, A., Mishchik, K., Bonse, J., Rosenfeld, A., Colombier, J. P., and Stoian, R., 2016, "Excitation and Relaxation Dynamics in Ultrafast Laser Irradiated Optical Glasses," High Power Laser Sci. Eng., **4**, p. e46.
[382] Zhang, N., Li, X., Jiang, L., Shi, X., Li, C., and Lu, Y., 2013, "Femtosecond Double-Pulse Fabrication of Hierarchical Nanostructures Based on Electron Dynamics Control for High Surface-Enhanced Raman Scattering," Opt. Lett., **38**(18), p. 3558.
[383] Garcia-Lechuga, M., Siegel, J., Hernandez-Rueda, J., and Solis, J., 2014, "Imaging the Ultrafast Kerr Effect, Free Carrier Generation, Relaxation and Ablation Dynamics of Lithium Niobate Irradiated With Femtosecond Laser Pulses," J. Appl. Phys., **116**(11), p. 113502.
[384] Garcia-Lechuga, M., Siegel, J., Hernandez-Rueda, J., and Solis, J., 2014, "Femtosecond Laser Ablation of Dielectric Materials in the Optical Breakdown Regime: Expansion of a Transparent Shell," Appl. Phys. Lett., **105**(11), p. 112902.
[385] Rapp, S., Heinrich, G., Domke, M., and Huber, H. P., 2014, "The Combination of Direct and Confined Laser Ablation Mechanisms for the Selective Structuring of Thin Silicon Nitride Layers," Phys. Procedia, **56**(C), pp. 998–1006.

[386] Wædegaard, K. J., Sandkamm, D. B., Mouskeftaras, A., Guizard, S., and Balling, P., 2014, "Probing Ultrashort-Pulse Laser Excitation of Sapphire: From the Initial Carrier Creation to Material Ablation," Europhys. Lett., **105**(4), p. 47001.
[387] Acharya, S., Chouthe, S., Graener, H., Böntgen, T., Sturm, C., Schmidt-Grund, R., Grundmann, M., and Seifert, G., 2014, "Ultrafast Dynamics of the Dielectric Functions of ZnO and BaTiO3 Thin Films After Intense Femtosecond Laser Excitation," J. Appl. Phys., **115**(5), p. 53508.
[388] Gulley, J. R., and Lanier, T. E., 2014, "Model for Ultrashort Laser Pulse-Induced Ionization Dynamics in Transparent Solids," Phys. Rev. B, **90**(15), p. 155119.
[389] Rethfeld, B., Rämer, A., Brouwer, N., Medvedev, N., and Osmani, O., 2014, "Electron Dynamics and Energy Dissipation in Highly Excited Dielectrics," Nucl. Instrum. Methods Phys. Res., Sect. B, **327**(1), pp. 78–88.
[390] Gruzdev, V., 2014, "Fundamental Mechanisms of Laser Damage of Dielectric Crystals by Ultrashort Pulse: Ionization Dynamics for the Keldysh Model," Opt. Eng., **53**(12), p. 122515.
[391] Weiner, A., 2000, "Femtosecond Pulse Shaping Using Spatial Light Modulators," Rev. Sci. Instrum., **71**(5), pp. 1929–1960.
[392] Weiner, A. M., 1995, "Femtosecond Optical Pulse Shaping and Processing," Prog. Quantum Electron., **19**(3), pp. 161–237.
[393] Li, M., Menon, S., Nibarger, J. P., and Gibson, G. N., 1999, "Ultrafast Electron Dynamics in Femtosecond Optical Breakdown of Dielectrics," Phys. Rev. Lett., **82**(11), pp. 2394–2397.
[394] Choi, T. Y., Hwang, D. J., and Grigoropoulos, C. P., 2002, "Femtosecond Laser Induced Ablation of Crystalline Silicon upon Double Beam Irradiation," Appl. Surf. Sci., **197**, pp. 720–725.
[395] Qi, Y., Qi, H., Wang, Q., Chen, Z., and Hu, Z., 2015, "The Influence of Double Pulse Delay and Ambient Pressure on Femtosecond Laser Ablation of Silicon," Opt. Laser Technol., **66**, pp. 68–77.
[396] Chowdhury, I. H., Xu, X., and Weiner, A. M., 2005, "Ultrafast Double-Pulse Ablation of Fused Silica," Appl. Phys. Lett., **86**(15), p. 151110.
[397] Zhang, K., Jiang, L., Li, X., Shi, X., Yu, D., Qu, L., and Lu, Y., 2014, "Femtosecond Laser Pulse-Train Induced Breakdown in Fused Silica: The Role of Seed Electrons," J. Phys. D: Appl. Phys., **47**(43), p. 435105.
[398] Chowdhury, I. H., Xu, X., and Weiner, A. M., 2003, "Ultrafast Pulse Train Micromachining," Proc. SPIE, **4978**, pp. 138–146.
[399] Englert, L., Rethfeld, B., Haag, L., Wollenhaupt, M., Sarpe-Tudoran, C., and Baumert, T., 2007, "Control of Ionization Processes in High Band Gap Materials via Tailored Femtosecond Pulses," Opt. Express, **15**(26), pp. 17855–17862.
[400] Englert, L., Wollenhaupt, M., Sarpe, C., Otto, D., and Baumert, T., 2012, "Morphology of Nanoscale Structures on Fused Silica Surfaces From Interaction With Temporally Tailored Femtosecond Pulses," J. Laser Appl., **24**(4), p. 42002.
[401] Englert, L., Wollenhaupt, M., Haag, L., Sarpe-Tudoran, C., Rethfeld, B., and Baumert, T., 2008, "Material Processing of Dielectrics With Temporally Asymmetric Shaped Femtosecond Laser Pulses on the Nanometer Scale," Appl. Phys. A, **92**(4), pp. 749–753.
[402] Ahn, S., Choi, J., Noh, J., and Cho, S. H., 2018, "High Aspect Ratio Nanoholes in Glass Generated by Femtosecond Laser Pulses With Picosecond Intervals," Opt. Lasers Eng., **101**, pp. 85–88.
[403] Rezaei, S., Li, J., and Herman, P. R., 2015, "Burst Train Generator of High Energy Femtosecond Laser Pulses for Driving Heat Accumulation Effect During Micromachining," Opt. Lett., **40**(9), pp. 2064–2067.
[404] Götte, N., Winkler, T., Meinl, T., Kusserow, T., Zielinski, B., Sarpe, C., Senftleben, A., Hillmer, H., and Baumert, T., 2016, "Temporal Airy Pulses for Controlled High Aspect Ratio Nanomachining of Dielectrics," Optica, **3**(4), pp. 389–395.
[405] Gyamfi, M., Costella, M., Willemsen, T., Jürgens, P., Mende, M., Jensen, L., and Ristau, D., 2016, "Dual Wavelength Laser Damage Mechanisms in the Ultra-Short Pulse Regime," Proceedings of SPIE 10014, Laser-Induced Damage in Optical Materials, Boulder, CO, Sept. 25–28, p. 100141B.
[406] Yu, X., Bian, Q., Zhao, B., Chang, Z., Corkum, P. B., and Lei, S., 2013, "Near-Infrared Femtosecond Laser Machining Initiated by Ultraviolet Multiphoton Ionization," Appl. Phys. Lett., **102**(10), p. 101111.
[407] Yu, X., Bian, Q., Chang, Z., Corkum, P. B., and Lei, S., 2013, "Femtosecond Laser Nanomachining Initiated by Ultraviolet Multiphoton Ionization," Opt. Express, **21**(20), pp. 24185–24190.
[408] Yu, X., Chang, Z., Corkum, P. B., and Lei, S., 2014, "Fabricating Nanostructures on Fused Silica Using Femtosecond Infrared Pulses Combined With Sub-Nanojoule Ultraviolet Pulses," Opt. Lett., **39**(19), pp. 5638–5640.
[409] Dickey, F. M., 2014, *Laser Beam Shaping: Theory and Techniques*, 2nd ed., CRC Press, Taylor & Francis Group, Boca Raton, FL.
[410] Dickey, F. M., and Lizotte, T. E., 2017, *Laser Beam Shaping Applications*, 2nd ed., CRC Press, Taylor & Francis Group, Boca Raton, FL.
[411] Gerchberg, R. W., and Saxton, W. O., 1972, "A Practical Algorithm for the Determination of Phase From Image and Diffraction Plane Pictures," Optik, **35**(2), pp. 237–246.
[412] Lopez, J., Mishchik, K., Chassagne, B., Javaux-Leger, C., Honninger, C., Mottay, E., and Kling, R., 2015, "Glass Cutting Using Ultrashort Pulsed Bessel Beams," International Congress on Applications of Lasers & Electro-Optics, pp. 60–69.
[413] Sanner, N., Huot, N., Audouard, E., Larat, C., Huignard, J.-P., and Loiseaux, B., 2005, "Programmable Focal Spot Shaping of Amplified Femtosecond Laser Pulses," Opt. Lett., **30**(12), pp. 1479–1481.
[414] Sanner, N., Huot, N., Audouard, E., Larat, C., and Huignard, J. P., 2007, "Direct Ultrafast Laser Micro-Structuring of Materials Using Programmable Beam Shaping," Opt. Lasers Eng., **45**(6), pp. 737–741.
[415] Li, J., Kuang, Z., Edwardson, S., Perrie, W., Liu, D., and Dearden, G., 2016, "Imaging-Based Amplitude Laser Beam Shaping for Material Processing by 2D Reflectivity Tuning of a Spatial Light Modulator," Appl. Opt., **55**(5), p. 1095.
[416] Turunen, J., and Friberg, A. T., 2010, "Chapter 1—Propagation-Invariant Optical Fields," Prog. Opt., **54**, pp. 1–88.
[417] Duocastella, M., and Arnold, C. B., 2012, "Bessel and Annular Beams for Materials Processing," Laser Photon. Rev., **6**(5), pp. 607–621.
[418] Wetzel, B., Xie, C., Lacourt, P.-A., Dudley, J. M., and Courvoisier, F., 2013, "Femtosecond Laser Fabrication of Micro and Nano-Disks in Single Layer Graphene Using Vortex Bessel Beams," Appl. Phys. Lett., **103**(24), p. 241111.
[419] Sahin, R., Ersoy, T., and Akturk, S., 2014, "Ablation of Metal Thin Films Using Femtosecond Laser Bessel Vortex Beams," Appl. Phys. A, **118**(1), pp. 125–129.
[420] Cheng, W., and Polynkin, P., 2014, "Micromachining of Borosilicate Glass Surfaces Using Femtosecond Higher-Order Bessel Beams," J. Opt. Soc. Am. B, **31**(11), p. C48.
[421] Xie, C., Jukna, V., Milián, C., Giust, R., Ouadghiri-Idrissi, I., Itina, T., Dudley, J. M., Couairon, A., and Courvoisier, F., 2015, "Tubular Filamentation for Laser Material Processing," Sci. Rep., **5**(1), p. 8914.
[422] Vasilyeu, R., Dudley, A., Khilo, N., and Forbes, A., 2009, "Generating Superpositions of Higher-Order Bessel Beams," Opt. Express, **17**(26), pp. 23389–23395.
[423] Yu, X., Trallero-Herrero, C. A., and Lei, S., 2016, "Materials Processing With Superposed Bessel Beams," Appl. Surf. Sci., **360**, pp. 833–839.
[424] Yang, L., Qian, D., Xin, C., Hu, Z., Ji, S., Wu, D., Hu, Y., Li, J., Huang, W., and Chu, J., 2017, "Two-Photon Polymerization of Microstructures by a Non-Diffraction Multifoci Pattern Generated From a Superposed Bessel Beam," Opt. Lett., **42**(4), pp. 743–746.
[425] Stoian, R., Bhuyan, M. K., Zhang, G., Cheng, G., Meyer, R., and Courvoisier, F., 2018, "Ultrafast Bessel Beams: Advanced Tools for Laser Materials Processing," Adv. Opt. Technol., **7**(3), pp. 165–174.
[426] Lenzner, M., Krüger, J., Sartania, S., Cheng, Z., Spielmann, C., Mourou, G., and Kautek, F., 1998, "Femtosecond Optical Breakdown in Dielectrics," Phys. Rev. Lett., **80**(18), pp. 4076–4079.
[427] Tien, A.-C., Backus, S., Kapteyn, H., Murnane, M., and Mourou, G., 1999, "Short-Pulse Laser Damage in Transparent Materials as a Function of Pulse Duration," Phys. Rev. Lett., **82**(19), pp. 3883–3886.
[428] Bonse, J., Baudach, S., Krüger, J., Kautek, W., and Lenzner, M., 2002, "Femtosecond Laser Ablation of Silicon-Modification Thresholds and Morphology," Appl. Phys. A Mater. Sci. Process., **74**(1), pp. 19–25.
[429] Keldysh, L., 1965, "Concerning the Theory of Impact Ionization in Semiconductors," Sov. Phys. JETP, **21(6)**, pp. 1135.
[430] Sanner, N., Utéza, O., Chimier, B., Sentis, M., Lassonde, P., Légaré, F., and Kieffer, J. C., 2010, "Toward Determinism in Surface Damaging of Dielectrics Using Few-Cycle Laser Pulses," Appl. Phys. Lett., **96**(7), p. 71111.
[431] Du, J., Li, Z., Kobayashi, T., Zhao, Y., and Leng, Y., 2014, *Pacific-Rim Laser Damage*, T. Jitsuno, J. Shao, and W. Rudolph, eds., International Society for Optics and Photonics, Bellingham, United States, p. 923805.
[432] Soileau, M. J., C Y., 2018, "Laser-Induced Periodic Structures on Optical Materials," Proceedings of the 2018 SPIE Laser Damage Symposium, Sept. 23–26.
[433] Kafka, K. R. P., Talisa, N., Tempea, G., Austin, D. R., Neacsu, C., and Chowdhury, E. A., 2016, "Few-Cycle Pulse Laser Induced Damage Threshold Determination of Ultra-Broadband Optics," Opt. Express, **24**(25), pp. 28858–28868.
[434] Pasquier, C., Blandin, P., Clady, R., Sanner, N., Sentis, M., Utéza, O., Li, Y., and Long, S. Y., 2015, "Handling Beam Propagation in Air for Nearly 10-fs Laser Damage Experiments," Opt. Commun., **355**, pp. 230–238.
[435] Karimi, E., Altucci, C., Tosa, V., Velotta, R., and Marrucci, L., 2013, "Influence of Generalized Focusing of Few-Cycle Gaussian Pulses in Attosecond Pulse Generation," Opt. Express, **21**(21), p. 24991.
[436] Juha, L., Bittner, M., Chvostova, D., Letal, V., Krasa, J., Otcenasek, Z., Kozlova, M., Polan, J., Präg, A. R., Rus, B., Stupka, M., Krzywinski, J., Andrejczuk, A., Pelka, J. B., Sobierajski, R., Ryc, L., Feldhaus, J., Boody, F. P., Grisham, M. E., Vaschenko, G. O., Menoni, C. S., and Rocca, J. J., 2005, "XUV-Laser Induced Ablation of PMMA With Nano-, Pico-, and Femtosecond Pulses," J. Electron. Spectrosc. Relat. Phenom., **144–147**, pp. 929–993.
[437] Jakubczak, K., Mocek, T., Chalupsky, J., Lee, G. H., Kim, T. K., Park, S. B., Nam, C. H., Hajkova, V., Toufarova, M., Juha, L., and Rus, B., 2011, "Enhanced Surface Structuring by Ultrafast XUV/NIR Dual Action," New J. Phys., **13**(5), p. 53049.
[438] Austin, D. R., Kafka, K. R. P., Lai, Y. H., Wang, Z., Blaga, C. I., and Chowdhury, E. A., 2018, "Femtosecond Laser Damage of Germanium From Near- to Mid-Infrared Wavelengths," Opt. Lett., **43**(15), p. 3702.
[439] Torres-Peiró, S., González-Ausejo, J., Mendoza-Yero, O., Mínguez-Vega, G., Andrés, P., and Lancis, J., 2013, "Parallel Laser Micromachining Based on Diffractive Optical Elements With Dispersion Compensated Femtosecond Pulses," Opt. Express, **21**(26), pp. 31830–31836.
[440] Pan, A., Si, J., Chen, T., Li, C., and Hou, X., 2016, "Fabrication of Two-Dimensional Periodic Structures on Silicon After Scanning Irradiation With Femtosecond Laser Multi-Beams," Appl. Surf. Sci., **368**, pp. 443–448.
[441] Mauclair, C., Cheng, G., Huot, N., Audouard, E., Rosenfeld, A., Hertel, I. V., and Stoian, R., 2009, "Dynamic Ultrafast Laser Spatial Tailoring for Parallel

Micromachining of Photonic Devices in Transparent Materials," Opt. Express, **17**(5), pp. 3531–3542.
[442] Kuang, Z., Perrie, W., Edwardson, S. P., Fearon, E., and Dearden, G., 2014, "Ultrafast Laser Parallel Microdrilling Using Multiple Annular Beams Generated by a Spatial Light Modulator," J. Phys. D: Appl. Phys., **47**(11), p. 115501.
[443] Sakakura, M., Sawano, T., Shimotsuma, Y., Miura, K., and Hirao, K., 2009, "Parallel Drawing of Multiple Bent Optical Waveguides Using a Spatial Light Modulator," Jpn. J. Appl. Phys., **48**(12), p. 126507.
[444] Bhuyan, M. K., Velpula, P. K., Colombier, J. P., Olivier, T., Faure, N., and Stoian, R., 2014, "Single-Shot High Aspect Ratio Bulk Nanostructuring of Fused Silica Using Chirp-Controlled Ultrafast Laser Bessel Beams," Appl. Phys. Lett., **104**(2), p. 021107.
[445] Meyer, R., Giust, R., Jacquot, M., Dudley, J. M., and Courvoisier, F., 2017, "Submicron-Quality Cleaving of Glass With Elliptical Ultrafast Bessel Beams," Appl. Phys. Lett., **111**(23), p. 231108.
[446] Bhuyan, M. K., Courvoisier, F., Lacourt, P. A., Jacquot, M., Salut, R., Furfaro, L., and Dudley, J. M., 2010, "High Aspect Ratio Nanochannel Machining Using Single Shot Femtosecond Bessel Beams," Appl. Phys. Lett., **97**(8), p. 081102.
[447] Hu, A., Peng, P., Alarifi, H., Zhang, X. Y., Guo, J. Y., Zhou, Y., and Duley, W. W., 2012, "Femtosecond Laser Welded Nanostructures and Plamonic Devices," J. Laser Appl., **24**(4), p. 042001.
[448] Peng, P., Hu, A., Gerlich, A. P., Zou, G., Liu, L., and Zhou, Y., 2015, "Joining of Silver Nanomaterials at Low Temperatures: Processes, Properties, and Applications," ACS Appl. Mater. Int., **7**(23), pp. 12597–12618.
[449] Ma, Y., Li, H., Bridges, D., Peng, P., Lawrie, B., Feng, Z., and Hu, A., 2016, "Zero-Dimensional to Three-Dimensional Nanojoining: Current Status and Potential Applications," RSC Adv., **6**(79), pp. 75916–75936.
[450] Huang, H., Sivayoganathan, M., Duley, W. W., and Zhou, Y., 2015, "High Integrity Interconnection of Silver Submicron/Nanoparticles on Silicon Wafer by Femtosecond Laser Irradiation," Nanotech, **26**(2), p. 025303.
[451] Garnett, E. C., Cai, W., Cha, J., Mahmood, F., Connor, S. T., Christoforo, M., Cui, Y., McGehee, M., and Brongersma, M. L., 2012, "Self-Limited Plasmonic Welding of Silver Nanowire Junctions," Nature Mater., **11**(3), pp. 241–249.
[452] Nian, Q., Saei, M., Xu, Y., Sabyasachi, G., Deng, B., Chen, Y., and Cheng, G. J., 2015, "Crystalline Nanojoining Silver Nanowire Percolated Networks on Flexible Substrate," ACS Nano, **9**(10), pp. 10018–10031.
[453] Alarifi, H., Atiş, M., Özdoğan, C., Hu, A., Yavuz, M., and Zhou, Y., 2013, "Determination of Complete Melting and Surface Premelting Points of Silver Nanoparticles by Molecular Dynamics Simulation," J. Phys. Chem. C, **117**(23), pp. 12289–12298.
[454] Marzbanrad, E., Hu, A., Zhao, B., and Zhou, Y., 2015, "Room Temperature Nanojoining of Triangular and Hexagonal Silver Nanodisks," J. Phys. Chem. C, **117**(32), pp. 16665–16676.
[455] Li, Q., Liu, G., Yang, H., Wang, W., Luo, S., Dai, S., and Qiu, M., 2016, "Optically Controlled Local Nanosoldering of Metal Nanowires," Appl. Phys. Lett., **108**(19), p. 193101.
[456] Yang, H., Lu, J., Ghosh, P., Chen, Z., Wang, W., Ye, H., Ye, Q., Qiu, M., and Li, Q., 2018, "Plasmonic-Enhanced Targeted Nanohealing of Metallic Nanostructures," Appl. Phys. Lett., **112**(7), p. 071108.
[457] Lin, L., Liu, L., Peng, P., Zhou, G., Duley, W. W., and Zhou, Y., 2016, "In Situ Nanojoining of Y- and T-Shaped Silver Nanowires Structures Using Femtosecond Laser Radiation," Nanotechnol, **27**(12), p. 125201.
[458] Lin, L., Liu, L., Musselman, K., Zou, G., Duley, W. W., and Zhou, Y., 2016, "Plasmonic-Radiation-Enhanced Metal Oxide Nanowire Heterojunctions for Controllable Multilevel Memory," Adv. Funct. Mater., **26**(33), pp. 5979–5986.
[459] Deng, Y., Bai, Y., Yu, Y., Deng, S., Tian, Y., Zhang, G., Zheng, C., Wu, J., and Hu, A., 2019, "Laser Nanojoining of Copper Nanowires," J. Laser Appl., **31**, p. 022414.
[460] Yalisove, S. M., Sugioka, K., and Grigoropoulos, C. P., 2016, "Advances and Opportunities of Ultrafast Laser Synthesis and Processing," MRS Bull., **41**(12), pp. 955–959.
[461] Hu, A., Rybachuk, M., Lu, Q.-B., and Duley, W. W., 2007, "Direct Synthesis of sp-Bonded Carbon Chains on Graphite Surface by Femtosecond Laser Irradiation," Appl. Phys. Lett., **91**(13), p. 131906.
[462] Hu, A., Sanderson, J., Zaidi, A. A., Wang, C., Zhang, T., and Duley, W. W., 2008, "Direct Synthesis of Polyyne Molecules in Acetone by Dissociation Using Femtosecond Laser Irradiation," Carbon, **46**(13), pp. 1823–1825.
[463] Rapp, L., Haberl, B., Pickard, C. J., Bradby, J., Gamaly, E. G., Williams, J. S., and Rode, A. V., 2015, "Experimental Evidence of New Tetragonal Polymorphs of Silicon Formed Through Ultrafast Laser-Induced Confined Micro-Explosion," Nature Comm., **6**(1), p. 7555.
[464] Matsuda, T., Sano, T., Arakawa, K., Sakata, O., Tajiri, H., and Hirose, A., 2014, "Femtosecond Laser-Driven Shock-Induced Dislocation Structures in Iron," Appl. Phys. Exp., **7**(12), p. 122704.
[465] Sano, T., Eimura, T., Kashiwabara, R., Matsuda, T., Isshiki, Y., Hirose, A., Tsutsumi, S., Arakawa, K., Hashimoto, T., Masaki, K., and Sano, Y., 2017, "Femtosecond Laser Peening of 2024 Aluminum Alloy Without a Sacrificial Overlay Under Atmospheric Conditions," J. Laser Appl., **29**(1), p. 012005.
[466] Majumdar, J. D., Gurevich, E. L., Kumari, R., and Ostendorf, A., 2016, "Investigation on Femtosecond Laser Irradiation Assisted Shock Peening of Medium Carbon (0.4% C) Steel," Appl. Surf. Sci., **364**, pp. 133–140.